DISSERTATION

TRACING CARBON FLOWS THROUGH ARCTIC AND ALPINE WATERSHEDS

Submitted by

Laurel M. Lynch

Graduate Degree Program in Ecology

In partial fulfillment of the requirements

For the Degree of Doctor of Philosophy

Colorado State University

Fort Collins, Colorado

Spring 2018

Doctoral Committee:

Advisor: Matthew D. Wallenstein

Claudia M. Boot
Timothy P. Covino
M. Francesca Cotrufo

ABSTRACT

TRACING CARBON FLOWS THROUGH ARCTIC AND ALPINE WATERSHEDS

Organic matter turnover and mobilization links the productivity of terrestrial and fluvial ecosystems and regulates global climate. The first part of this dissertation reviews how our conceptual framework of soil organic matter (SOM) and dissolved organic matter (DOM) cycling has evolved, and emphasizes the role of microbial communities in controlling SOM stability. Chapter two investigates how fresh carbon (C) influences SOM cycling in soils underlying two dominant Arctic plant species. We amended soils colonized by *Eriophorum vaginatum*—a tussock-forming sedge—and *Betula nana*—a competitive dwarf shrub—with glucose, and employed stable isotope tracing to quantify substrate conversion to CO_2, incorporation in microbial biomass, and retention in bulk soil. We measured responses during peak biomass, fall senescence, and spring thaw to assess interactive effects of glucose amendment and season. We also captured legacy responses to amendment by assessing the fate of glucose over short, intermediate, and longer-term periods. We found that glucose conversion to CO_2 was twice as high in tussock soils, while stabilization in bulk soils was significantly higher in shrub soils. Our results highlight the extraordinary C storage capacity of these soils, and suggest shrub expansion could mitigate C losses even as Arctic soils warm.

Chapter three evaluates the mobilization and transformation potential DOM of flowing through an Arctic hillslope. Widespread permafrost thaw is expected to increase CO_2 release from soils to the atmosphere and transform the hydrological routing of water and DOM across Arctic landscapes. We traced the mobilization potential of DOM at two landscape positions

(hillslope and riparian) and from two soil horizons (organic and mineral) using bromide, and characterized the chemical composition of DOM using solution state ^{1}H-NMR and fluorescence spectroscopy. We found that compounds mobilized through the porous organic horizon were associated with plant-derived molecules, while those flowing through mineral soils had a microbial fingerprint. Landscape position also influenced the chemical diversity of DOM, which increased during downslope transport from hillslope to riparian soils. While the chemical composition of DOM varied across the landscape, the potential for rapid lateral flow across Arctic hillslopes and along the mineral-permafrost interface was uniformly high, suggesting DOM mobilization is an important mechanism of C loss from Arctic soils.

Chapter four explores how geomorphic complexity and seasonal hydrology influence the cycling and transformation of DOM in alpine headwater streams. We collected surface and hyporheic water samples from two watersheds varying in channel complexity (single-thread and multi-thread) at eight time points spanning the seasonal hydrograph. We found that connectivity across the terrestrial-aquatic interface was maximized during peak discharge and decreased through the season. The chemical composition of DOM, evaluated using electron impact gas chromatography mass spectrometry and fluorescence spectroscopy, varied with watershed connectivity, with increasingly divergent DOM profiles observed with a loss of hydrologic connectivity. We suggest that widespread channel simplification, resulting from land-use and management changes, will reduce DOM processing and compromise ecosystem function.

ACKNOWLEDGMENTS

I have been incredibly fortunate to have the guidance and support of many groups and individuals throughout my dissertation work. I would first like to thank my PhD advisor, Matthew Wallenstein, who provided exceptional research opportunities and mentorship. I was also fortunate to have the support and guidance of amazing committee members, Claudia Boot, Francesca Cotrufo, and Timothy Covino, who contributed substantially to my growth as an ecosystem ecologist and selflessly shared their respective expertise. Thank you to Malak Tfaily and David Hoyt for being amazing mentors while I completed my dissertation work at the Pacific Northwest National Laboratory. I would especially like to thank Megan Machmuller, with whom I spent many hours doing field and lab work in Alaska and Colorado, and who was immensely encouraging during my time at CSU. Many thanks as well to Carolyn Livensperger and Peter Baas for helping me with snowy field work at Toolik, and for being such great friends. Nick Sutfin and Tim Fegel, in addition to being amazing friends, helped develop the third chapter of this dissertation. I would also like to thank Sarah Fulton-Smith, whose support extends far beyond science, and Jessica Ernakovich, for being an amazing collaborator and mentor.

Much of this work was made possible by Daniel Reuss, who kept the EcoCore labs running, and to Michelle Haddix for helping with protocol training and development. I am immensely grateful for my consultations with Ann Hess and Monique Rocca, who significantly improved my understanding of statistics. I would also like to thank the Toolik GIS team, Jason Stuckey, Randy Fulweber, and Jorge Noguera, for collecting high-resolution GPS data at my field sites.

Finally, I would like to thank those who inspired my early scientific development, and my family. In particular, I would like to thank John Schade and Stephanie Schmidt, who introduced me to biogeochemistry at St Olaf College and helped me design my first research experiment. Thank you to Roger Reuss, Knut Kielland, and Michaela Swanson for hiring me for my first research experience and introducing me to extracellular enzymes, mycorrhizae, lynx, and snowshoe hare. I would also like to thank two of my exceptional high school teachers: Cynthia Beale, my incredibly inspirational and supportive biology teacher, and Carrie Heimer, my English teacher who helped me develop my interest in literature and writing. Most especially, I want to thank my parents for their love and support, and for encouraging my passion for outdoor adventures, scholarship, and the arts, and, of course, to my partner, Alex Maas.

I would also like to acknowledge my collaborators on chapter two (Megan Machmuller, Francesca Cotrufo, Eldor Paul, Matthew Wallenstein), chapter three (Timothy Covino, Claudia Boot, Megan Machmuller, Francesca Cotrufo, Chris Rithner, David Hoyt, Matthew Wallenstein) and chapter four (Nick Sutfin, Timothy Fegel, Claudia Boot, Timothy Covino Matthew Wallenstein).

This work was funded by the NSF Faculty Early Career Development Program (grant 255228), the Department of Energy Terrestrial and Ecosystem Science Program (grant DE-SC0010568), the NSF IWATER: Integrated Water, Atmosphere, Ecosystems Education and Research Program at Colorado State University (grant DGE-0966346), and the DOE Science Graduate Student Research Program (grant DE-SC0014664). Research support at Toolik Lake Field Station was provided by the Arctic LTER Program (grant 1637459).

TABLE OF CONTENTS

CHAPTER 1- INTRODCUTION

Soils store over three times as much carbon (C) as the atmosphere (Ontl and Schulte, 2012), making them critical climate regulators (Oelkers and Cole, 2008). The largest soil organic C stocks are located in high latitude and alpine regions (Koven et al., 2009; Tarnocai et al., 2009), where cold temperatures and saturated conditions limit rates of soil organic matter (SOM) decomposition (Ernakovich et al., 2014; Hicks Pries et al., 2013).These temperature-stabilized systems may exert a disproportionate influence on soil C cycling as climate warms (Dutta et al., 2006; Schaefer et al., 2011; Schmidt et al., 2011; Vonk et al., 2013) given current C storage capacities (Crowther et al., 2016) and rapid warming of northern ecosystems (Meehl et al., 2013; Serreze and Barry, 2011). Additionally, decomposition rates have a higher temperature sensitivity than net primary productivity (Kirschbaum, 1995), suggesting greater plant growth may be insufficient in balancing C losses. Climate perturbation will also transform the hydrology (Frey and McClelland, 2009; J. Rowland et al., 2010), permafrost extent (Jorgenson et al., 2001; Liljedahl et al., 2016), species composition (Crimmins et al., 2009; Sturm et al., 2001), and disturbance regimes (Westerling, 2006) of tundra and alpine ecosystems (Pachauri et al., 2014). Ecosystem ecology, which addresses interactions between the abiotic environment and living organisms as an integrated system (Chapin III et al., 2011), is fundamental in describing how C cycling and energy flows are influenced by human activity, whether directly through transformation of the physical environment or indirectly through land-use versus climate change. In this dissertation, I employ an ecosystems approach to trace the production, consumption, and transformation of C as it is mobilized from upland soils and exported through headwater streams.

In the past several decades views on organic C cycling have undergone significant revision. Traditional models of SOM and dissolved organic matter (DOM) dynamics suggest recalcitrant plant products—lignin derivatives, humic substances, quinone-type structures—form a stable C pool that resists further turnover (Couteaux et al., 1995; Meentemeyer and Berg, 1986; Sparks, 2003; Waksman and Stevens, 1930). The majority of evidence supporting these models was generated in the laboratory, where bulk SOM was extracted under strong acid and base conditions to isolate humin, humic-acid, and fulvic-acid fractions. The advent of higher-resolution and non-destructive analytical techniques revealed that these operationally-defined fractions are not detectable in natural soils. As a result, humification theory has been widely replaced by soil continuum models (Cotrufo et al., 2013; Dungait et al., 2012; Grandy and Neff, 2008; Kleber and Johnson, 2010; Lehmann and Kleber, 2015; Marschner et al., 2008; Schimel and Schaeffer, 2012), which emphasize the role of microbial communities in promoting SOM formation. In particular, microbial residues, including metabolites and necromass, appear to persist in 'stable' soil pools with slower turnover rates, and include amide, aliphatic, carboxylic, aromatic, and *O*-alkyl moieties (Kallenbach et al., 2016; Lehmann et al., 2008; Liang et al., 2017).

Microbial substrate use efficiency (SUE) exerts a primary control on C fate by determining the fraction of soil C that is released to the atmosphere as CO_2 or CH_4, incorporated into microbial biomass, or stabilized in the soil-mineral matrix (Cotrufo et al., 2013). SUE is defined as the ratio of growth to respiration ([$\mu/(\mu+R]$, where μ is biomass growth and R is respiration) (Sinsabaugh et al., 2013). Lower quality plant material, including compounds with higher C:N and/or lower energy yields, require microbial communities to synthesize and excrete extracellular enzymes that attack and transform plant residues (Liang et al., 2017). These

catabolic pathways are associated with low SUE and high evolution of CO_2 and/or CH_4 to the atmosphere. Priming has been proposed as a dramatic example of low SUE, where deposition of fresh plant-derived materials stimulates microbial decomposition and destabilization of existing SOM stocks (Fontaine et al., 2007, 2004; Kuzyakov, 2002; Kuzyakov et al., 2000). Priming has been found to increase CO_2 evolution by as much as 400% (Zhu and Cheng, 2011); if priming becomes a dominant mechanism in SOM-rich tundra soils, a strong positive feedback to warming could be activated (Schmidt et al., 2011). In contrast, higher-quality plant material may be preferentially assimilated into microbial biomass. The transformation and re-synthesis of plant-derived material into relatively stable microbe-derived compounds—including cell wall fragments and osmolytes—may promote SOM formation and stabilization (Liang et al., 2017; Joshua Schimel et al., 2007). The primary mechanisms of SOM retention include chemical bonding on reactive soil minerals (Kaiser and Kalbitz, 2012; Kögel-Knabner et al., 2008; Vogel et al., 2014) and occlusion in soil aggregates (Bachmann et al., n.d.; Lehmann et al., 2007; Mueller et al., 2012; Vogel et al., 2014). In chapter two we test whether inputs of low molecular weight carbon induce SOM priming or stabilization in Arctic tundra soils colonized by vegetation with contrasting litter quality.

The chemical composition of DOM integrates microbial metabolism across the landscape (Figure 1.1). Unlike SOM, DOM is comprised of low-molecular weight compounds that are directly available for microbial uptake (Kalbitz et al., 2003) and thus represent a critical intermediary in global C cycling (Battin et al., 2009a; Vonk et al., 2013). The movement of DOM through upland soils and across the terrestrial-aquatic interface was traditionally viewed as a selective chromatograph, where DOM produced through plant and microbial activity in the organic horizon leached vertically until it sorbed on reactive mineral surfaces or was exported to

depth or the fluvial network (Neff and Asner, 2001). This view has been revised by Kaiser and Kalbitz (2012) who suggest variable concentrations and fluxes of DOM in the soil profile result from sequential sorption and desorption, combined with intensive microbial processing. The mobilization potential of DOM, which depends upon its reactivity and pore-water connectivity (Smith et al., 2017), influences the residence time of organic matter in terrestrial environments (Battin et al., 2009a; Singer et al., 2012). In chapter three we test how the chemical composition of DOM varies with landscape position and flowpath velocity on a permafrost-impacted hillslope.

Energetic linkages between terrestrial and fluvial systems are shaped by landscape complexity (Battin et al., 2009a). Like the terrestrial environment, where highly heterogeneous soil matrices can be bypassed by preferential flow, fluvial networks also exhibit varying degrees of channel complexity. This is particularly evident in mountainous headwater streams where channels alternate between simple, single-channel segments and complex segments with multiple channels of flow across the valley bottom (Livers and Wohl, 2016; Wegener et al., 2017; Wohl, 2013). Compounds entrained in slow flowpaths are more likely to be metabolized by microbial communities (Battin et al., 2009a; Singer et al., 2012) resulting in a convergent chemical profile (Kellerman et al., 2014) that reflects intensive, sequential metabolism (Liang et al., 2017). In contrast, DOM flowing through an integrated landscape, such as a swift, channelized stream, could expedite the delivery of young, divergent DOM chemistries to downstream environments. In chapter four we explore how geomorphic complexity and fluvial hydrology interactively influence the chemical composition of DOM flowing through multi-thread and single-channel headwater streams.

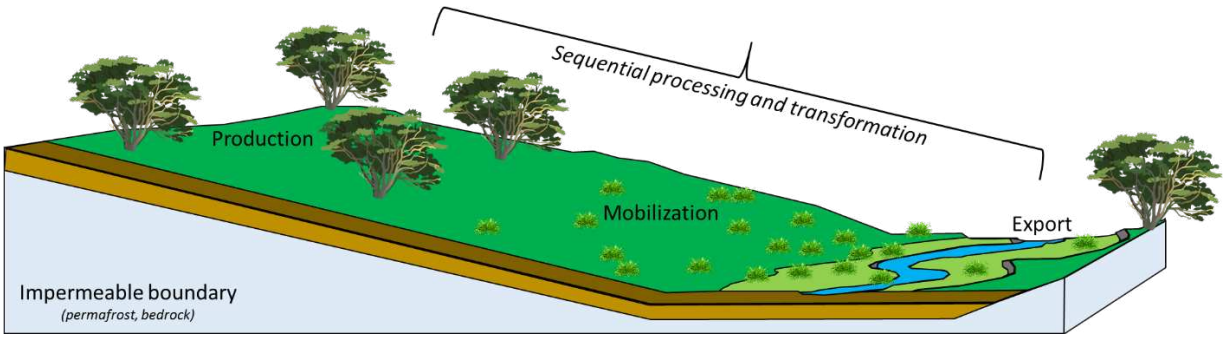

Figure 1.1- In this dissertation, I explore how organic matter produced in upland soils (and throughout the landscape) can be mobilized through hillslope flowpaths and exported through headwater streams. These flows of energy not only link terrestrial and aquatic systems, but represent a continuum of sequential processing and transformation that produces highly diverse organic matter and metabolite profiles.

REFERENCES

Bardgett, R. D., C. Freeman, and N. J. Ostle (2008), Microbial contributions to climate change through carbon cycle feedbacks., *ISME J.*, *2*(8), 805–814.

Baron, J. S., T. M. Schmidt, and M. D. Hartman (2009), Climate-induced changes in high elevation stream nitrate dynamics, *Glob. Chang. Biol.*, *15*(7), 1777–1789, doi:10.1111/j.1365-2486.2009.01847.x.

Battin, T. J., K. Besemer, M. M. Bengtsson, A. M. Romani, and A. I. Packmann (2016), The ecology and biogeochemistry of stream biofilms, *Nat. Rev. Microbiol.*, *14*(4), 251–263, doi:10.1038/nrmicro.2016.15.

Beaulieu, J. J. et al. (2011), Nitrous oxide emission from denitrification in stream and river networks., *Proc. Natl. Acad. Sci. U. S. A.*, *108*(1), 214–219, doi:10.1073/pnas.1011464108.

Bormann, A. F. H., and G. E. Likens (1967), Nutrient Cycling, *Science (80-.).*, *155*(3761), 424–429.

Burrows, R. M. . B., J. B. . Fellman, R. H. . Magierowski, and L. A. . B. Barmuta (2013), Allochthonous dissolved organic matter controls bacterial carbon production in old-growth and clearfelled headwater streams, *Freshw. Sci.*, *32*(3), 821–836, doi:10.1899/12-163.1.

Butman, D., and P. a. Raymond (2011), Significant efflux of carbon dioxide from streams and rivers in the United States, *Nat. Geosci.*, *4*(12), 839–842, doi:10.1038/ngeo1294.

Campeau, A., J.-F. Lapierre, D. Vachon, and P. a. del Giorgio (2014), Regional contribution of CO 2 and CH 4 fluxes from the fluvial network in a lowland boreal landscape of Québec, *Global Biogeochem. Cycles*, *1*, n/a–n/a, doi:10.1002/2013GB004685.

Cole, J. J. et al. (2007), Plumbing the Global Carbon Cycle : Integrating Inland Waters into the Terrestrial Carbon Budget, *Ecosystems*, *10*, 171–184, doi:10.1007/s10021-006-9013-8.

Crawford, J. T., M. M. Dornblaser, E. H. Stanley, D. W. Clow, and G. Robert (2014), Source limitation of carbon gas emissions in high-elevation mountain streams and lakes.

Dodds, W. K., and V. H. Smith (2016), Nitrogen , phosphorus , and eutrophication in streams, *Inl. Waters*, *6*, 155–164, doi:10.5268/IW-6.2.909.

Fahey, T. J. et al. (2005), The biogeochemistry of carbon at Hubbard Brook, *Biogeochemistry*, *75*(1), 109–176, doi:10.1007/s10533-004-6321-y.

Fisher, S. G., N. B. Grimm, E. Martí, R. M. Holmes, and J. B. J. Jr. (1998), Material Spiraling in Stream Corridors: A Telescoping Ecosystem Model, *Ecosystems*, *1*(1), 19–34, doi:10.1007/s100219900003.

Freixa, A. (2016), Function and Structure of River Sediment Biofilms and Their Role in Dissolved Organic Matter Utilization,

Frey, K. E., J. W. McClelland, R. M. Holmes, and L. C. Smith (2007), Impacts of climate warming and permafrost thaw on the riverine transport of nitrogen and phosphorus to the Kara Sea, *J. Geophys. Res.*, *112*(G4), 10, doi:G04s5810.1029/2006jg000369.

Hood, E., M. N. Gooseff, and S. L. Johnson (2006), Changes in the character of stream water dissolved organic carbon during flushing in three small watersheds, Oregon, *J. Geophys. Res. Biogeosciences*, *111*(1), 1–8, doi:10.1029/2005JG000082.

Kokic, J., M. B. M. Wallin, H. E. Chmiel, B. a Denfeld, and S. Sobek (2014), Carbon dioxide evasion from headwater systems strongly contributes to the total export of carbon from a small boreal lake catchment, *J. ...*, (Dic), 1–16, doi:10.1002/2014JG002706.Received.

Lansdown, K., C. M. Heppell, M. Trimmer, a. Binley, a. L. Heathwaite, P. Byrne, and H. Zhang (2015), The interplay between transport and reaction rates as controls on nitrate attenuation in permeable, streambed sediments, *J. Geophys. Res. Biogeosciences*, 1–17, doi:10.1002/2014JG002874.

Lawrence, D. J., B. Stewart-Koster, J. D. Olden, A. S. Ruesch, C. E. Torgersen, J. J. Lawler, D. P. Butcher, and J. K. Crown (2014), The interactive effects of climate change, riparian management, and a nonnative predator on stream-rearing salmon, *Ecol. Appl.*, *24*(4), 895–912, doi:10.1890/13-0753.1.

Lovett, G. M., C. G. Jones, M. G. Turner, and K. C. Weathers (2005), *Heterogeneous Landscapes Ecosystem Function in Heterogeneous Landscapes*.

Mast, M. A., D. W. Clow, J. S. Baron, and G. A. Wetherbee (2014), Links between N Deposition and Nitrate Export from a High- Elevation Watershed in the Colorado Front Range, *Environ. Sci. Technol.*, *48*(24), 14258–14265.

Newbold, J. D., J. W. Elwood, R. V. O'Neill, and W. Van Winkle (1981), Measuring Nutrient Spiralling in Streams, *Can. J. Fish. Aquat. Sci.*, *38*(7), 860–863, doi:10.1139/f81-114.

Poff, N. L., and J. K. H. Zimmerman (2010), Ecological responses to altered flow regimes: A literature review to inform the science and management of environmental flows, *Freshw. Biol.*, *55*(1), 194–205, doi:10.1111/j.1365-2427.2009.02272.x.

Shelley, F., F. Abdullahi, J. Grey, and M. Trimmer (2015), Microbial methane cycling in the bed of a chalk river: oxidation has the potential to match methanogenesis enhanced by warming, *Freshw. Biol.*, *60*, 150–160, doi:10.1111/fwb.12480.

Spencer, R. G. M., P. J. Mann, T. Dittmar, T. I. Eglinton, C. McIntyre, R. M. Holmes, N. Zimov, and A. Stubbins (2015), Detecting the Signature of Permafrost Thaw in Arctic Rivers, *Geophys. Res. Lett.*, *1*(850), n/a–n/a, doi:10.1002/2015GL063498.

Stanley, E. H., N. J. Casson, S. T. Christel, J. T. Crawford, L. C. Loken, and S. Oliver (2015), The Ecology of Methane in Streams and Rivers: Patterns, Controls, and Global Significance, *Ecol. Monogr.*, *1*, 1689–1699, doi:10.1017/CBO9781107415324.004.

Vannote, R. L., G. W. Minshall, K. W. Cummins, J. R. Sedell, and C. E. Cushing (1980), The River Continuum Concept, *Can. J. Fish. Aquat. Sci.*, *37*(1), 130–137, doi:10.1139/f80-017.

Yamashita, Y., B. D. Kloeppel, J. Knoepp, G. L. Zausen, and R. Jaff?? (2011), Effects of Watershed History on Dissolved Organic Matter Characteristics in Headwater Streams, *Ecosystems*, *14*(7), 1110–1122, doi:10.1007/s10021-011-9469-z.

CHAPTER 2- TRACKING THE FATE OF FRESH CARBON IN THE ARCTIC TUNDRA: WILL SHRUB EXPANSION ALTER RESPONSES OF SOIL ORGANIC MATTER TO GLOBAL WARMING?[1]

INTRODUCTION

The vulnerability of vast carbon (C) stocks stored in Arctic soils to rapid climate warming is widely recognized (Crowther et al., 2016; Mack et al., 2004). But, climate warming is also increasing plant productivity, which could either ameliorate or enhance soil C loss (Natali et al., 2012; Sistla et al., 2013). The potential for C inputs to balance losses will depend on how efficiently plant-derived C is incorporated into microbial products, the precursor of soil organic matter (SOM) formation, *versus* converted to CO_2 and released to the atmosphere (Cotrufo et al., 2013). In addition, new plant litter and root exudate inputs might enhance the decomposition of old SOM through a process known as priming (Fontaine et al., 2003; Kuzyakov, 2002). Thus, enhanced plant productivity in the Arctic could either promote the formation of new soil C, or increase losses of native soil C, making vegetation responses to warming a critical regulator of global C cycling.

The net effects of rapid climate change on Arctic soil C stocks are mixed, with evidence of massive greenhouse gas release to the atmosphere (Commane et al., 2017; Crowther et al., 2016; Mack et al., 2004; Schuur et al., 2008), as well as recovery of soil C stocks following perturbation (Jiang et al., 2015; Natali et al., 2012; Sistla et al., 2013). Several responses to warming will likely modulate the balance between C release and storage. Warmer winters

[1] This chapter is in review at Soil Biology and Biochemistry: Lynch, L.M., Machmuller M.B., Cotrufo, M.F., Paul, E.A., Wallenstein, M.D., 2018. Tracking the fate of fresh carbon in the Arctic tundra: Will shrub expansion alter responses of soil organic matter to warming?

(Christensen et al., 2013) are degrading permafrost and deepening active layer thaw depths (Hodgkins et al., 2014; Liljedahl et al., 2016), which could expose newly liberated C to rapid microbial metabolism (Mackelprang et al., 2011; Marín-Spiotta et al., 2014). At the same time, lengthening growing seasons (Ernakovich et al., 2014; Livensperger et al., 2016) have fundamentally altered vegetation composition and productivity (Chapin et al., 1995; Deslippe and Simard, 2011; Sturm et al., 2001), the effects of which are diffusing belowground (Hartley *et al.*, 2012). Specifically, greater plant productivity is expected to increase the release of root exudates belowground (Brüggemann et al., 2011), which are primarily composed of low molecular weight C compounds (LMW-C) (Jones et al., 2009). These LMW-C compounds may stimulate decomposition of native SOM (Hartley et al., 2012; Mack et al., 2004) by inducing a positive priming effect to relieve microbial nutrient limitation (Kuzyakov, 2002). As a result, greater extracellular enzyme production could increase nutrient mobilization from native SOM and contribute to net soil C loss (Kuzyakov, 2010). Alternatively, new LMW-C inputs could reduce SOM turnover if microbial substrate use efficiency (SUE) increases and microbial products are stabilized through organo-mineral complexation (Cotrufo et al., 2013; Kallenbach et al., 2016; Schmidt et al., 2011).

The influence of vegetation on belowground nutrient availability may influence the net effect of LMW-C inputs on soil C stocks (Hartley et al., 2012). Widespread increases in primary productivity have been attributed to rapid expansion of *Betula nana* shrubs (Sturm et al., 2001). The success of these shrubs is facilitated by phenotypic traits that allow them to outcompete other species, including *Eriophorum vaginatum,* a dominant tussock-forming sedge (Bret-Harte et al., 2001; Chapin et al., 1995; Deslippe and Simard, 2011; Koyama et al., 2013; Shaver et al., 2001; Sistla et al., 2013). These traits include developmental plasticity (Bret-Harte et al., 2001),

formation of N-acquiring and C-sharing ectomycorrhizal networks (Deslippe and Simard, 2011), and snow entrapment, which facilitates over-winter SOM mineralization and release of nutrients for shrub uptake the following spring (Schimel et al., 2004; Sturm et al., 2001). Associations between *B. nana* and N-acquiring ectomycorrhizal networks increase shrub litter and soil N concentrations (Deslippe and Simard, 2011) relative to non-mycorrhizal, N poorer, *E. vaginatum* systems (Sullivan et al., 2007). The difference in N availability belowground could increase the magnitude of priming resulting from new LMW-C inputs in *E. vaginatum* soils, particularly during peak plant productivity when nutrient competition is intensified (Zhu et al., 2016). Thus, cascading effects of *B. nana* expansion may release microbial energetic and nutrient constraints relative to *E. vaginatum* soils, reducing the magnitude of SOM priming.

To test the effect of LMW-C inputs on native soil C stocks, we applied ^{13}C-enriched glucose—a model root exudate (Dijkstra et al., 2011; Strickland et al., 2012)—to Arctic tundra soils underlying *E. vaginatum* and *B. nana*. We used two-pool isotope mixing models to track the proportion of LMW-C converted to CO_2, assimilated in microbial biomass, transformed to dissolved organic matter, and retained in bulk soil. We captured the influence of season on LMW-C fate by amending soils in July (peak biomass), September (senescence), and May (spring thaw). To determine whether LMW-C persisted longer-term, we measured responses 54 and 306 days following amendment. We posit that the fate of LMW-C and the magnitude and direction of priming is driven by SOM stoichiometry (e.g. C:N). With this rationale, we test three predictions: (1) LMW-C input increases SOM turnover, with the largest priming effect—and lowest microbial SUE—in higher C:N soils underlying *E. vaginatum*; (2) the magnitude of these effects vary seasonally and are negatively correlated with soil N concentrations; (3) the

proportion of LMW-C retained belowground is positively correlated with microbial SUE (Figure 2.1).

METHODS

SITE DESCRIPTION

We established study plots in May 2014 in a moist acidic tundra site near Toolik Lake Field Station, Alaska, USA (68˚ 38'N, 149˚ 34'W). Mean annual temperature at Toolik Field Station is -8°C, with average summer temperatures near 10°C and average winter temperatures near -20°C (Hobbie and Kling, 2014). Mean annual precipitation is 318 mm, with 43% falling as snow (Schimel et al., 2004). The region is dominated by *Eriophorum vaginatum,* a tussock forming sedge, *Betula nana,* a dwarf birch, and mosses, which together comprise approximately 45% of above and belowground biomass (g m^{-2}) (Hobbie and Chapin, 1998). The soils are classified as Ruptic Histic Aquiturbels (Borden et al., 2010) and have an average pH of 4.9. Average soil C stocks in the top 20 cm were 2,150 ± 335 g C m^{-2} in soils underlying *B. nana* and 2,282 ± 296 g C m^{-2} in soils underlying *E. vaginatum.* We observed the deepest active layers at our plots in July 2014, averaging 10 cm beneath *B. nana* and >20 cm beneath *E. vaginatum.* Unfortunately, we did not measure species-specific soil temperatures, however previous research has shown temperatures are similar between graminoid and shrub dominated communities (Bradley-Cook et al., 2016). Thus, although areas colonized by dense, tall shrubs may increase latent heat fluxes (McFadden, 1998) and could reduce temperatures relative to within-tussock soils (Chapin III et al., 1979), these effects are not always propagated belowground (Sturm et al., 2001).

We selected three time periods for our study that represent important seasonal stages in the Arctic: peak productivity (July 24–August 6, 2014), senescence (September 6–September 18,

2014), and thaw (May 19–May 30, 2015). Precipitation and temperature data for each sampling period were acquired from the Toolik Long Term Ecological Research database (Shaver and Laundre, 2010). Cumulative precipitation was 39.6 mm during peak plant productivity, 2.0 mm during senescence, and 55.3 mm during thaw. Mean soil temperatures at 5 cm depth were 9.1 (± 0.6) °C during peak plant productivity, 3.0 (± 0.5) °C during senescence, and 6.65 (± 0.3) °C during thaw. Average annual precipitation and soil temperatures are reported for 2014, 2015, and the ten-year average (2005-2015) in SI Table 2.1.

EXPERIMENTAL DESIGN

Our experiment consisted of three factors: vegetation type (*B. nana* or *E. vaginatum),* LMW-C addition (amended or control), and month (July, September, or May). We replicated each treatment four times in a fully randomized block design, where each 5x5 m^2 block was spaced 10 m apart. Our experimental unit was a PVC collar (10 cm diameter and 15 cm tall), which we installed around a tussock or shrub plant, maintaining a minimum spacing of 1 m between collars.

We installed 12 collars in each block (2 vegetation types * 2 additions * 3 months) in May 2014 and let them equilibrate for 45 days before amending soils within treatment collars with LMW-C. Soils were amended July 28, 2014, September 11, 2014, or May 22, 2015. We amended each collar with ^{13}C-enriched (10 atom%) glucose solution at 640 μg C g^{-1} soil. This corresponded to approximately 36 g glucose m^{-2}, assuming a 10 cm organic horizon and a bulk density of 0.075 g cm^{-3}. The LMW-C addition increased average soil C concentrations in the top 20 cm by 1.7%; we selected this relatively low tracer concentration to avoid inducing a direct C fertilization effect and to minimize impacts on ongoing metabolic processes (Dijkstra et al., 2011). To achieve even distribution throughout the amended soil profile, we added 5 ml of

substrate with a 20-gauge needle (Becton Dickinson) at five equidistantly spaced points, continuously injecting substrate from 5 cm depth to the soil surface.

Two additional collars were installed around *B. nana* and *E. vaginatum* plants in each block allowing us to monitor the influence of elevated LMW-C availability on intermediate and long-term Arctic C cycling. These collars were amended July 28, 2014 and harvested either 49 days (September 11, 2014) or 306 days (May 30, 2015) following amendment. Control collars in each block remained undisturbed for the duration of the experiment and were used as background end members in the two-pool isotope-mixing model (see *Data Analysis*).

CO_2 MEASUREMENTS

LMW-C amended and control (non-amended) soils were measured in the field for CO_2 concentrations (ppm) and $^{13}CO_2$ enrichment (‰) using a Picarro G2101-*i* (Picarro Inc., Sunnyvale, CA, USA) portable cavity ring-down spectroscopy analyzer (CRDSA). The CRDSA was frequently calibrated using high-purity CO_2 calibrant gas with a range of CO_2 concentrations and isotopic values (Cambridge Isotope Laboratories CLM-3783-10; Airgas UHP300). CO_2 concentrations and ^{13}C- CO_2 isotope values were validated with a Li-Cor LI 6252 Infrared gas analyzer (Li-Cor Inc., Lincoln, NE, USA) and a PreCon Delta V IRMS coupled to a GC-isolink unit (Thermo Scientific, Waltham, MA, USA) at Colorado State University.

To allow continuous flux measurements at our field site, we coupled the CRDSA to an external recirculating vacuum pump and eliminated water interference using a magnesium perchlorate water trap (<0.03% H_2O; Agilent Technologies MT120-4). We used Bev-A-Line stainless steel flexible tubing (Swagelok 321-4-X-24DFR) to connect the CRDSA to the water trap and recirculation pump, as well as to a 10 cm diameter PVC cap fit with two 6.35 mm

Swagelok stainless steel ports (SS-4-VCR-6-DM). The connection of the PVC cap and collar formed a gas tight seal that was fitted with a foam gasket (LiCor 8100-632).

CO_2 and $\delta^{13}C$-CO_2 was measured in the amended soils after six and twelve hours, and one, three, five, seven, and ten days. Amended soils incubated for intermediate length were measured again four times after approximately 1.5 months (43, 44, 48, 49 days) of *in situ* incubation, and long-term soils were measured again after approximately 11 months (44, 50, 302, and 305 days) of *in situ* incubation. Control soils were measured for $^{13}CO_2$ flux twelve times during the course of the study (five times in July, five times in September, and two times in May). Corrections were applied to CO_2 effluxes using an average hourly soil temperature at 5 cm depth to account for variability. We connected the CRDSA to each collar for a sufficient period of time to allow an increase of at least 100 ppm CO_2 , and $^{-}5‰$ $\delta^{13}C$ for control soils and $^{+}100‰$ $\delta^{13}C$ for treatment soils. This range of CO_2 concentration and isotope enrichment was sufficient to quantify the exchange processes of CO_2 between terrestrial and atmospheric reservoirs and to apply the Keeling plot method to estimate ^{13}C of the soil CO_2 efflux (Cotrufo et al., 2014; Keeling, 1958; Köhler et al., 2006). We calculated the ^{13}C-CO_2 signature as the y-intercept of the linear regression of ^{13}C versus the inverse CO_2 concentration ($r^2 \geq 0.98$). We flushed the CRDSA with ambient air between measurements and began subsequent measurements after CO_2 concentrations and isotope enrichment returned to background levels.

SOIL COLLECTION AND PROCESSING

At each harvest date (July 29, 2014, September 21, or May 31, 2015) we collected control and LMW-C amended soils by cutting around the PVC collar with an ethanol-sterilized, serrated knife. We split soil cores into a surface sample (0-10 cm) and a subsurface sample (10-20 cm), which roughly corresponded to the organic and mineral horizon (± 5.3 cm). Each sample

was bagged individually and shipped frozen to Colorado State University for analysis, where they were stored until processing. In the laboratory, green litter and live roots were removed and samples were thoroughly homogenized by hand. Soils were sub-sampled for gravimetric water content, C and N elemental and isotopic analyses, extractable nutrients, microbial biomass, and potential extracellular enzyme activities, as described below. We ground soils to a fine powder using liquid N and a mortar and pestle, and measured %C, %N, and ^{13}C using a Carlo Erba NA 1500 elemental analyzer (CE Instruments, Lancanshire, UK) coupled to a VG Isochrom continuous flow isotope ratio mass spectrometer (Isoprime, Inc., Manchester, UK).

EXTRACTABLE NUTRIENTS AND MICROBIAL BIOMASS

Microbial biomass and soil nutrient analyses were conducted following a modified method described in Weintraub et al. (2007). We extracted samples and soil-free blanks with 25 ml of 0.05 M potassium sulfate and agitated them on an orbital shaker for one hour. To extract microbial biomass, we evenly distributed 2 ml of ethanol-free chloroform over 5 g wet weight soil subsamples and incubated them at room temperature for 24 hours in a stoppered 250 ml Erlenmeyer flask. Following incubation, we vented flasks in a fume hood for at least 30 minutes until the chloroform had fully evaporated (Witt et al., 2000). We filtered both control and fumigated samples through No. 1 Whatman paper and analyzed total extractable organic carbon (TOC) and total dissolved nitrogen (TDN) with a Shimadzu TOC-L (Shimadzu Scientific Instruments, Inc.). We measured extractable ammonium and nitrate with an Alpkem flow solution IV automated wet chemistry system (O.I. Analytical College Station, TX). Total organic nitrogen (TON) was calculated as the difference between TDN and total inorganic nitrogen (TIN = ammonium + nitrate). We calculated extractable microbial biomass (MB) C and N as the

difference between paired chloroform-fumigated and non-fumigated subsamples and no correction factors (k_{ec}) were applied (Weintraub et al., 2007).

To quantify the pool of soluble LMW-C and LMW-C incorporation in MB, we lyophilized extracts of chloroform fumigated and non-fumigated subsamples using a FreeZone 6 Liter console freeze dry system (Labcono, Kansas City, MO). We analyzed lyophilized subsamples for %C and $\delta^{13}C$ with a Carlo Erba NA 1500 elemental analyzer (CE Instruments, Lancanshire, UK) coupled to a VG Isochrom continuous flow isotope ratio mass spectrometer (Isoprime, Inc., Manchester, UK), and applied the isotopic mixing method as described below (see *Data Analysis*).

EXTRACELLULAR ENZYME ACTIVITIES

We assayed potential activities of seven hydrolytic extracellular enzymes (pEEA) [α-Glucosidase (AG), β-Glucosidase (BG), Cellobiohydrolase (CB), and β-Xylosidase (XYL), which are involved in C-acquisition, N-acetyl glucosaminidase (NAG) and Leucine aminopeptidase (LAP), which are involved in N-acquisition, and Acid phosphatase (AP), which is involved in P-acquisition] using the 96-well microplate fluorometric method described in detail elsewhere (Bell et al., 2013; Koyama et al., 2013; Wallenstein et al., 2009). Briefly, we homogenized 0.5 g of organic soil or 1.0 g of mineral soil for 45 seconds with 91 ml of 50 mM sodium acetate buffer (pH 4.9) in a Waring blender. Soil slurries were mixed on a stir plate and 800 µl subsamples were added to a deep 96-well microplate using a wide orifice pipette tip for organic samples and a narrow orifice pipette tip for mineral samples. Substrate concentrations, soil masses, and incubation lengths were determined based on tests prior to the experiment in order to capture the maximum potential enzyme activity (V_{max}). We pipetted 200 µl of 200 µM fluorescing substrate for all substrates—except AP, where we used 200 µl of 600 µM AP—into

the sample assay wells and incubated them for three hours at 25°C. We also prepared standards for each soil slurry using a range of concentrations of 4-methylumbellifferone or 7-amino-4-methylcoumarin (LAP only). When the incubation was complete, we centrifuged plates for three minutes at 1500 rpm (~350 xg) and transferred 250 µl from each well into black 96-well plates. Substrate fluorescence was measured on a Tecan Infinite M200 microplate reader at an excitation wavelength of 365 nm and an emission wavelength of 450 nm (Tecan Trading AG, Switzerland). Data are presented as nmol g dry soil^{-1} hour^{-1}.

DATA ANALYSIS

We applied a two-source mixing model (Post, 2002) to assess the relative contribution of native SOM C *versus* LMW-C to the C pool of interest (i.e., respired CO_2, microbial biomass C, or bulk soil C), as follows:

$$f_{LMW\text{-}C} = (\delta_A - \delta_C) / (\delta_{LMW\text{-}C} - \delta_C),$$

where $f_{LMW\text{-}C}$ is the fraction of the C pool derived from ^{13}C-glucose; δ_A and δ_C are the $\delta^{13}C$ values of the C pool sampled from LMW-C amended and control collars, respectively; and $\delta_{LMW\text{-}C}$ is the $\delta^{13}C$ of the 10 atom% glucose substrate. We calculated the fraction of the C pool derived from SOM as the difference between total and LMW-C-derived C pool. We defined the priming effect as a significant increase in SOM-derived respiration resulting from the input of LMW-C, and calculated it as the difference between treatment and control collar SOM-derived respiration (Kuzyakov, 2010). We defined microbial substrate use efficiency (SUE) as the partitioning of LMW-C between growth and respiration (Manzoni et al., 2012):

$$SUE = {}^{13}MB / ({}^{13}MB + {}^{13}CO_2),$$

where ^{13}MB represents LMW-C assimilated in microbial biomass (g C m^{-2}), and $^{13}CO_2$ represents the fraction of LMW-C converted to CO_2 (g C m^{-2}). Similarly, we define substrate retention efficiency as the partitioning of LMW-C between bulk soils and respiration:

$$\text{Retention Efficiency} = {}^{13}C_{\text{Bulk Soil}} / ({}^{13}C_{\text{Bulk Soil}} + {}^{13}CO_2),$$

We performed all statistical analyses using R version 3.3.1. When necessary, we applied transformations to meet the assumptions of normality, evaluated with Shapiro-Wilk tests and Q-Q plots. We used linear mixed-effect models to identify the main effects of vegetation type, LMW-C amendment, and season, and all 2-way and 3-way interactions on our dependent variable of interest using the lme4 package (Bates et al., 2016). Similarly, we tested for main effects of depth, vegetation type, and treatment, conditional on season (SI Table 2.2). Vegetation type, LMW-C amendment, season, depth, and all interactions were included as categorical fixed effects, while our blocking design and block interactions were included as categorical random effects. We also examined whether amendment influenced LMW-C recovery in soil pools after 49 and 306 days of incubation as above. Due to underlying heterogeneity in soil C stocks we conducted additional analyses to confirm that our findings were robust. We include results from models where soil C is included in the linear mixed-effect model as an additive covariate (with no interactions) (SI Table 2.3) and results following normalization of all data to soil C stocks (g^{-1} soil C) (SI Table 2.4). Results from both models are consistent with values scaled to collar area

(m^{-2}). Therefore, we report all factor units in g m^{-2} for the remainder of this manuscript to correct for bulk density to 20 cm depth and allow direct comparison of coefficients between treatments.

We used AICc model selection criteria for small sample sizes (Barton, 2016) to identify factors driving the fraction of LMW-C converted to CO_2 and the proportion of LMW-C retained belowground. If two variables were highly correlated (>0.5), one variable was excluded from AICc model selection. As potential extracellular enzyme activities (pEEA) were highly collinear, we used an initial AICc model selection including all seven pEEAs against each dependent variable of interest. Finally, we built the full regression model using extractable and non-extractable pools of C and N, organic and inorganic N, microbial biomass C and N, soil temperature, and AICc-selected pEEAs. Models with the lowest AICc score were considered to have the best fit.

RESULTS

LMW-C AMENDMENT, MONTH, AND VEGETATION TYPE EFFECTS ON BIOGEOCHEMICAL PARAMETERS

In contrast to our hypothesis, we found no evidence of priming after LMW-C addition from soils underlying either vegetation type or in any month (Figure 2.2). Specifically, there was no significant main effect of treatment (LMW-C addition) or interaction (with month or vegetation) on SOM-derived CO_2 efflux (SI Table 2.5). However, SOM-derived CO_2 efflux was significantly influenced by month and was lower in September than July ($F_{2,15}$=7.94, p<0.01). Following LMW-C amendment, total CO_2 efflux (sum of LMW- and SOM- CO_2) exhibited significant interactions between vegetation type and treatment, as well as between treatment and month (SI Table 2.4). Overall, LMW-C amendment increased total CO_2 efflux by approximately 400% in *B. nana* soils and 650% in *E. vaginatum* soils relative to paired controls ($F_{2,36}$=8.36,

$p<0.001$, Table 2.1). These results were consistent when accounting for soil C heterogeneity among plots, including soil C concentrations in the model (SI Table 2.3a), and normalizing values with soil C (SI Table 2.4). Additionally, LMW-C additions had the largest effect on total CO_2 efflux in May, and were nine times higher from soils underlying *B. nana* and 14 times higher from soils underlying *E. vaginatum* relative to paired controls ($p<0.01$, Table 2.1).

MBC and pEEAs were influenced more by month than by treatment or vegetation type, and displayed no significant 2-way or 3-way interactions (Table 2.1, SI Table 2.6). MBC was significantly lower in May than July or September ($F_{2,36}=11.84$, $p<0.001$. There was a significant interaction between treatment and vegetation type for MBN ($F_{1,36}=5.90$, $p<0.05$), which was driven by higher biomass N in amended soils underlying *B. nana* in May than September. While MBC did not vary by soil depth or vegetation type in any season, MBN pools were 1.5 times higher in organic than mineral soils under both vegetation types in September ($F_{1,20}=5.46$, $p<0.05$, SI Table 2.2). BG was the only pEEA stimulated by LMW-C amendment ($F_{2,36}=8.54$, $p<0.01$), while XYL, NAG, and LAP varied significantly with season, exhibiting lower activities in May than other months (SI Table 2.6; $p<0.05$). There was a significant depth effect in July for all enzymes except NAG, and in May for all enzymes except XYL, where pEEAs were significantly higher in the organic than the mineral soil horizon. In September, we observed a significant interaction between depth and treatment, with activities of three C-cycling enzymes (BG, CB and XYL) stimulated by LMW-C amendment in the organic horizon. Activities for all other enzymes in September were significantly higher in the organic than mineral horizon.

We found a significant effect of month and LMW-C amendment on soil C pools, with no significant interactions (Table 2.1). TOC exhibited a significant three-way interaction between treatment, vegetation, and month ($F_{2,33}=4.82$, $p<0.05$), which was driven by larger extractable C

from soils underlying *B. nana* in July than May. Total soil C stocks and TOC concentrations did not vary by depth (SI Table 2.2). All three soil N pools, including soil N, TDN, and TIN exhibited significant interactions between vegetation type and month (Table 2.1). Soil N stocks were 1.2 times greater in *B. nana* soils than *E. vaginatum* soils in July, ($F_{2,33}$=4.56, p<0.05), but were not significantly different in other months. N stocks in *B. nana* soils were significantly lower in September than July (p<0.01). We observed a significant main effect of depth on soil N stocks, which were nearly twice as large in the mineral horizon relative to the organic horizon in September ($F_{1,20}$=6.44, p<0.05), and May ($F_{1,20}$=6.24, p<0.05, SI Table 2.2). Total dissolved N pools were nearly twice as large in soils underlying *B. nana* in July and May than September, and were also larger in *B. nana* than *E. vaginatum* soils during those months ($F_{2,33}$=3.79, p<0.05). TDN concentrations were 3.5 times higher in the organic than mineral soil horizons in July ($F_{1,22}$=6.86, p<0.05), but were three times higher in the mineral horizon in September ($F_{1,22}$=5.66, p<0.05) and two times higher in May ($F_{1,22}$=3.99, p<0.05) relative to the organic horizon (SI Table 2.2). TIN concentrations were twice as high in *B. nana* soils in July compared to other months, and twice as high in *E. vaginatum* soils in September compared to other months (p<0.05). We observed a significant main effect of depth on TIN concentrations only in May, when availability was twice as high in the mineral than organic soil horizons ($F_{1,20}$=4.95, p<0.05, SI Table 2.2).

VEGETATION AND MONTH EFFECTS ON THE FATE OF LMW-C

There were significant main effects of vegetation and month (no interaction) on LMW-CO2 efflux, which was 2.4 times higher from soils underlying E. vaginatum than B. nana (Figure 2.2b,c; $F_{1,18}$=17.74, $p<0.001$), and higher in May than July (Figure 2.2a,c $F_{2,18}$=3.84, $p<0.05$). There was a significant effect of vegetation on LMW-C retention efficiencies, which were 1.5 times higher in soils underlying B. nana than E. vaginatum (Figure 2.3a; $F_{1,18}$=4.63, $p<0.01$). Month significantly influenced microbial SUE, which was lowest in September ($F_{2,18}$=7.83, $p<0.01$), with no effect of vegetation type or interactions between month and vegetation type (Figure 2.3b, SI Table 2.5).

LEGACY EFFECTS OF LMW-C ADDITION

Soils amended with LMW-C in July and measured after 49 and 306 days of *in situ* incubation exhibited significant legacy effects (Figure 2.4). LMW-CO_2 losses were greater from soils underlying *E. vaginatum* than *B. nana* after 10 and 49 days of incubation (Figure 2.4a; $F_{1,34}$=11.88, $p<0.01$). Microbial SUE was highest after 10 days and negligible 49 and 306 days following amendment ($F_{2,34}$=19.80, $p<0.001$), while assimilation of LMW-C in MB did not exhibit legacy effects (Figure 2.4b). In contrast, LMW-C retention efficiencies were significantly greater 49 and 306 days following amendment than after 10 days (Figure 2.4c; $F_{2,34}$=32.78, $p<0.001$) under both vegetation types. SOM-derived respiration was not different than control systems and the priming effect was not observed during any measurement period.

THE INFLUENCE OF BIOGEOCHEMICAL VARIABLES ON LMW-C FATE

Explanatory variables controlling LMW-C conversion to CO_2, microbial SUE, and LMW-C retention in bulk soils were explored using AICc model selection (Figure 2.5). The best-fit model explaining LMW-CO_2 efflux included soil C:N, TOC:TDN, AP, soil C, and TOC

(Figure 2.5a; full AICc model score: 182.90, best-fit AICc model score: 150.54). In contrast to our expectations, TOC exerted a larger influence (greater effect on AICc score) than N status (Figure 2.5a) and exhibited an inverse relationship with LMW-CO_2 efflux ($p<0.001$). Potential AP enzyme activities (nmol g dry $soil^{-1}$ MBC^{-1}) ($p<0.05$), soil C:N ($p<0.05$), and soil C ($p<0.01$) were also negatively related with LMW-CO_2 efflux, while TOC:TDN was positively related ($p<0.05$). The best-fit model explaining microbial SUE included soil temperature and TOC:TDN (Figure 2.5b, full AICc model score: 24.51, best-fit AICc model score: -3.7), suggesting a strong seasonal influence on metabolic efficiency. As predicted, the best-fit model explaining LMW-C retention efficiencies included MBC and extractable C:N (Figure 2.5c, full AICc model score: 21.93, best-fit model score: 2.51).

DISCUSSION

Complex interactions among plants, soils, and microbes regulate soil C storage and the magnitude of the Arctic C-climate feedback. Currently, the dominant paradigm is that warming will alleviate temperature constraints on microbial activity and increase rates of decomposition and soil C loss to the atmosphere (Commane et al., 2017; Crowther et al., 2016; Mack et al., 2004; Mackelprang et al., 2011). However, our results highlight the exceptional C storage capacity of Arctic soils, and suggest shrub expansion could mitigate soil C losses to the atmosphere as the Arctic warms (Figure 2.1).

Plant traits, particularly rooting architecture and exudate production, strongly influence soil chemistry and the long-term stability of native SOM stocks (Jones et al., 2009; Zhu et al., 2016). Unlike *B. nana* shrubs, *E. vaginatum* tussocks do not form ectomycorrhizal (ECM) associations, and their soil microbial communities have been shown to become progressively N-limited throughout the growing season (McMahon and Schimel, 2017). *E. vaginatum* also

produce lower quality fine root litter with a 30% higher C:N ratio than those produced by *B. nana* (Hobbie, 1996; Sullivan et al., 2007), likely contributing to the lower N concentrations we observed in tussock relative to shrub soils. Tussock roots can extend from the soil surface to the permafrost interface (Iversen et al., 2015) and directly supply mineral soils with labile C, which is expected to stimulate microbial mining of nutrients from SOM (Chen et al., 2013) and induce a positive priming effect, as previously observed in several laboratory incubation studies (Fontaine et al., 2004; Wild et al., 2014). On the other hand, shrub expansion is predicted to shift rooting distributions upward into the organic horizon (Iversen et al., 2015), where minimal or negligible priming has been observed in laboratory studies (Fontaine et al., 2007; Wild et al., 2014). Taken together, this suggests that a shallower root distribution with shrub expansion should reduce TOC and N availability at depth. Our data, however, do not support this. Rather, we found significantly higher N concentrations, particularly in mineral soils colonized by *B. nana* shrubs, and no differences between in TOC concentration between soil horizons. Additionally, pEEAs were significantly lower in mineral relative to organic soil horizons, which could explain a lack of priming in mineral soils. Overall, greater LMW-C retention in shrub soils suggests shrub expansion may increase microbial activity and C-cycling in the priming-resistant organic horizon, and increase N availability at depth, where priming might otherwise occur.

Plant litter quality and soil chemistry control microbial SUE, which in turn regulate mechanisms of SOM formation and retention (Cotrufo et al., 2013; Dijkstra et al., 2015). We found that apparent SUE tended to be higher in soils underlying *B. nana*, resulting in significantly greater LMW-C retention, particularly after nine months of incubation. As high-quality shrub litter more closely matches microbial stoichiometry (Chen et al., 2013) shrub expansion may facilitate stabilization of microbial products within the soil matrix (Dohnalkova

et al., 2017; Schmidt et al., 2011). Although we did not observe SOM priming, the conversion of LMW-C to CO_2 was twice as high from soils underlying *E. vaginatum,* indicating activation of catabolic pathways and preferential transfer of new C sources to the atmosphere. Potential activities of BG, an extracellular enzyme involved in C-acquisition, also increased following LMW-C addition in tussock soils. While increased activities of C-targeting enzymes do not support positive priming effects associated with the nutrient mining hypothesis (Chen et al., 2013; Rousk et al., 2016), they do indicate mineralization of C-rich substrates, potentially from turnover of tussock litter. Laboratory incubation experiments have shown that the *potential* for priming exists in a wide range of soils. But these experiments often add a high substrate concentration at a single time point that do not closely mimic constant inputs of lower concentration through root exudation (Cheng *et al.*, 2003; Fontaine *et al.*, 2003; Brant *et al.*, 2006; Blagodatskaya & Kuzyakov, 2008; Pisani *et al.*, 2016). Thus, it is unclear from these experiments whether priming will be stimulated by increased C inputs in critical systems like Arctic tundra. In this first *in situ* experiment conducted in the Arctic, we did not find strong evidence of priming. However, our addition of a single, energy-rich substrate, may have been utilized by a subset of the microbial community that is not representative of the slower-growing communities typically associated with SOM priming (Fontaine and Barot, 2005) that utilize the full chemical diversity of root exudate compounds. The lack of mycorrhizal associations with *E. vaginatum* tussocks could explain the negligible priming effects we observed, as the production of oxidative enzymes by fungal communities are considered to be a rate-limiting step for SOM mineralization (Rousk et al., 2014). While shrub-colonized soils have greater fungal abundance and enzymatic potential for SOM priming, higher soil N concentrations can reduce microbial production of extracellular enzymes targeting complex organic matter (Carreiro et al.,

2000). Additionally, the co-addition of C and N has been shown to stimulate N-mineralization from SOM by up to 300% in Arctic soils (Rousk et al., 2016); if we had amended soils with a more complex substrate we may have induced a positive priming effect (Fontaine and Barot, 2005). Thus, we cannot rule out the possibility of priming as this system changes.

Our results confirm the importance of seasonal sampling in the Arctic, as interactions between season and vegetation type controlled the fate of LMW-C. When LMW-C was added to shrub soils in May, a large proportion was retained belowground. This retention may be caused by greater microbial assimilation of labile C during spring thaw, and production of microbial necromass, which contributes to relatively stable mineral associated organic matter (MAOM) and SOM formation (Averill and Waring, 2017; Cotrufo et al., 2013; Schmidt et al., 2011). In contrast, LMW-C additions in tussock soils were largely emitted back to the atmosphere as CO_2. In July, the influence of LMW-C amendments was reduced, with significantly lower LMW-CO_2 production from soils underlying both vegetation types. Greater belowground rhizosphere inputs during peak plant productivity may reduce microbial reliance upon exogenous LMW-C. In shrub soils, higher activities of N and P acquiring extracellular enzymes, indicate greater nutrient accessibility (Wallenstein et al., 2009), which can lead to more efficient microbial communities (McLaren et al., 2017) and the stabilization of microbial-derived products belowground (Dohnalkova et al., 2017; Tfaily et al., 2014). During fall senescence, C-rich plant litter is deposited at the soil surface, while roots are actively acquiring and translocating nutrients belowground (Chapin and Bloom, 1976; Iversen et al., 2015). During this period, extracellular enzyme activities were highest in soils underlying both vegetation types, perhaps indicating sufficient nutrient availability for enzyme production, litter depolymerization, and SOM decomposition (McMahon and Schimel, 2017; Wallenstein et al., 2009). While seasonal

dynamics provide important insights on short-term mechanisms controlling the fate of new C, it remains critical to determine whether these responses are transient or of sufficient duration and magnitude to influence the C-climate feedback.

Few studies have examined the longer-term fate of new C inputs in the Arctic, significantly limiting certainty surrounding the interaction of climate warming and shrub expansion on C cycling. During the initial stages of *in situ* incubation, microbial communities underlying both vegetation types respired LMW-C derived CO_2 to the atmosphere. However, less than half of the LMW-C added was respired from beneath either vegetation type, potentially as a result of efficient metabolism and SOM formation (Blagodatskaya and Kuzyakov, 2008; Cotrufo et al., 2015; Hill et al., 2008). After two months of *in situ* incubation, LMW-C incorporation in microbial biomass pools and conversion to CO_2 did not differ relative to control systems, however after ten months LMW-CO_2 efflux was significantly greater from soils underlying *E. vaginatum* relative to *B. nana*. While it is unlikely that LMW-C substrate remained untransformed within the dissolved SOM pool (Dijkstra et al., 2015; Hill et al., 2008), predation within the rhizosphere and turnover of microbial products may contribute to longer-term LMW-C derived efflux (Moore et al., 2003). More significantly, the proportion of LMW-C retained in the soil *versus* lost as CO_2 was higher in soils underlying *B. nana,* which could indicate efficient SOM stabilization via microbial assimilation of dissolved organic matter and retention of microbial byproducts (Cotrufo et al., 2015). While further work is needed to determine the long-term stability and efficiency of C transformation through metabolic pathways, our longer-term perspective provides evidence that new C inputs contribute to SOM formation, particularly in shrub-dominated soils. This effect could be strengthened as climate warming thaws permafrost

soils and exposes mineral surfaces able to stabilize microbial products (Schmidt et al., 2011; Wieder et al., 2013).

Our observations of lower CO_2 efflux and higher substrate retention in shrub-dominated soils may not be ubiquitous—as their expansion will not entirely eliminate other plant species (Elmendorf et al., 2012; Livensperger et al., 2016)—and may not persist throughout time. As the climate changes, microbial access to soil substrates and SOM stability will be regulated by the interactions between soil moisture and temperature. The years in which we conducted the *in situ* priming experiment were representative of longer-term seasonal treads, however hydrologic connectivity has been projected to increase with high-latitude warming (J. C. Rowland et al., 2010). Currently, shrubs are expanding into areas with high potential for moisture accumulation and drainage, specifically valley slopes and floodplains (Naito and Cairns, 2011). Local landscape characteristics, including the balance between thermokarst formation (Abbott and Jones, 2015) *versus* hillslope drainage (Kittler et al., 2018), will influence microbial accessibility to substrates, and the balance between SOM priming and formation. Substrate availability is positively correlated with moisture, as enhanced pore connectivity facilitates SOC transport from protected to active C pools, where it can be metabolized by microorganisms (Bailey et al., 2017). Similarly, warmer soil temperatures are associated with increased rates of SOM mineralization (Crowther et al., 2016; Hartley et al., 2008), although additional stressors may induce transient (Allison et al., 2010; Sistla et al., 2013), or even negative (Allison and Treseder, 2008) responses. Therefore, the complex interplay between soil temperature and moisture conditions, which were not exhaustively captured in this study, may alter the balance between SOM retention and priming.

In conclusion, we found that LMW-C conversion to CO_2 and retention in the soil matrix is influenced by a number of biogeochemical parameters relating primarily to nutrient availability. Specifically, soils underlying shrubs have higher soil N concentrations and greater retention of added glucose, likely a function of the stoichiometric controls on microbial SUE. In contrast, the activity of C-degrading enzymes and conversion of new LMW-C inputs to CO_2 suggests the cycling of labile C is rapid in the C-rich soils underlying *E. vaginatum.* These results support our hypothesis that soil N status and access to labile energy sources, such as root exudates, will determine the fate of new C sources in the Arctic. While large-scale CLM models predict C storage in the Arctic will decrease under warming scenarios (Crowther et al., 2016; Thornton et al., 2009; Wieder et al., 2013), our results suggest shrub expansion may mitigate turnover of new C sources. Thus, the interactions between shrubs and microbial metabolic efficiency act as critical controls on the direction and magnitude of the Arctic C-climate feedback.

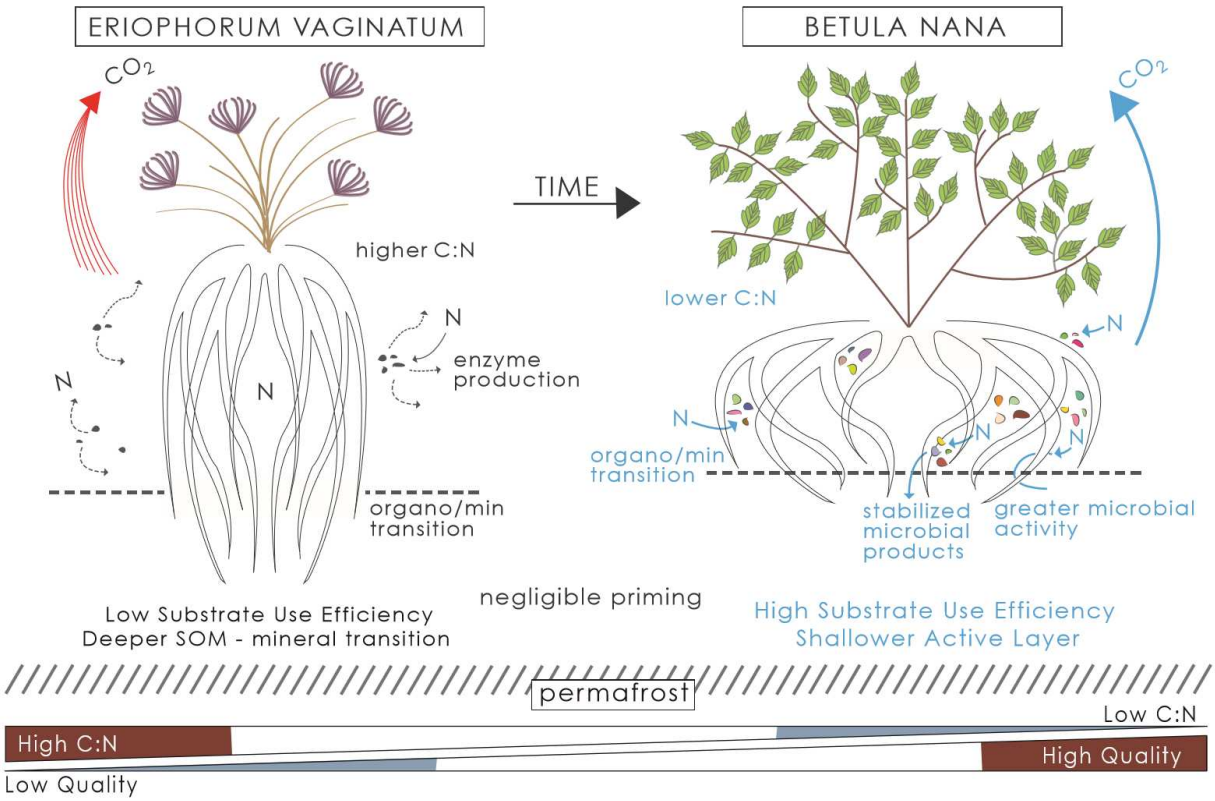

Figure 2.1. Conceptual model depicting the fate of LMW-C as influenced by vegetation type and soil chemistry. Plant traits (e.g. litter chemistry, root architecture, depth to mineral horizon) influence soil chemistry and lead to divergent microbial functions. Higher microbial substrate use efficiencies in soils underlying *B. nana* contribute to soil organic matter formation. Arrow sizes indicate the magnitude of CO_2 efflux.

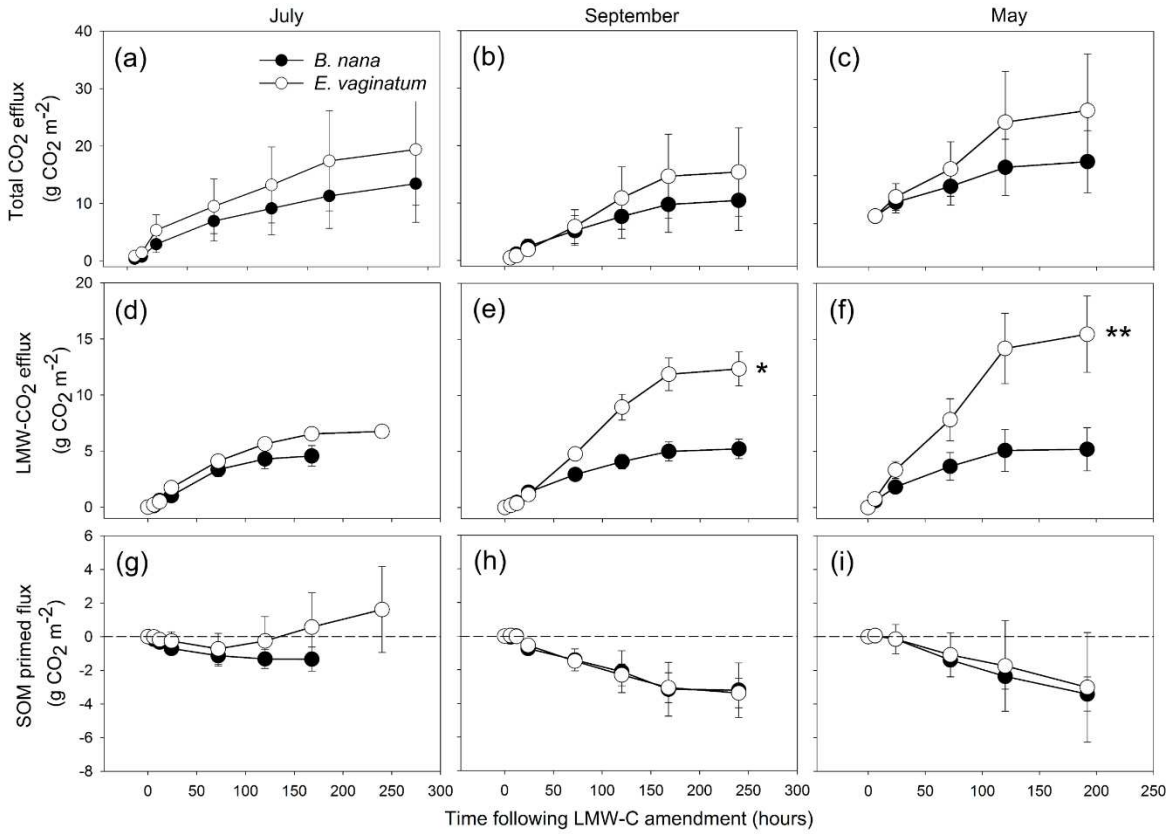

Figure 2.2. Cumulative respiration from soils underlying *B. nana* (closed symbols) and *E. vaginatum* (open symbols). Total CO_2 efflux (g m^{-2}) (upper panel) in July (a), September (b), and May (c), CO_2 efflux (g m^{-2}) derived from LMW-C (middle panel) in July (d), September (e), and May (f), and the difference between amendment and control CO_2 efflux (lower panel) in July (g), September (h), and May (i). Values below y=0 on SOM primed flux y-axis indicate negative priming (or SOM formation), while values above indicate positive priming (excess C lost as CO_2 in amended compared to control soils resulting from metabolism of native SOM stocks). Points represent means ± standard error (n=4). Significant differences between vegetation type and LMW-C treatment are reported as * $p < 0.05$, or ** $p < 0.01$.

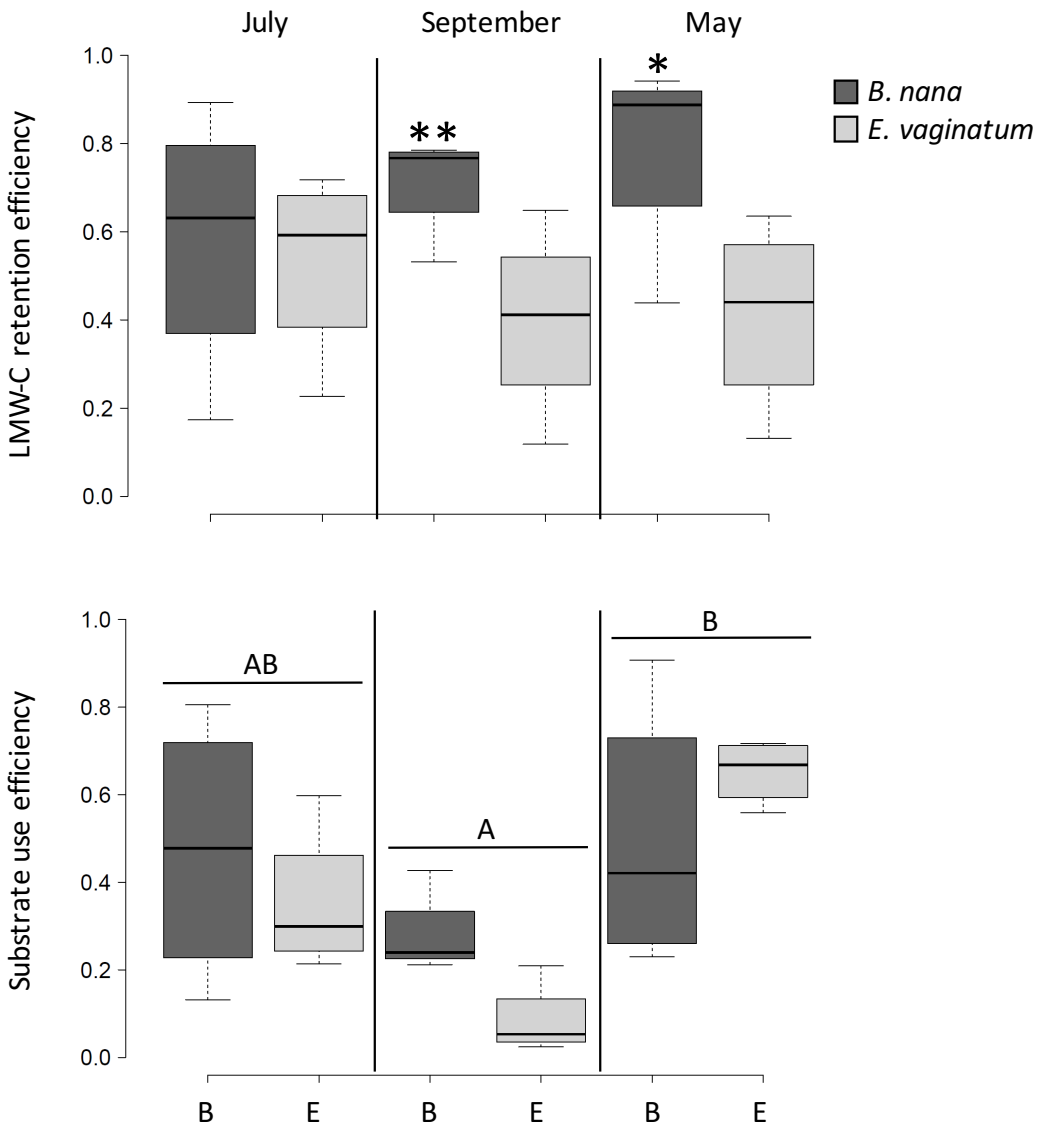

Figure 2.3. Boxplots representing LMW-C retention efficiencies (a) and substrate use efficiencies (b) by vegetation type and month for short-term (10 day) incubation periods. *B. nana* (B) are displayed in charcoal boxes, and *E. vaginatum* (E) in light gray boxes. Significant differences between vegetation type are reported as * $p < 0.05$, or ** $p < 0.01$. Significant differences between months are indicated by letters ($p<0.05$). There were no significant interactions between month and LMW-C amendment. Each box spans the interquartile range and whiskers extend to the minimum and maximum of the distribution (n=4).

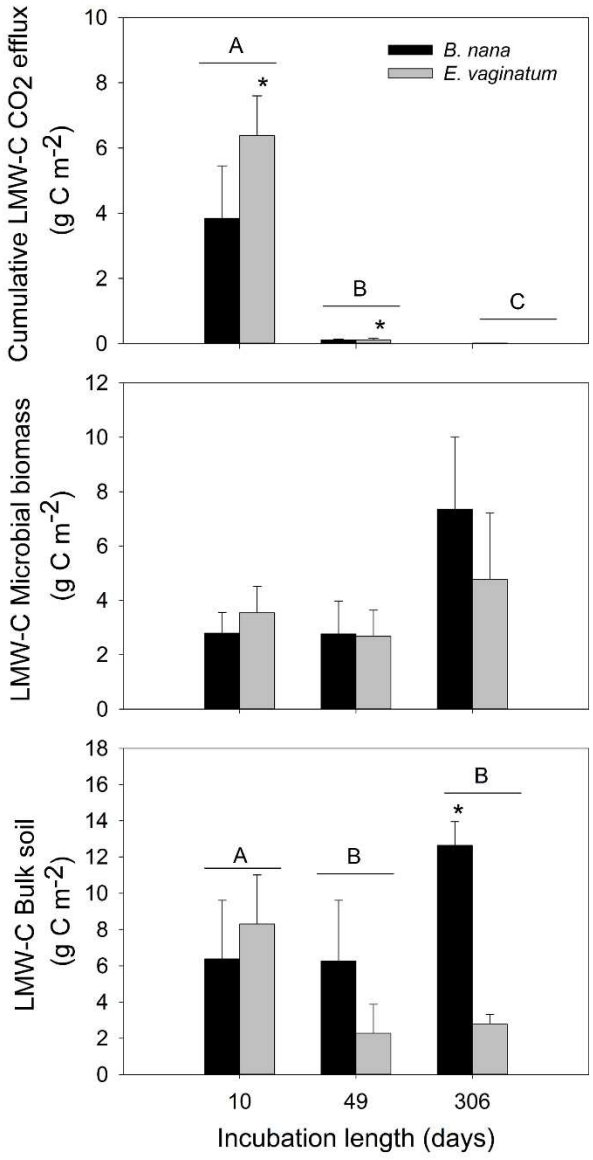

Figure 2.4. Legacy effect of LMW-C measured after 10 (short), 49 (intermediate), and 306 (long) days of *in situ* incubation. *B. nana* are shown in black and *E. vaginatum* are shown in light gray. Panels represent cumulative LMW-C derived CO_2 efflux (a), LMW-C assimilation in microbial biomass (b), and LMW-C recovery in bulk soil (c) relative to a non-amended control. Bars represent means (g ^{13}C-CO_2 m^{-2}) ± standard error (n=4). Significant differences between vegetation type are reported as * $p < 0.05$, or ** $p < 0.01$. Significant differences between months are indicated by letters ($p<0.05$). There were no interactions between month and LMW-C amendment.

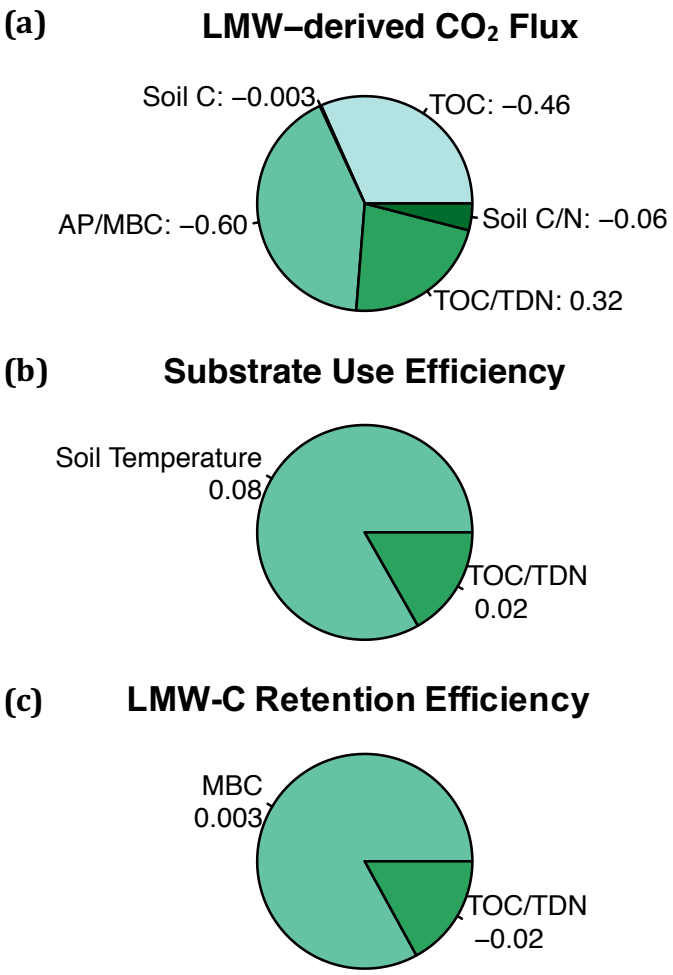

Figure 2.5. Pie charts display the coefficient strength of biogeochemical parameters included in best-fit AICc-selected models for LMW-derived CO_2 flux (a), microbial substrate use efficiency (b), and LMW-C retention efficiency (c). Selected parameters include soil and dissolved pools of C and N (Soil C, Soil N, TOC, TDN), microbial biomass C (MBC), activity of acid phosphatase relative to MBC (AP/MBC), and soil temperature at 5 cm depth (°C).

Table 2.1. Biogeochemical characteristics of soils underlying *B. nana* and *E. vaginatum*. The average followed by the standard error (± 1 S.E.) in parentheses for total CO_2 efflux, soil C and N, dissolved C and N (TOC, TDN), and microbial biomass C and N (MBC, MBN) (n=4). The level of significance from the 3-way ANOVA model including vegetation (V), treatment (T), month (M), all 2-way and 3-way interactions are reported as * $p < 0.05$, ** $p < 0.01$, *** $p < 0.001$, or non-significant (n.s.).

Month	Vegetation/ Treatment	CO_2 Flux ($g\ m^{-2}$)	Soil C ($g\ m^{-2}$)	Soil N ($g\ m^{-2}$)	TOC ($g\ m^{-2}$)	TDN ($g\ m^{-2}$)	TIN ($ug\ m^{-2}$)	MBC ($g\ C\ m^{-2}$)	MBN ($g\ N\ m^{-2}$)
July	*B. nana*								
	Control	5.70 (0.44)	2788.98 (310.12)	85.95 (7.64)	27.48 (2.40)	1.88 (0.56)	10.98 (5.91)	59.18 (13.74)	7.13 (2.04)
	Amended	12.12 (2.88)	3407.54 (223.61)	94.04 (14.46	10.87 (3.55)	1.62 (0.45)	44.62 (16.42)	51.41 (6.99)	6.02 (0.76)
	E. vaginatum								
	Control	6.93 (0.55)	2859.55 (382.04)	44.61 (9.45)	13.41 (1.35)	0.60 (0.05)	4.80 (1.90)	55.25 (11.53)	4.97 (1.17)
	Amended	19.41 (1.73)	2919.19 (287.17)	63.62 (17.54)	11.88 (1.34)	0.72 (0.14)	7.08 (1.99)	67.84 (12.35)	11.20 (3.49)
September	*B. nana*								
	Control	7.79 (1.03)	1658.17 (330.93)	21.02 (11.13)	10.09 (3.74)	0.74 (0.21)	4.34 (1.89)	44.94 (25.34)	3.07 (1.49)
	Amended	10.46 (0.49)	2551.58 (429.46)	70.46 (13.79)	8.50 (1.27)	0.75 (0.18)	4.65 (2.51)	36.81 (8.11)	4.03 (1.38)
	E. vaginatum								
	Control	5.77 (0.64)	2104.85 (385.80)	43.92 (12.37)	10.01 (1.32)	0.70 (0.11)	11.53 (5.75)	55.84 (18.25)	4.50 (1.48)
	Amended	15.41 (2.02)	3335.89 (137.46)	76.43 (5.43)	9.36 (1.78)	0.86 (0.29)	18.34 (7.68)	41.74 (6.50)	4.21 (0.68)
May	*B. nana*								
	Control	1.45 (0.23)	2002.79 (333.86)	68.05 (15.60)	28.05 (4.68)	1.45 (0.36)	10.64 (3.32)	118.18 (13.74)	9.35 (0.69)
	Amended	12.90 (2.17)	2086.96 (456.49)	71.15 (19.01)	14.48 (2.73)	1.57 (0.59)	14.75 (6.76)	111.28 (38.76)	7.96 (2.40)
	E. vaginatum								
	Control	1.66 (0.22)	1882.44 (679.71)	39.20 (12.06)	14.17 (3.71)	0.66 (0.13)	3.28 (0.87)	53.66 (17.24)	4.64 (1.66)
	Amended	23.55 (5.90)	3233.73 (306.74)	76.73 (11.75)	26.86 (4.72)	1.13 (0.11)	8.04 (2.98)	155.54 (30.50)	9.32 (1.39)
Source of variance									
T		***	**	***	*	n.s.	n.s.	n.s.	n.s.
V		**	n.s.	n.s.	n.s.	**	n.s.	n.s.	n.s.
M		***	*	n.s.	***	*	n.s.	***	**
T*V		**	n.s.	n.s.	***	n.s.	n.s.	n.s.	*
T*M		***	n.s.	n.s.	n.s.	n.s.	n.s.	n.s.	n.s.
V*M		n.s.	n.s.	*	n.s.	*	*	n.s.	n.s.
T*V*M		n.s.	n.s.	n.s.	*	n.s.	n.s.	n.s.	n.s.

REFERENCES

Barton, K., 2016. MuMIN: Multi-model inference. CRAN Repository.

Bates, D., Maechler Martin, Walker, S., 2016. Package "lme4": Linear Mixed-Effects Models. CRAN Repository 1–113. doi:10.18637/jss.v067.i01

Bell, C.W., Fricks, B.E., Rocca, J.D., Steinweg, J.M., McMahon, S.K., Wallenstein, M.D., 2013. High-throughput fluorometric measurement of potential soil extracellular enzyme activities. Journal of Visualized Experiments : JoVE. doi:10.3791/50961

Blagodatskaya, E., Kuzyakov, Y., 2008. Mechanisms of real and apparent priming effects and their dependence on soil microbial biomass and community structure: critical review. Biology and Fertility of Soils 45, 115–131. doi:10.1007/s00374-008-0334-y

Brant, J.B., Sulzman, E.W., Myrold, D.D., 2006. Microbial community utilization of added carbon substrates in response to long-term carbon input manipulation. Soil Biology and Biochemistry 38, 2219–2232. doi:10.1016/j.soilbio.2006.01.022

Bret-Harte, M.S., Shaver, G.R., Zoerner, J.P., Johnstone, J.F., Wagner, J.L., Chavez, A.S., Gunkelman, R.F., Lippert, S.C., Laundre, J.A., 2001. Developmental plasticity allows Betula nana to dominate tundra subjected to an altered environment. Ecology 82, 18–32. doi:10.1890/0012-9658(2001)082[0018:DPABNT]2.0.CO;2

Brüggemann, N., Gessler, A., Kayler, Z., Keel, S.G., Badeck, F., Barthel, M., Boeckx, P., Buchmann, N., Brugnoli, E., Esperschütz, J., Gavrichkova, O., Ghashghaie, J., Gomez-Casanovas, N., Keitel, C., Knohl, A., Kuptz, D., Palacio, S., Salmon, Y., Uchida, Y., Bahn, M., 2011. Carbon allocation and carbon isotope fluxes in the plant-soil-atmosphere continuum: A review. Biogeosciences 8, 3457–3489. doi:10.5194/bg-8-3457-2011

Buckeridge, K.M., Grogan, P., 2010. Deepened snow increases late thaw biogeochemical pulses in mesic low arctic tundra. Biogeochemistry 101, 105–121. doi:10.1007/s10533-010-9426-5

Chapin, A.F.S., Bloom, A., 1976. Phosphate absorption : Adaptation of tundra graminoids to a low temperature, low phosphorus environment. Oikos 27, 111–121. doi:10.1007/BF00258285

Chapin, F.S., Shaver, G.R., Giblin, A.E., Nadelhoffer, K.J., Laundre, J.A., 1995. Responses of Arctic tundra to experimental and observed changes in climate. Ecology 76, 694–711. doi:10.2307/1939337

Chen, R., Senbayram, M., Blagodatsky, S., Myachina, O., Dittert, K., Lin, X., Blagodatskaya, E., Kuzyakov, Y., 2013. Soil C and N availability determine the priming effect: Microbial N mining and stoichiometric decomposition theories. Global Change Biology 20, 2356–2367. doi:10.1111/gcb.12475

Cheng, W., Johnson, D.W., Fu, S., 2003. Rhizosphere effects on decomposition: Controls of plant species, phenology, and fertilization. Soil Science Society of America Journal 67, 1418–1427. doi:doi:10.2136/sssaj2003.1418

Christensen, J.H., Kumar, K.K., Aldria, E., An, S.-I., Cavalcanti, I.F. a., Castro, M. De, Dong, W., Goswami, P., Hall, A., Kanyanga, J.K., Kitoh, A., Kossin, J., Lau, N.-C., Renwick, J., Stephenson, D.B., Xie, S.-P., Zhou, T., 2013. Climate Phenomena and their relevance for future regional climate change, in: Stocker, T.F., Qin, D., Plattner, G.K., Tignor, M., Allen, S.K., Boschung, J., Nauels, A., Xia, Y., Bex, V., Midgley, P.M. (Eds.), Climate Change 2013: The Physical Science Basis. Contribution of Working Group I to the Fifth

Assessment Report of the Intergovernmental Panel on Climate Change. Cambridge University Press, Cambridge, United Kingdom and New York, NY, USA. doi:10.1017/CBO9781107415324.028

Clemmensen, K.E., Bahr, A., Ovaskainen, O., Dahlberg, A., Ekblad, A., Wallander, H., Stenlid, J., Finlay, R.D., Wardle, D.A., Lindahl, B.D., 2013. Roots and Associated Fungi Drive Long-Term Carbon Sequestration in Boreal Forest. Science 339, 1615–1618. doi:10.1126/science.1231923

Cleveland, C.C., Liptzin, D., 2007. C:N:P stoichiometry in soil: Is there a "Redfield ratio" for the microbial biomass? Biogeochemistry 85, 235–252. doi:10.1007/s10533-007-9132-0

Commane, R., Lindaas, J., Benmergui, J., Luus, K.A., Chang, R.Y.-W., Daube, B.C., Euskirchen, E.S., Henderson, J.M., Karion, A., Miller, J.B., Miller, S.M., Parazoo, N.C., Randerson, J.T., Sweeney, C., Tans, P., Thoning, K., Veraverbeke, S., Miller, C.E., Wofsy, S.C., 2017. Carbon dioxide sources from Alaska driven by increasing early winter respiration from Arctic tundra. Proceedings of the National Academy of Sciences 201618567. doi:10.1073/PNAS.1618567114

Cotrufo, M.F., Soong, J., Vandegehuchte, M.L., Nguyen, T., Denef, K., Ashley Shaw, E., Sylvain, Z.A., De Tomasel, C.M., Nielsen, U.N., Wall, D.H., 2014. Naphthalene addition to soil surfaces: A feasible method to reduce soil micro-arthropods with negligible direct effects on soil C dynamics. Applied Soil Ecology 74, 21–29. doi:10.1016/j.apsoil.2013.09.008

Cotrufo, M.F., Soong, J.L., Horton, A.J., Campbell, E.E., Haddix, M.L., Wall, D.H., Parton, W.J., 2015. Formation of soil organic matter via biochemical and physical pathways of litter mass loss. Nature Geoscience 8, 776–779. doi:10.1038/ngeo2520

Cotrufo, M.F., Wallenstein, M.D., Boot, C.M., Denef, K., Paul, E., 2013. The Microbial Efficiency-Matrix Stabilization (MEMS) framework integrates plant litter decomposition with soil organic matter stabilization: Do labile plant inputs form stable soil organic matter? Global Change Biology 19, 988–995. doi:10.1111/gcb.12113

Crowther, T., Todd-Brown, K., Rowe, C., Wieder, W., Carey, J., Machmuller, M., Snoek, L., Fang, S., Zhou, G., Allison, S., Blair, J., Bridgham, S., Burton, A., Carrillo, Y., Reich, P., Clark, J., Classen, A., Dijkstra, F., Elberling, B., Emmett, B., Estiarte, M., Frey, S., Guo, J., Harte, J., Jiang, L., Johnson, B., Kröel-Dulay, G., Larsen, K., Laudon, H., Lavallee, J., Luo, Y., Lupascu, M., Ma, L., Marhan, S., Michelsen, A., Mohan, J., Niu, S., Pendall, E., Penuelas, J., Pfeifer-Meister, L., Poll, C., Reinsch, S., Reynolds, L., Schmidth, I., Sistla, S., Sokol, N., Templer, P., Treseder, K., Welker, J., Bradford, M., 2016. Quantifying global soil C losses in response to warming. Nature 104, 104–108. doi:10.1038/nature20150

Deslippe, J.R., Simard, S.W., 2011. Below-ground carbon transfer among Betula nana may increase with warming in Arctic tundra. New Phytologist 192, 689–698. doi:10.1111/j.1469-8137.2011.03835.x

Dijkstra, P., Salpas, E., Fairbanks, D., Miller, E.B., Hagerty, S.B., van Groenigen, K.J., Hungate, B.A., Marks, J.C., Koch, G.W., Schwartz, E., 2015. High carbon use efficiency in soil microbial communities is related to balanced growth, not storage compound synthesis. Soil Biology and Biochemistry 89, 35–43. doi:10.1016/j.soilbio.2015.06.021

Dijkstra, P., Thomas, S.C., Heinrich, P.L., Koch, G.W., Schwartz, E., Hungate, B.A., 2011. Effect of temperature on metabolic activity of intact microbial communities: Evidence for altered metabolic pathway activity but not for increased maintenance respiration and reduced carbon use efficiency. Soil Biology and Biochemistry 43, 2023–2031.

doi:10.1016/j.soilbio.2011.05.018
Elmendorf, S.C., Henry, G.H.R., Hollister, R.D., Björk, R.G., Bjorkman, A.D., Callaghan, T. V., Collier, L.S., Cooper, E.J., Cornelissen, J.H.C., Day, T.A., Fosaa, A.M., Gould, W.A., Grétarsdóttir, J., Harte, J., Hermanutz, L., Hik, D.S., Hofgaard, A., Jarrad, F., Jónsdóttir, I.S., Keuper, F., Klanderud, K., Klein, J.A., Koh, S., Kudo, G., Lang, S.I., Loewen, V., May, J.L., Mercado, J., Michelsen, A., Molau, U., Myers-Smith, I.H., Oberbauer, S.F., Pieper, S., Post, E., Rixen, C., Robinson, C.H., Schmidt, N.M., Shaver, G.R., Stenström, A., Tolvanen, A., Totland, Ø., Troxler, T., Wahren, C.H., Webber, P.J., Welker, J.M., Wookey, P.A., 2012. Global assessment of experimental climate warming on tundra vegetation: Heterogeneity over space and time. Ecology Letters 15, 164–175. doi:10.1111/j.1461-0248.2011.01716.x
Ernakovich, J.G., Hopping, K.A., Berdanier, A.B., Simpson, R.T., Kachergis, E.J., Steltzer, H., Wallenstein, M.D., 2014. Predicted responses of arctic and alpine ecosystems to altered seasonality under climate change. Global Change Biology 20, 3256–3269. doi:10.1111/gcb.12568
Ernakovich, J.G., Lynch, L.M., Brewer, P.E., Calderon, F.J., Wallenstein, M.D., 2017. Redox and temperature-sensitive changes in microbial communities and soil chemistry dictate greenhouse gas loss from thawed permafrost. Biogeochemistry. doi:10.1007/s10533-017-0354-5
Fontaine, S., Bardoux, G., Abbadie, L., Mariotti, A., 2004. Carbon input to soil may decrease soil carbon content. Ecology Letters 7, 314–320. doi:10.1111/j.1461-0248.2004.00579.x
Fontaine, S., Mariotti, A., Abbadie, L., 2003. The priming effect of organic matter: a question of microbial competition? Soil Biology and Biochemistry 35, 837–843. doi:10.1016/S0038-0717(03)00123-8
Hartley, I.P., Garnett, M., Sommerkorn, M., Hopkins, D.W., Fletcher, B.J., Sloan, V.L., Phoenix, G.K., Wookey, P. a., 2012. A potential loss of carbon associated with greater plant growth in the European Arctic. Nature Climate Change 2, 875–879. doi:10.1038/nclimate1575
Hill, P.W., Farrar, J.F., Jones, D.L., 2008. Decoupling of microbial glucose uptake and mineralization in soil. Soil Biology and Biochemistry 40, 616–624. doi:10.1016/j.soilbio.2007.09.008
Hobbie, J.E., Kling, G.W. (Eds.), 2014. A Changing Arctic: Ecological Consequences for Tundra. Oxford University Press.
Hobbie, S.E., 1996. Temperature and plant species control over litter decomposition in Alaskan tundra. Ecological Monographs 66, 503–522. doi:10.2307/2963492
Hobbie, S.E., Chapin, F.S., 1998. The response of tundra plant biomass, aboveground production, nitrogen, and CO2 flux to experimental warming. Ecology 79, 1526–1544. doi:10.1890/0012-9658(1998)079[1526:TROTPB]2.0.CO;2
Hodgkins, S.B., Tfaily, M.M., McCalley, C.K., Logan, T. a, Crill, P.M., Saleska, S.R., Rich, V.I., Chanton, J.P., 2014. Changes in peat chemistry associated with permafrost thaw increase greenhouse gas production. Proceedings of the National Academy of Sciences of the United States of America 111, 5819–24. doi:10.1073/pnas.1314641111
Iversen, C.M., Sloan, V.L., Sullivan, P.F., Euskirchen, E.S., Mcguire, A.D., Norby, R.J., Walker, A.P., Warren, J.M., Wullschleger, S.D., 2015. The unseen iceberg: Plant roots in arctic tundra. New Phytologist 205, 34–58. doi:10.1111/nph.13003
Jiang, Y., Rastetter, E.B., Rocha, A. V., Pearce, A.R., Kwiatkowski, B.L., Shaver, G.R., 2015. Modeling Carbon-Nutrient interactions during the early recovery of tundra after fire.

Ecological Applications 25, 1640–1652. doi:10.1890/14-1921.1
Jones, D.L., Nguyen, C., Finlay, R.D., 2009. Carbon flow in the rhizosphere: Carbon trading at the soil-root interface. Plant and Soil 321, 5–33. doi:10.1007/s11104-009-9925-0
Kallenbach, C.M., Grandy, A., Frey, S.D., 2016. Direct evidence for microbial-derived soil organic matter formation and its ecophysiological controls. Nature Communications 7, 1–10. doi:10.1038/ncomms13630
Köhler, P., Schmitt, J., Fischer, H., 2006. On the application and interpretation of Keeling plots in paleo climate research--deciphering δ13C of atmospheric CO2 measured in ice cores. Biogeosciences 3, 539–556. doi:10.5194/bg-3-539-2006
Koyama, A., Wallenstein, M.D., Simpson, R.T., Moore, J.C., 2013. Carbon-degrading enzyme activities stimulated by increased nutrient availability in Arctic tundra soils. PLoS ONE 8, 1–12. doi:10.1371/journal.pone.0077212
Kuzyakov, Y., 2010. Priming effects: Interactions between living and dead organic matter. Soil Biology and Biochemistry 42, 1363–1371. doi:10.1016/j.soilbio.2010.04.003
Kuzyakov, Y., 2002. Review: Factors affecting rhizosphere priming effects. Journal of Plant Nutrition and Soil Science 165, 382–396. doi:10.1002/1522-2624(200208)165:4<382::AID-JPLN382>3.0.CO;2
Liljedahl, A.K., Boike, J., Daanen, R.P., Fedorov, A.N., Frost, G. V., Grosse, G., Hinzman, L.D., Iijma, Y., Jorgenson, J.C., Matveyeva, N., Necsoiu, M., Raynolds, M.K., Romanovsky, V.E., Schulla, J., Tape, K.D., Walker, D.A., Wilson, C., Yabuki, H., Zona, D., 2016. Pan-Arctic ice-wedge degradation in warming permafrost and influence on tundra hydrology. Nature Geoscience 9, 312–318. doi:10.1038/ngeo2674
Livensperger, C., Steltzer, H., Darrouzet-Nardi, A., Sullivan, P.F., Wallenstein, M.D., Weintraub, M.N., 2016. Earlier snowmelt and warming lead to earlier but not necessarily more plant growth. AoB Plants 8, 1–15. doi:10.1093/aobpla/plw021
Mack, M.C., Schuur, E.A., Bret-Harte, M.S., Shaver, G.R., Chapin III, F.S., 2004. Ecosystem carbon storage in arctic tundra reduced by long-term nutrient fertilization. Nature 431, 440–443. doi:10.1038/nature02887
Mackelprang, R., Waldrop, M.P., DeAngelis, K.M., David, M.M., Chavarria, K.L., Blazewicz, S.J., Rubin, E.M., Jansson, J.K., 2011. Metagenomic analysis of a permafrost microbial community reveals a rapid response to thaw. Nature 480, 368–71. doi:10.1038/nature10576
Manzoni, S., Taylor, P., Richter, A., Porporato, A., Ågren, G.I., 2012. Environmental and stoichiometric controls on microbial carbon-use efficiency in soils. New Phytologist 196, 79–91. doi:10.1111/j.1469-8137.2012.04225.x
Marín-Spiotta, E., Gruley, K.E., Crawford, J., Atkinson, E.E., Miesel, J.R., Greene, S., Cardona-Correa, C., Spencer, R.G.M., 2014. Paradigm shifts in soil organic matter research affect interpretations of aquatic carbon cycling: Transcending disciplinary and ecosystem boundaries. Biogeochemistry 117, 279–297. doi:10.1007/s10533-013-9949-7
Marschner, B., Brodowski, S., Dreves, A., Gleixner, G., Gude, A., Grootes, P.M., Hamer, U., Heim, A., Jandl, G., Ji, R., Kaiser, K., Kalbitz, K., Kramer, C., Leinweber, P., Rethemeyer, J., Schäffer, A., Schmidt, M.W.I., Schwark, L., Wiesenberg, G.L.B., 2008. How relevant is recalcitrance for the stabilization of organic matter in soils? Journal of Plant Nutrition and Soil Science 171, 91–110. doi:10.1002/jpln.200700049
McLaren, J.R., Buckeridge, K.M., van de Weg, M.J., Shaver, G.R., Schimel, J.P., Gough, L., 2017. Shrub encroachment in Arctic tundra: Betula nana effects on above- and belowground litter decomposition. Ecology 98, 1361–1376. doi:10.1002/ecy.1790

McMahon, S., Schimel, J.P., 2017. Shifting patterns of microbial N-metabolism across seasons in upland Alaskan tundra soils. Soil Biology and Biochemistry 105, 96–107. doi:10.1016/j.soilbio.2016.11.012
Melle, C., Wallenstein, M., Darrouzet-Nardi, A., Weintraub, M.N., 2015. Microbial activity is not always limited by nitrogen in Arctic tundra soils. Soil Biology and Biochemistry 90, 52–61. doi:10.1016/j.soilbio.2015.07.023
Miltner, A., Bombach, P., Schmidt-Brücken, B., Kästner, M., 2012. SOM genesis: Microbial biomass as a significant source. Biogeochemistry 111, 41–55. doi:10.1007/s10533-011-9658-z
Moore, J.C., McCann, K., Setälä, H., De Ruiter, P.C., 2003. Top-down is bottom-up: Does predation in the rhizosphere regulate aboveground dynamics? Ecology 84, 846–857. doi:10.1890/0012-9658(2003)084[0846:TIBDPI]2.0.CO;2
Naito, A.T., Cairns, D.M., 2011. Relationships between Arctic shrub dynamics and topographically derived hydrologic characteristics. Environmental Research Letters 6, 45506. doi:10.1088/1748-9326/6/4/045506
Natali, S.M., Schuur, E.A.G., Rubin, R.L., 2012. Increased plant productivity in Alaskan tundra as a result of experimental warming of soil and permafrost. Journal of Ecology 100, 488–498. doi:10.1111/j.1365-2745.2011.01925.x
Osterkamp, T.E., Romanovsky, V.E., 1999. Evidence for warming and thawing of discontinuous permafrost in Alaska. Permafrost and Periglacial Processes 10, 17–37. doi:10.1002/(SICI)1099-1530(199901/03)10:1<17::AID-PPP303>3.0.CO;2-4
Pisani, O., Lin, L.H., Lun, O.O.Y., Lajtha, K., Nadelhoffer, K.J., Simpson, A.J., Simpson, M.J., 2016. Long-term doubling of litter inputs accelerates soil organic matter degradation and reduces soil carbon stocks. Biogeochemistry 127, 1–14. doi:10.1007/s10533-015-0171-7
Post, D.M., 2002. Using stable isotopes to estimate trophic position: models, methods, and assumptions. Ecology 83, 703–718. doi:10.2307/3071875
Rousk, K., Michelsen, A., Rousk, J., 2016. Microbial control of soil organic matter mineralization responses to labile carbon in subarctic climate change treatments. Global Change Biology 22, 4150–4161. doi:10.1111/gcb.13296
Schimel, J.P., Bilbrough, C., Welker, J.M., 2004. Increased snow depth affects microbial activity and nitrogen mineralization in two Arctic tundra communities. Soil Biology & Biochemistry 36, 217–227. doi:10.1016/j.soilbio.2003.09.008
Schmidt, M.W.I., Torn, M.S., Abiven, S., Dittmar, T., Guggenberger, G., Janssens, I. a., Kleber, M., Kögel-Knabner, I., Lehmann, J., Manning, D. a. C., Nannipieri, P., Rasse, D.P., Weiner, S., Trumbore, S.E., 2011. Persistence of soil organic matter as an ecosystem property. Nature 478, 49–56. doi:10.1038/nature10386
Schuur, E.A.G., Bockheim, J., Canadell, J.G., Euskirchen, E., Field, C.B., Goryachkin, S. V., Hagemann, S., Kuhry, P., Lafleur, P.M., Lee, H., Mazhitova, G., Nelson, F.E., Rinke, A., Romanovsky, V.E., Shiklomanov, N., Tarnocai, C., Venevsky, S., Vogel, J.G., Zimov, S.A., 2008. Vulnerability of permafrost carbon to climate change: Implications for the global carbon cycle. BioScience 58, 701–714. doi:10.1641/B580807
Shaver, G.R., Bret-harte, M.S., Jones, M.H., Johnstone, J., Gough, L., Laundre, J.A., Chapin III, F.S., 2001. Species Composition Interacts with Fertilizer to Control Long-Term Change in Tundra Productivity. Ecology 82, 3163–3181. doi:10.1890/0012-9658(2001)082[3163:SCIWFT]2.0.CO;2
Shaver, G.R., Laundre, J.A., 2010. Arctic LTER Data Catalog [WWW Document]. Arctic LTER

Database. URL http://arc-lter.ecosystems.mbl.edu/data-catalog
Sistla, S.A., Moore, J.C., Simpson, R.T., Gough, L., Shaver, G.R., Schimel, J.P., 2013. Long-term warming restructures Arctic tundra without changing net soil carbon storage. Nature 497, 615–618. doi:10.1038/nature12129
Strickland, M.S., Wickings, K., Bradford, M.A., 2012. The fate of glucose, a low molecular weight compound of root exudates, in the belowground foodweb of forests and pastures. Soil Biology and Biochemistry 49, 23–29. doi:10.1016/j.soilbio.2012.02.001
Sturm, M., Racine, C., Tape, K., 2001. Climate change. Increasing shrub abundance in the Arctic. Nature 411, 546–547. doi:10.1038/35079180
Sullivan, P.F., Sommerkorn, M., Rueth, H.M., Nadelhoffer, K.J., Shaver, G.R., Welker, J.M., 2007. Climate and species affect fine root production with long-term fertilization in acidic tussock tundra near Toolik Lake, Alaska. Oecologia 153, 643–652. doi:10.1007/s00442-007-0753-8
Thornton, P.E., Doney, S.C., Lindsay, K., Moore, J.K., Mahowald, N., Randerson, J.T., Fung, I., Lamarque, J.F., Feddema, J.J., Lee, Y.H., 2009. Carbon-nitrogen interactions regulate climate-carbon cycle feedbacks: results from an atmosphere-ocean general circulation model. Biogeosciences 6, 2099–2120. doi:10.5194/bg-6-2099-2009
Vogel, C., Mueller, C.W., Hoschen, C., Buegger, F., Heister, K., Schulz, S., Schloter, M., Kogel-Knabner, I., 2014. Submicron structures provide preferential spots for carbon and nitrogen sequestration in soils. Nature Communications 5, 1–7. doi:10.1038/ncomms3947
Waldrop, M.P., Wickland, K.P., White Iii, R., Berhe, A.A., Harden, J.W., Romanovsky, V.E., 2010. Molecular investigations into a globally important carbon pool: permafrost-protected carbon in Alaskan soils. Global Change Biology 16, 2543–2554. doi:10.1111/j.1365-2486.2009.02141.x
Wallenstein, M.D., McMahon, S.K., Schimel, J.P., 2009. Seasonal variation in enzyme activities and temperature sensitivities in Arctic tundra soils. Global Change Biology 15, 1631–1639. doi:10.1111/j.1365-2486.2008.01819.x
Weintraub, M.N., Schimel, J.P., 2005. Seasonal protein dynamics in Alaskan arctic tundra soils. Soil Biology and Biochemistry 37, 1469–1475. doi:10.1016/j.soilbio.2005.01.005
Weintraub, M.N., Scott-Denton, L.E., Schmidt, S.K., Monson, R.K., 2007. The effects of tree rhizodeposition on soil exoenzyme activity, dissolved organic carbon, and nutrient availability in a subalpine forest ecosystem. Oecologia 154, 327–338. doi:10.1007/s00442-007-0804-1
Wieder, W.R., Bonan, G.B., Allison, S.D., 2013. Global soil carbon projections are improved by modelling microbial processes. Nature Climate Change 3, 909–912. doi:10.1038/nclimate1951
Wild, B., Schnecker, J., Alves, R.J.E., Barsukov, P., Barta, J., Capek, P., Gentsch, N., Gittel, A., Guggenberger, G., Lashchinskiy, N., Mikutta, R., 2014. Input of easily available organic C and N stimulates microbial decomposition of soil organic matter in arctic permafrost soil. Soil Biology and Biochemistry 75, 143–151. doi:10.1016/j.soilbio.2014.04.014
Zhu, Q., Iversen, C.M., Riley, W.J., Slette, I.J., Vander Stel, H.M., 2016. Root traits explain observed tundra vegetation nitrogen uptake patterns: Implications for trait-based land models. Journal of Geophysical Research: Biogeosciences 121, 3101–3112. doi:10.1002/2016JG003554

CHAPTER 3- FROM SOILS TO STREAMS: MOBILIZATION POTENTIALS OF DISSOLVED ORGANIC MATTER FLOWING THROUGH ARCTIC SOILS[2]

INTRODUCTION

Widespread permafrost thaw in high-latitude regions (Koven et al., 2009; Osterkamp and Romanovsky, 1999) is predicted to increase CO_2 release from soils to the atmosphere (Ernakovich et al., 2017; Natali et al., 2015; Schuur et al., 2009) and transform the hydrology of Arctic watersheds (Frey and McClelland, 2009; J. C. Rowland et al., 2010; White et al., 2007). While permafrost boundaries currently limit subsurface storage and control the routing of water, carbon (C), nutrients, and sediment across Arctic landscapes (J. C. Rowland et al., 2010), permafrost loss is projected to increase soil drainage and the connectivity of surface and subsurface flowpaths (Walvoord and Kurylyk, 2016), with implications for watershed biogeochemistry (Covino, 2017). Of particular interest is the fate of dissolved organic matter (DOM), which comprises the dominant and most mobile form of organic C in soil pore-waters (Jansen et al., 2014; Kalbitz et al., 2003). The vast chemical diversity of DOM shapes microbial metabolism, links terrestrial (Ernakovich et al., 2017) and aquatic environments (Battin et al., 2009b; Kellerman et al., 2014), and influences landscape C balances (Mu et al., 2017). Understanding the chemical composition and mobilization potential of DOM is thus essential in determining the proportion of newly produced and thawed soil C that is converted and released to the atmosphere as CO_2, incorporated into microbial biomass, or complexed and stabilized in the soil mineral matrix. These dynamics will influence whether Arctic catchments, which

[2] This manuscript is in preparation: Lynch, L.M., Covino, T.P., Boot, C.M., Machmuller, M.B., Cotrufo, M.F., Rithner, C., Hoyt, D., Wallentsein, M.D., 2018. From soils to streams: Mobilization potentials of dissolved organic matter flowing through Arctic soils..

currently contain nearly half of global soil organic C reservoirs, remain a globally relevant C sink.

Geophysical factors, including soil moisture and hillslope angle, vary between hillslope and riparian ecotones (Anderson et al., 2008; Kane et al., 1989; Klaus et al., 2013; Seibert et al., 2009; Weiler and McDonnell, 2006), modulating the residence time (Mu et al., 2017) and transformation potentials (Battin et al., 2009a) of DOM within a catchment. Although DOM export through mineral soils and exchange with organic horizons is limited by low permeability and hydraulic conductivity (Cooper et al., 2017; Santeford, 1978), preferential flow mechanisms, including pipe networks (Carey and Woo, 2000), water tracks (Bowden et al., 2008), desiccation and contraction cracks (Lachenbruch, 1962; Woo, 2012), and macropore flow (Weiler and McDonnell, 2006) may increase exchange between soil horizons and mass loading of DOM to recipient streams (Covino, 2017), particularly as permafrost thaws. While antecedent soil moisture conditions typically control when, and how extensively, preferential flow networks are activated (Weiler and McDonnell, 2006), there is evidence that water in saturated mineral soils can be discharged to porous organic horizons even during dry conditions and later released directly to streams during storm events (Hinton et al., 1994; Kirchner, 2003). Storm events can also reconnect isolated regions on the hillslope (Stieglitz et al., 2003), transiently connectivity hillslope-riparian ecotones and flushing significant quantities of DOM to the stream network (Bergstrom et al., 2016; Hopp and McDonnell, 2009; Jencso et al., 2010). Although permafrost-influenced soils are an important source of chemical energy to stream ecosystems, we currently lack a quantitative understanding of how DOM is cycled through hillslope environments and how the residence time of water parcels in different landscape positions influences its reactivity.

The residence time of water and DOM as it is conveyed from hillslope environments across the terrestrial-aquatic interface determines how extensively microbial communities can metabolize and alter DOM chemistry before it enters the aquatic environment (Battin et al., 2009a; Mu et al., 2017). Substrates with low physicochemical reactivity, including aromatic compounds and those with high C:N, may be utilized by microbial communities with low metabolic efficiency, resulting in catabolic release of CO_2 and CH_4 to the atmosphere (Cotrufo et al., 2013). In contrast, substrates with higher physicochemical reactivity, such as oxygen-bearing or low C:N compounds, may be preferentially incorporated into microbial biomass (Liang et al., 2017). Resulting microbial residues, including detrital proteins and lipids, promote organic matter aggregation and stabilization within the soil matrix (Koven et al., 2009). Although increasing mineral exposure could sequester DOM at the permafrost thaw front (Schmidt et al., 2011), this immobilization is likely transient, as microbial processing can desorb compounds, with a microbial fingerprint, back into the soil pore-water matrix (Kaiser and Kalbitz, 2012). Additionally, recently produced plant-materials can stimulate the turnover of mineral organic matter through priming (Fontaine et al., 2007; Wild et al., 2014), a mechanism that may compete with DOM retention and increase sequential processing. Because pore-water DOM has the potential to structure downslope metabolism and in-stream productivity, it is essential to understand how hillslope environments influence its transport and chemical transformation.

DOM is comprised of an amalgam of compounds including those recently produced plant products, microbial metabolites, and organic matter fragments that have been extensively degraded and reprocessed (Liang et al., 2017). Consequently, DOM is one of the most complex natural mixtures, and requires the adoption of higher-resolution chemical techniques to determine its structural composition (Kellerman et al., 2014; G. C. Woods et al., 2011),

transformation in pore-water environments (Ward and Cory, 2015), influence on terrestrial C balances (Roth et al., 2014). Solution state ^{1}H-NMR offers a powerful, non-targeted approach that can quantitatively classify DOM structures and metabolites (Simpson et al., 2012). Nearly 75% of DOM composition has been linked with two major structural regions: CRAMs (carboxylic-rich alicyclic materials, which are associated with ester, carboxylic acid, and ketone groups) and MDLT (materials derived from linear terpenoids, including relatively hydrophobic aliphatic-type materials) (Hertkorn et al., 2006; Gwen C. Woods et al., 2011). Additional contributions are made by conformationally larger compounds, including carbohydrates and aromatics (Woods et al., 2009). Using these chemical fingerprints to infer microbial processes and C reactivity is central to understanding the fate of DOM as it is cycled in soil pore-waters.

In this study, we used a suite of complementary approaches, including solution-state ^{1}H-NMR and fluorescence spectroscopy, to characterize the chemical composition of pore-water DOM collected from two landscape positions (hillslope, riparian) and two soil horizons (organic, mineral). We assessed the mobilization and exchange potentials of DOM flowing through organic soils *versus* along the mineral-permafrost interface using bromide, a conservative salt tracer. We hypothesized that (1) DOM is rapidly exported through porous organic relative to mineral soils, with minimal exchange between the two horizons, and (2) DOM composition converges from hillslope to riparian sites as sequential, intensive microbial anabolism homogenizes substrate chemistry. With this rationale, we tested two predictions: (1) organic and mineral soil horizons act as independent reactors, with distinct chemistries propagated downslope, and (2) DOM diversity is significantly higher in hillslope than riparian sites.

METHODS

SITE DESCRIPTION

Imnavait Creek is located in the northern foothills of the Brooks Range in Alaska, USA (68º37'N, 149º17'W) (Figure 3.1). The small headwater basin is completely underlain by permafrost and drains approximately 2 km^2. Soil substrates were deposited during the Sagavanirktok glaciation, approximately 300,000 years ago, and classified as Histic Pergelic Cryaquepts (Walker and Walker, 1996). The porous organic horizon is comprised of live and dead roots, and the mineral horizon is made of silt overlying rocky glacial till and meltwater deposits capped by thick loess and solifluction lobes (Walker and Walker, 1996). The maximum thaw depth during sampling was 60 cm.

Dry prostrate shrub and fruticose-lichen tundra dominate the hillcrest and shoulder of the Imnavait Creek watershed. The dominant hillslope species are *Eriophorum* vaginatum, a tussock-forming sedge, *Betula nana,* a dwarf birch shrub, and mosses. Near the stream channel *Sphagnum* mosses become dominant, increasing soil acidity and reducing active layer thickness (Walker and Walker, 1996). Imnavait Creek is a shallow beaded stream; ponded sections form at ice-wedge polygon intersections and are connected by short water courses (Walker and Walker, 1996). For the duration of this study—August 1 to August 23, 2016—cumulative precipitation was 58 mm, air temperature at 1 m ranged from -1.6ºC to 18ºC, average soil temperatures were 8ºC in the organic horizon (10 cm deep) and 4ºC in the mineral horizon (50 cm deep), and average *in situ* soil moistures were 32% (Toolik Lake EDC, Imnavait Creek SNOTEL Site # 968, 930 m elevation, North Slope County, 68°37'N by 149°18'W).

LYSIMETER ARRAY

Two landscape positions (hillslope and riparian) were selected to assess preferential flow pathways through organic and mineral soil horizons. On August 2, 2016, we installed three replicated nests of clustered soil pore-water samplers, hereafter referred to as lysimeters (1900L series from Soil Moisture Equipment Corp., Goleta, CA), at each landscape position, with six lysimeters per nest (n=36, Figure 3.1). Within each nest we arrayed lysimeters in pairs, with one sampler installed in the organic horizon (12 cm deep) and the second installed at the mineral-permafrost interface (approximately 50 cm deep). The mineral horizon lysimeter was installed 25 cm directly downslope from the paired organic horizon lysimeter to minimize disturbance. Two pairs of lysimeters were installed directly downslope from each other to assess primary flow pathways and the third pair was installed on a 45 degree angle to capture lateral flow (Figure 3.1).

We installed each lysimeter by digging a 10-cm diameter hole using a Dutch-style sandy soils auger, placing the lysimeter to the appropriate depth, and backfilling around the porous ceramic cup with silica flour to establish good hydraulic contact between the soil matrix and sampling cup. We finished backfilling around the PVC tube with excavated soil. To collect pore-water samples, we established a 65-centibar vacuum using a gauged vacuum hand pump (Soil Moisture Equipment Corp.) and sealed the lysimeter by folding over the Neoprene tubing and securing it with clamping rings. We extracted samples from each lysimeter using 50 ml syringe or 1 L Erlenmeyer extraction kits. Extraction lines and flasks were thoroughly rinsed six times with reverse osmosis water following collection of each sample. The location of each lysimeter was determined using a Trimble GeoXT mapping grade receiver. Spatial characteristics were extracted from LiDAR data collected by Vierling et al. (2013). Elevation was calculated using

the NAVD88 (vertical datum) and Geoid 12A. Relative topographic position was calculated as the difference between the maximum and minimum elevation at the location of each lysimeter, with a resolution of 25 cm, and aspect was measured relative to true north. Spatial characteristics are reported in Supplementary Table 3.1.

PORE-WATER CHEMISTRIES

We allowed the lysimeters to equilibrate for one week and purged them twice to eliminate any samples influenced by soil disturbance. On August 8 and 12, 2016 we collected pore-waters for detailed chemical analysis into sterile 60 ml amber borosilicate bottles, placed each bottle on ice in the field, froze them within two hours of collection, and transported them to Colorado State University for analysis (described below, Table 3.3). Dissolved organic carbon (DOC) and total dissolved nitrogen (TDN) concentrations were measured on a Shimadzu TOC-L (Shimadzu Scientific Instruments, Inc.), with detection limits of 4 ppb for DOC and 5 ppb for TDN. Inorganic nitrogen and phosphate (PO_4) concentrations were measured on an Alpkem flow solution IV automated wet chemistry system (O.I. Analytical College Station, TX), with detection limits of 0.5 mg/L for inorganic N and 0.05 mg/L for PO_4.

OPTICAL FLUROSCENCE

We used fluorescence excitation-emission matrices (EEMS) and specific UV absorbance to characterize the chromophoric and fluorescent properties of pore-water samples using an Aqualog spectrofluorometer with a xenon excitation source (Horiba-Jobin Yvone Scientific Edison, NJ). We normalized samples to 5 mg C L^{-1}, set the excitation and emission slits to a 3-nm band-pass, and incrementally increased wavelengths in 3-nm steps from 200 to 800 nm. A sealed cuvette of fluorescence-free DI water was used as a blank and analyzed between every ten samples to correct for instrument drift. Following spectral analysis, each sample was corrected

for inner-filter effects, Rayleigh scatter was masked using first and second grating orders, and the spectra were corrected by the sample blank to minimize the influence of water Raman peaks (Ward and Cory, 2015). We calculated DOC normalized specific UV absorbance at 254 nm ($SUVA_{254}$) by dividing the absorbance at 254 nm by the pathlength (m) and DOC concentration (mg C L^{-1}). Resulting $SUVA_{254}$ values, reported as L mg C^{-1} m^{-1}, are used as an indicator of aromaticity (Weishaar et al., 2003). We quantified EEMS using the fluorescence regional integration (FRI) approach as outlined by Chen et al. (2003) to identify five spectral regions (Matlab R2016b). Regions I and II are related to simple aromatic proteins (tyrosine and tryptophan-like), region III to fulvic-acid type material, region IV to soluble microbial byproduct-like material, and region V to humic acid-type organics (Chen *et al.*, 2003). The FRI approach is well suited to capturing the underlying heterogeneity and compositional quality of aromatic DOM in soil pore-waters because it quantifies regions of wavelength-dependent fluorescent intensities, rather than selecting several data points per spectra (Chen et al., 2003).

NUCLEAR MAGNETIC RESONANCE SPECTROSCOPY

We lyophilized 60 ml of frozen water collected from each lysimeter using a FreeZone 6 Liter Console Freeze Dry System (Labconco Corp. Kansas City, MO). We relativized pore-waters to the lowest C concentration (0.73 mg C L^{-1}) and re-suspended samples in a mixture of 10% deuterium (Cambridge Isotope Laboratories) and 90% HPLC-grade water (Sigma Aldrich). We transferred reconstituted samples to Wilmad 535-PP NMR tubes (Wilmad Glass, SP-Industries, Inc.) for high-precision analysis (McCay, 2009). All ^{1}H-NMR spectra were collected with a Varian Inova 500 MHz NMR spectrometer using a 1D nuclear Overhauser effect spectroscopy (NOESY) pre-saturation experiment. Each experiment was performed with an actively shielded z-gradient and a 3919 WATERGATE pulse sequence, which is favored in

solution-state NMR for suppressing the water solvent peak at 4.7 ppm (Adams et al., 2013; McCay, 2009). We acquired spectra with 32 k time domain points and 1,024 scans at 298 K, and reduced baseline distortions around the suppressed water peak using Crude and Whittaker smoothing. NMR regions were assigned the following chemical shifts: MDLT (0.6-1.6 ppm), CRAM (1.6-3.2 ppm), carbohydrates (3.2-4.5 ppm), and aromatics (6.5-8.5 ppm) (Kalbitz et al., 2003; Woods et al., 2009). NMR spectra were integrated to calculate the relative contribution of each index in describing the chemical composition of pore-water DOM (G. C. Woods et al., 2011; Woods et al., 2009).

A subset of samples were diluted by 10% (v/v) with 5 mM DSS (mM 2,2-dimethyl-2-silapentane-5-sulfonate-d6) as an internal standard at 0 ppm, and analyzed at the Pacific Northwest National Laboratory using a Varian Direct Drive 600 MHz NMR spectrometer equipped with a 5 mm triple-resonance salt-tolerant cold probe. The 1D spectra were processed using Chenomx NMR Suite 8.1 software, with peak quantification assigned relative to the DSS internal standard. Candidate metabolites were identified by matching the chemical shift, intensity information, and J-coupling to metabolite libraries available in the Chenomx library. We procured the InChI code for each annotated metabolite from PubChem and used ClassyFire to identify its chemical taxonomy (Djoumbou Feunang et al., 2016).

KBr TRACER ADDITIONS

To assess whether DOM mobilization differed between landscape position and soil horizon we used potassium bromide (KBr) as a conservative hillslope tracer. We selected KBr because of low background concentrations at our site, minimal sorption to soil minerals, and low toxicity (Davis et al., 1980). At each nest, we applied 1 L of 5 M KBr solution to the soil surface on August 12, 2016 (infiltration was instantaneous). We sampled lysimeters five and eight hours

after application (insufficient soil moisture at the hillslope site precluded extraction after eight hours), and then daily from August 13-22, 2016, for a total of fourteen samples per lysimeter at the riparian site and thirteen samples per lysimeter at the hillslope site. We measured bromide concentrations on a Dionex ICS-3000 Ion Chromatograph at the Fort Collins Biogeochemistry Laboratory, CO (U.S. Forest Service), with a detection limit of 0.01 mg/L. We calculated bromide recovery by integrating under the breakthrough curve (BTC) and transforming the tracer BTC to a cumulative distribution using the following equation:

$$\text{Bromide recovery} = \int_0^t \mathrm{T_c}(t)dt,$$

where T_c is the background-corrected bromide concentration. We then scaled the cumulative distribution from 0 – 1 by dividing by each value in the cumulative distribution by total solute recovery. We calculated the arrival (5% recovery), and median (50% recovery) transit times for the intercepted solute at each lysimeter (Runkel, 2015). We calculated modal velocity as the time to reach peak tracer concentration divided by the distance of each lysimeter from the KBr application site.

STATISTICAL ANALYSIS

We used linear mixed-effects models to test the effect of landscape position (hillslope *versus* riparian) and soil layer (organic *versus* mineral) on DOM properties using the lme4 package (Bates et al., 2016) in R version 3.3.1. Landscape position, soil layer, and their interaction were included as categorical fixed effects, and the blocked nest design was included as a categorical random effect. Data were log transformed when necessary to meet assumptions of normality, evaluated with Shapiro-Wilk tests. Model residuals were visually inspected for constant and homogenous variance using Q-Q and residual *versus* fitted plots and formally tested

with normal and studentized Breusch-Pagan tests and non-constant variance scores. We summarized our model output using the lsmeans package, which provides pairwise comparisons among least-squares means and Tukey's HSD adjusted p-values (Lenth, 2016). We assessed bromide transit time distributions using repeat measures ANOVA, where landscape position, soil layer, distance of each lysimeter from the bromide application site, and time were included as categorical fixed effects, and the blocked nest design and lysimeter were included as categorical random effects.

We identified relationships between our dependent variable of interest (bromide transit time distributions, pore-water chemistry, EEMS regions, NMR indices) and potential predictor spatial variables using multiple linear regression analysis. We identified highly correlated variables using Pearson correlation plots (Supplemental Figure 3.1) and calculated variation inflation factors (VIF) for each parameter in the model using the *vif* function in the R *car* package (Fox and Monette, 1992). We assigned a VIF cutoff value of two (Zuur et al., 2010) and sequentially removed variables until only independent predictor variables remained (Duffy et al., 2016). Potential variables for the initial regression analysis included surface roughness, slope angle, aspect, distance from Imnavait creek, and bulk density. Stepwise multiple linear regressions were conducted following Sutfin and Wohl (2017) using the *step* function in the R *stats* package. We normalized TDN, PO_4, and EEMS regions IV and V using boxcox power transformations in the R *MASS* package and verified assumptions of normality and constant and homogenous variance as above.

We used MetaboAnalyst 3.0 (Xia and Wishart, 2016) to process and analyze NMR metabolites (following removal of the solvent peak at a shift of 4.5-5.0 ppm). We sum-normalized and z-transformed variables and removed non-informative spectral regions using

interquartile range filtering, a recommended data pre-treatment step for untargeted metabolomics datasets (Hackstadt and Hess, 2009). We determined whether samples clustered by categorical factors (landscape position or soil horizon), using Partial Least Squares–Discriminant Analysis (PLS–DA), a method commonly applied to chemometric datasets (Grootveld, 2014), using the *plsr* function in the R *pls* package (Wehrens and Mevik, 2007). We explored relationships between the distribution and intensity of our metabolites and hypothetical classification system (landscape position or soil horizon) using random forest classification and B/W permutation tests, and assessed the performance of each generated model with 10-fold cross validation methods. For each model, we generated 2,000 permutations to test whether our hypothetical classification systems were significantly better than those arising through random chance (Grootveld, 2014).

RESULTS

INFLUENCE OF LANDSCAPE POSITION AND SOIL HORIZON ON PORE-WATER CHEMISTRY

Contrary to our expectations, variation in DOC concentrations was not explained by landscape position or soil horizon (Figure 3.2). We observed significant interactions between landscape position and soil horizon for TDN and ammonium (NH_4) pools (Figure 3.2). Total dissolved N pools were 1.6 times higher in pore-waters collected at the mineral-permafrost interface than those collected from the organic horizon of the riparian corridor ($F_{1,28}$=0.58, $p<0.01$, Figure 3.2) and NH_4 concentrations were twice as high in riparian mineral soils than all others ($F_{1,28}$=1.69, $p<0.001$). Nitrate concentrations were below detection limit (<0.01 ppm) across landscape position and depth. We observed main effects of landscape position and soil horizon (no interaction) on pore-water PO_4 concentrations, which were 14% higher in overlying

organic than mineral soils ($F_{1,32}$=21.26, p<0.001) and 10% higher on the hillslope than along the riparian corridor ($F_{1,32}$=16.07, p<0.001, Figure 3.2). DOC:TDN ratios were significantly higher at the hillslope than riparian sites, suggesting N becomes more available as DOM cycles downslope ($F_{1,28}$=6.26, p=0.02). We also observed higher TDN:PO_4 at the hillslope sites, suggesting PO_4 concentrations are higher in the wetter riparian zone ($F_{1,28}$=4.26, p<0.05).

Optical fluorescence characteristics were not influenced by landscape position, but differed significantly between soil horizons, suggesting exchange between organic and mineral compartments is limited (Table 3.1). The relative percent intensities for EEMS regions II and IV, related to simple aromatics and soluble microbial-type proteins, were 12% and 6% higher in pore-waters collected at the permafrost-mineral interface than those collected in the upper organic horizon ($F_{1,28}$=37.25, p<0.001, and $F_{1,28}$=21.12, p<0.001, respectively). In contrast, regions III and V, related to plant-derived compounds, exhibited 25% and 8% higher relative fluorescence intensities in the organic than the mineral horizon ($F_{1,28}$=15.10, p<0.001, $F_{1,32}$=18.94, p<0.001, respectively). Regressing region IV against region V revealed a strongly negative relationship (adjusted r^2 = 0.54), providing supporting evidence that microbial-derived products are enriched at depth (Supplemental Figure 3.2). We also observed a significant interaction between landscape position and soil horizon on DOM aromaticity, with significantly higher $SUVA_{254}$ values observed in mineral than organic soil horizons of hillslope sites ($F_{1,28}$=0.14, p<0.01). Pore-waters collected from the mineral horizon clustered apart from those collected from the organic horizon (Figure 3.3), with separation driven in the positive direction by EEMS region II and bulk density, and in the negative direction by PO_4.

METABOLITE CHARACTERIZATION

We observed significant structural variability in the pore-water chemistries collected from hillslope and riparian landscapes as well as from organic and mineral soil horizons (Figure 3.4). Together, the first two PLS-DA components explained 35% of the variance, with maximal classification performance achieved with five components (r^2=0.87; CV accuracy=0.61). The overall random forest OOB error was 0.56, with the best classification achieved for riparian organic pore-waters (0.33). Classification error was highest (0.78) for hillslope mineral soils, which were comprised of a core set of metabolites common across the landscape.

Aromatic and MDLT components, which are indicative of microbial-derived aliphatic chains, were 8% and 6% higher in organic soil horizons than at the mineral-permafrost interface ($p<0.01$). We observed a significant interaction between landscape position and soil horizon on CRAMs signals, which were enriched along the permafrost interface of the riparian zone and are typically associated with highly processed, refractory compounds (Hertkorn et al., 2006). Carbohydrate signals accounted for only 8% of all spectral features and were marginally higher at hillslope sites ($p=0.08$). Formate, a derivative of C3 plants, and acetate were consistently the most abundant metabolites, with higher concentrations in hillslope soils. Fermentation byproducts, including methanol, isopropanol, and lactate were also present, and enriched in mineral soils. Several fatty acids, including suberate, butyrate, and isovalerate, were present in relatively low concentrations (<22 umol) across sites and indicative of microbial metabolism. As metabolite diversity was typically higher in riparian than hillslope ecotones, we have evidence supporting our first hypothesis

ENVIRONMENTAL DRIVERS OF DOM MOBILIZATION

We observed a significant interaction between soil horizon and sampling time ($F_{2,48}$=1.94, p<0.05) on bromide transit distributions, such that solutes flowed more quickly through organic than mineral horizons. These results were supported by the modal velocities, which were five times faster in organic than mineral soils ($F_{1,28}$=7.98, p<0.01). Thus, for DOM to travel a distance of one meter, would require approximately five days through organic soils and nine days through mineral soils. Together, landscape position and soil bulk density explained 23% of the variability in bromide arrival time (p=0.02), while slope angle, site aspect, and soil bulk density explained the median arrival of bromide (adjusted r^2=0.32, p<0.01). These spatial variables reduced the best-fit AIC model scores by 3.2 and 12, relative to the null models. Our results suggest that solute pulses may be rapidly exported through the organic horizon, but transport through the mineral compartments is considerably slower. Additionally, we observed the most rapid solute velocities at lysimeters installed nearest the application site ($F_{2,20}$=0.46, p<0.05), but solute velocities were similar one meter away, regardless of whether they were installed directly downslope from the application site, or on a 45º angle. This observation highlights the potential for lateral flow across Arctic hillslopes. We observed no difference in the total volume of pore-water collected from across different landscape positions or soil horizons.

DISCUSSION

Rapid warming in high-latitude regions is expected to thaw permafrost and mobilize pore-water DOM through deep flowpaths. The results of this study advance our understanding of how the transport and transformation of DOM determines its fate. Linking hillslope connectivity with DOM chemistry provides unique insight in to pore-water cycling and is critical in understanding the interactive metabolism of terrestrial and aquatic environments. We found that

compounds mobilized through the porous organic horizon were associated with plant-derived molecules, while those flowing through mineral soils had a microbial fingerprint. Landscape position also influenced the structural diversity of DOM, which increased during downslope transport from hillslope to riparian soils. While the chemical composition of DOM varied across the landscape, the potential for rapid lateral flow across Arctic hillslopes and along the mineral-permafrost interface was uniformly high, suggesting DOM mobilization is an important mechanism of C loss from Arctic soils.

DOM composition was strongly related to soil horizon. We observed the highest relative fluorescent intensities of fulvic and humic type acids, which are typically associated with plant-derived compounds, in pore-waters collected from the organic horizon. During microbial decomposition, plant-derived molecules are broken into smaller compounds, increasing the relative proportion of polar and ionizable groups (Lehmann and Kleber, 2015). Resulting fragments are more soluble in water and can be preferentially leached from organic to mineral soil horizons (Zhang et al., 2017). The soil profile may thus act as a dynamic chromatograph (Kaiser and Kalbitz, 2012), where compounds are selectively retained or leached depending on their solubility, association with the soil mineral matrix, and chemical reactivity (Lehmann and Kleber, 2015). Across landscape position, we observed selective retention of MDLT compounds—hydrophobic, aliphatic species (Woods, 2012)—in the organic horizon, as well as high concentrations of chromophoric DOM ($SUVA_{254}$) at depth, suggesting these exchange mechanisms fractionate the chemical composition of DOM across the soil profile (Zhang et al., 2017).

The reactivity of organic matter typically increases with fragmentation, and could result in physicochemical complexation with soil minerals (Lehmann and Kleber, 2015). Chemical

stabilization has been proposed as a mechanism of DOM retention in the Arctic (Schmidt et al., 2011), however, isotherm studies suggest DOC adsorbs to mineral surfaces as a monolayer, which could preclude substantial DOM removal from C-rich soils (Mayer, 1994). As we observed similar DOC concentrations exported through mineral and organic soil horizons, large DOM pools appear to be mobile at depth and may be the result of continual DOM sorption and dissolution from the mineral matrix (Kaiser and Kalbitz, 2012). Therefore, the chemical signature of DOM leaching from surface to deep horizons and flowing along the permafrost-interface may reflect sequential and intensive microbial processing during export (Liang et al., 2017; Zhang et al., 2017). We observed significantly higher concentrations of hydrophobic, aliphatic-rich MDLT compounds in the organic horizon and high concentrations of chromophoric DOM ($SUVA_{254}$) in pore-waters at the permafrost-mineral interface. Leaching of DOM from rhizosphere organic soils to permafrost-influenced mineral soils is likely an important mechanism of organic matter translocation (Zhang 2017) with the potential to stimulate deep-horizon catabolism (Fontaine et al., 2007). We therefore reject our original hypothesis that organic and mineral horizons act as independent reactors due to differences in permeability and hydraulic conductivity Rather, our data suggest organic soils continually supply surface matter to deep flowpaths, which contribute to transient subsurface storage or export across the terrestrial-aquatic interface.

Pore-waters collected at the mineral-permafrost interface had the highest and most variable relative fluorescent intensities of simple aromatic proteins and soluble microbial byproducts (Chen et al., 2003). Although we observed higher $SUVA_{254}$ values at depth ^{1}H-NMR shift regions associated with aromatics (6.5-7.8 ppm), including lignin and protein side-chains (Pautler et al., 2010), were lower in deep mineral than organic soils. This observation highlights

the need for careful interpretation of EEMS and SUVA indices, which resolve only the chromophoric fraction of DOM (cDOM) (Spencer et al., 2015; Zhang et al., 2017). The most abundant metabolites collected at the permafrost-mineral interface were nonchromophoric compounds, including formate and fumarate—carboxylic acids associated with microbial degradation of aromatic compounds—and xanthine, a purine-derived metabolite associated with secondary plant metabolism (Djoumbou Feunang et al., 2016). We also observed higher ammonium concentrations in permafrost-influenced pore-waters, suggesting turnover of deep organic matter (Ward and Cory, 2015) could increase N availability at depth, amplifying the direct effects of warming on microbial activity (Schmidt et al., 2011). Together our results suggest warming-induced thaw at the permafrost-mineral interface will increase the fraction of cDOM and N-rich microbial products released to the fluvial network.

Landscape characteristics, including topography and topology, are often modeled as first order controls on runoff characteristics and hillslope-riparian connectivity and appear to control DOM chemodiversity at our sites (Jencso et al., 2010). However, the distribution of metabolite diversity was opposite of our prediction, with higher diversity observed in riparian than hillslope sites. While the structural chemistry of hillslope soils was relatively homogenous, carbohydrate concentrations were slightly elevated in the upper soil profile. Hillslope soils are colonized by productive dwarf shrub and tussock-forming sedge communities. The assimilation of carbohydrates and other labile plant-derived compounds into microbial biomass (Ernakovich et al., 2017) could result in the chemical convergence we observed at the hillslope sites (Liang et al., 2017). Recent evidence suggests widespread shrub expansion, a result of high-latitude warming (Sturm et al., 2001), will shift rooting distributions (Iversen et al., 2015), and deposition of labile root exudates (Zhu et al., 2016), upward into surface organic horizons, which are less

vulnerable to priming than energy depleted mineral soils (Fontaine et al., 2007; Wild et al., 2014). If microbial communities utilize newly deposited organic matter with high efficiency, warming could lessen organic matter conversion to CO_2 or CH_4, leading either to DOM stabilization in the soil matrix (Schmidt et al., 2011) or mass loading to the fluvial network (Covino, 2017).

Pore-waters collected from riparian soils exhibited higher chemodiversity than those collected from hillslope soils. This downslope divergence in DOM composition could be related to sequential catabolism during transport (Liang et al., 2017; Mu et al., 2017) or to the accumulation of compounds in a less favorable, or spatially heterogeneous, redox environment. Large aromatic contributions, linked with microbial-derived protein side chains, suggest higher microbial activity occurs in the organic horizon of riparian soils (Pautler et al., 2010). We also observed an increasing abundance of CRAM—carboxyl rich alicyclic materials (Woods, 2012)—in riparian mineral soils, which are associated with refractory, microbial-derived products (Zhang et al., 2017). CRAM compounds are the most abundant chemical class comprising deep ocean DOM (Hertkorn et al., 2006) and could represent a direct link between terrestrial source and oceanic sink. We also observed a significant decrease in pore-water C:N, suggesting DOM pools acquire an increasingly microbial signature during downslope export independent of soil horizon. Greater DOM diversity in riparian soils could also be due to diverse microbial communities exploiting multiple redox niches (Ernakovich and Wallenstein, 2015; Vos et al., 2013). Spatial heterogeneity of redox gradients have been linked to the activation of metabolic pathways utilizing alternate terminal electron acceptors to degrade DOM (Boye et al., 2017; Danczak et al., 2016), including siderophores and other chelating agents that are abundant in low-lying Arctic environments (Lipson et al., 2012). We consistently observed high

concentrations of metabolites associated with fermentation pathways (including acetate, formate, acetyl phosphate, and methanol) in riparian soils. These metabolites were far less abundant or absent in organic hillslope soils. The combination of variable redox gradients and siderophore availability could contribute to organic matter catabolism in riparian soils. While highly processed DOM is expected to be a poor energy substrate (Marín-Spiotta et al., 2014), there is evidence these compounds have high biological and photochemical lability (Vonk et al., 2013) in lakes (Gwen C. Woods et al., 2011) and rivers (Spencer et al., 2015).

The release of pore-water DOM across the terrestrial-aquatic interface is related to the connectivity of hillslope flowpaths (Ameli et al., 2016; Tetzlaff et al., 2015) and seasonal variability in subsurface storage capacities (Koch et al., 2013). While DOM transport through mineral-dominated soils is considered limited by low permeability, we observed no difference in solute traveltime velocities between soil horizons and landscape position, even late in the growing season. Additionally, total intercepted pore-water volumes did not vary spatially, suggesting preferential flow through deep soil horizons may limit Arctic DOM storage (Carey and Woo, 2000; Koch et al., 2013). While solute departure times were not explained by measured hillslope characteristics, bulk density, which exerts a control on lateral flow as a result of its depth-variable resistance properties (Quinton et al., 2000), was a significant predictor for arrival and median travel times. Reductions in soil volume with ground ice loss (Plug and West, 2009) could impede subsurface transmissivity in the future, but does not currently appear to limit flows. Previous work at Imnavait Creek has shown that small stormflow events are sufficient to re-establish flowpath connectivity across hillslopes (Kane et al., 1989). As increasing precipitation is projected for Arctic terrestrial ecosystems (Hinzman et al., 2005; Peterson et al., 2002), hillslope connectivity may become an increasingly important mechanism of DOM export.

Together, our results suggest high C-storage capacities of Arctic soils are balanced by the potential for rapid DOM mobilization across the terrestrial-aquatic interface. While the chromatographic influence of surface soils and flowpath connectivity will determine the persistence and movement of terrestrial-derived organic matter across the landscape, the chemical composition of mobilized DOM will structure microbial metabolism throughout terrestrial and fluvial networks. Our work highlights the need to integrate landscape and spatial characteristics into a framework of C transport in Arctic watersheds.

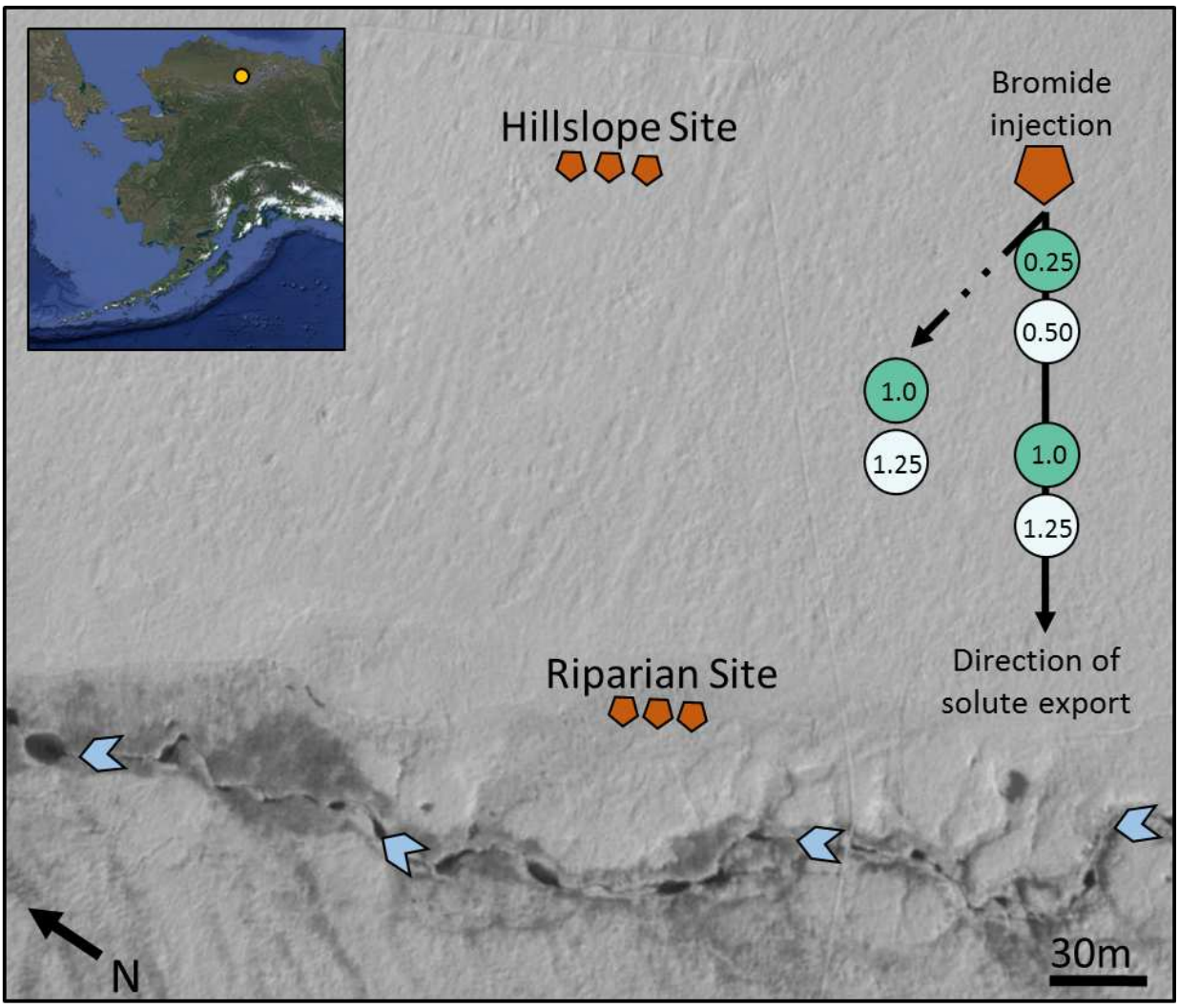

Figure 3.1. Site map, with flow direction of Imnavait Creek shown by blue arrows, and location in northern Alaska by yellow marker in inset map. Bromide was applied in three areas (brown pentagons) at two landscape positions (hillslope and riparian) to trace preferential flow paths and exchange potentials between organic and mineral soil horizons. Six lysimeters below each application zone (detailed schematic shown on right) captured bromide movement in the organic (dark circles) and mineral (light circles) soil horizons. Values in each circle represent the distance from bromide application.

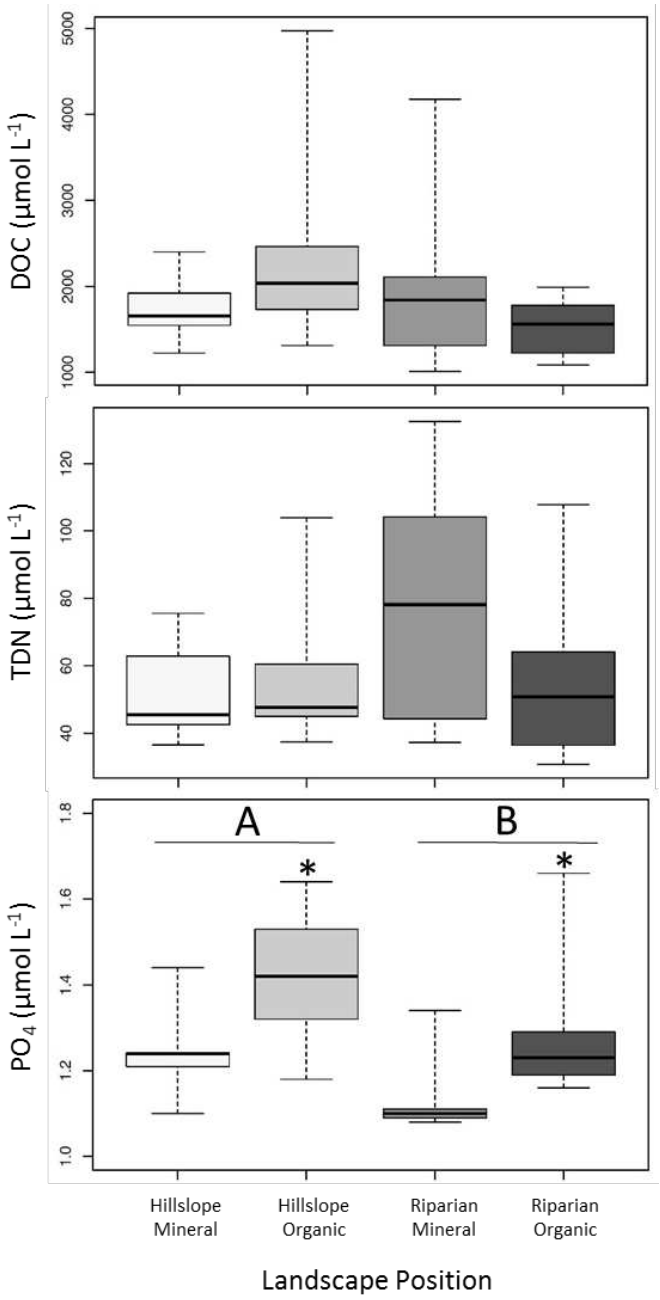

Figure 3.2. Boxplot panels display pore water dissolved organic carbon (DOC), total dissolved nitrogen (TDN), and phosphate (PO_4) concentrations collected from organic and mineral soil horizons in the hillslope or riparian area. Each box spans the interquartile range and whiskers extend the entire data range (n=9). Significant differences between landscape position (hillslope and riparian) are indicated by letters ($p<0.05$), and significant differences between soil horizons are reported as * ($p<0.05$). There was a significant interaction between site and soil horizon for TDN pools.

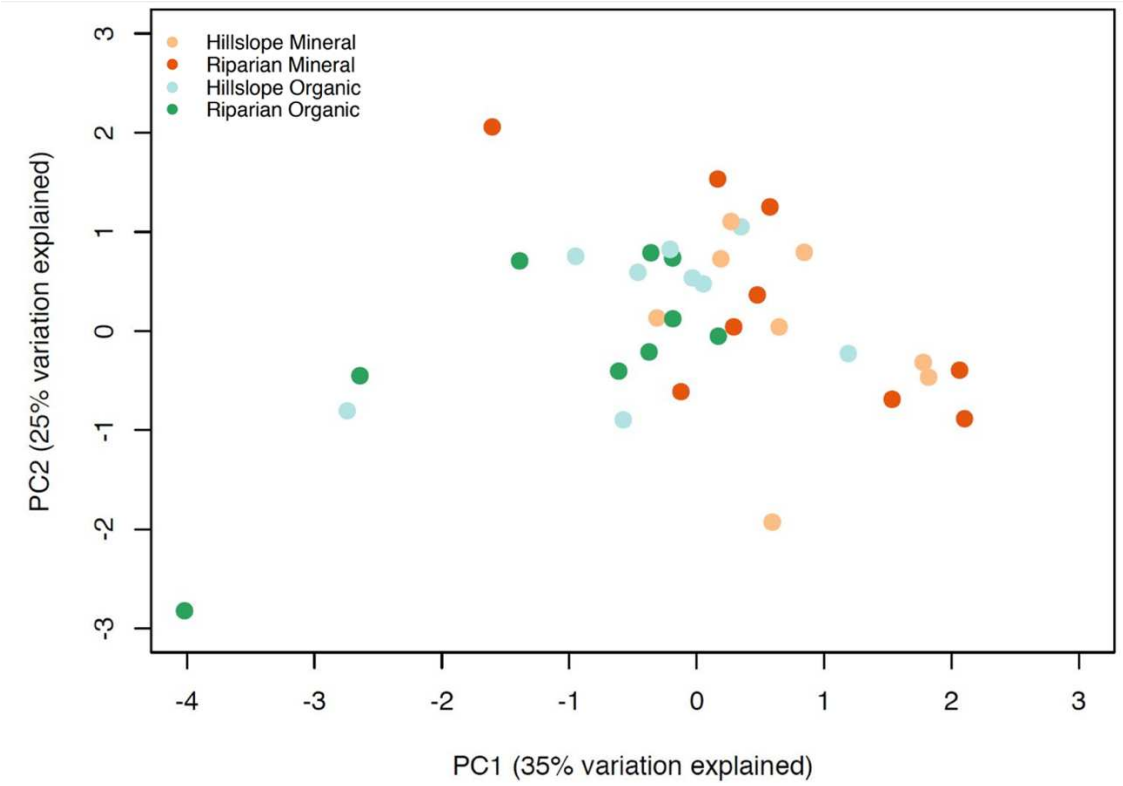

Figure 3.3. Two-dimensional PCA ordination showing the segregation of pore waters collected from mineral (red-hued) or organic (green-hued) soil layers at hillslope (circle) or riparian (square) location. Individual data points are replicates (n=9). Sample separation along PC1 is driven by EEMS region IV (soluble microbial-type proteins) in the negative direction and phosphate availability in the positive direction; separation along PC2 is driven by C and ammonium pools in the negative direction and EEMS region 1 (fulvic-type acids) in the positive direction.

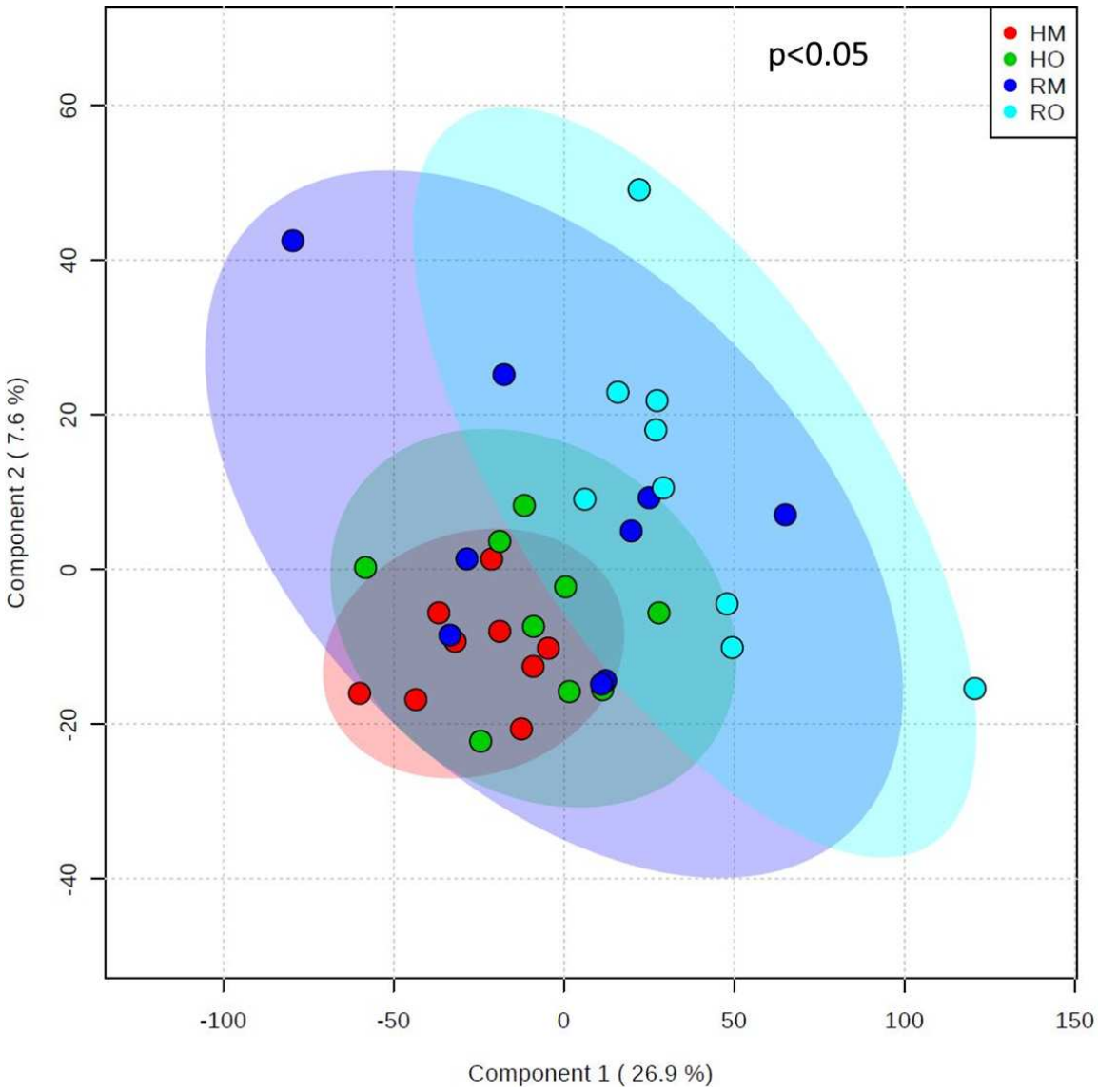

Figure 3.4. PLS-DA plot of metabolites clustered by landscape position (H: hillslope, R: riparian) and soil horizon (M: mineral, O: organic). Each circle represents a sample and shaded ellipses represent 95% confidence intervals for each *a-priori* cluster. Ellipse overlap signifies no significant difference between clusters. 2,000 permutations were generated to test whether our classification systems (landscape position and soil horizon) were significantly better than those arising through random chance.

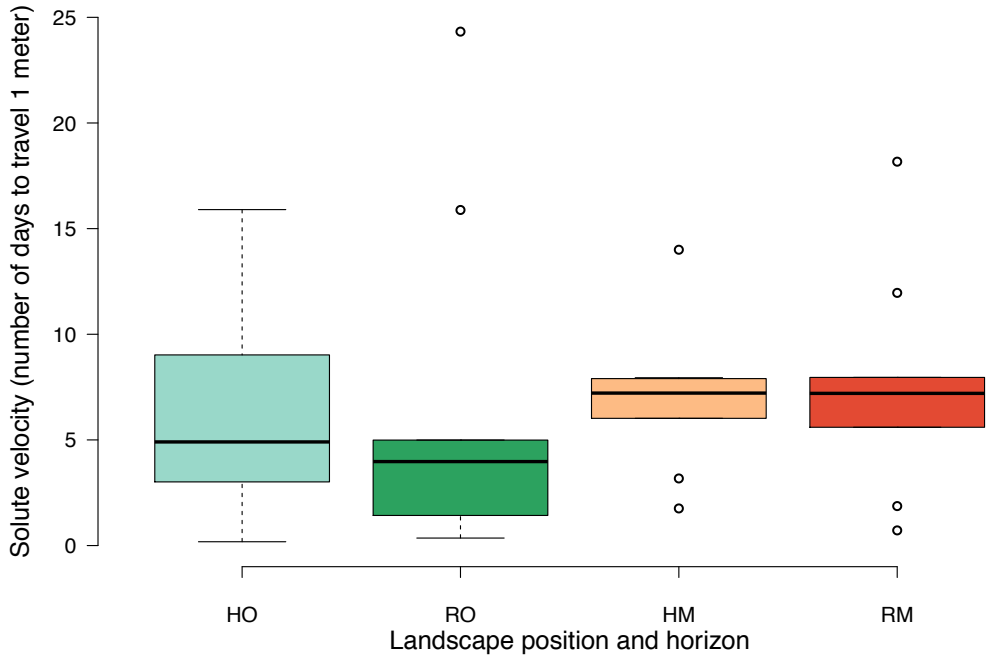

Figure 3.5. Solute velocity as a function of time after bromide addition, from organic (green) or mineral (red) soil horizons located in the hillslope (H) or riparian (R) location. Solute velocities were significantly faster through organic than mineral soil layers ($p<0.01$), with no differences between hillslope and riparian sites ($p=0.43$). Each box spans the interquartile range and whiskers extend to the minimum and maximum of the distribution ($n=4$).

Table 3.1. Biogeochemical characteristics of soil pore water samples collected from hillslope or riparian sites. At each site, samples were collected from either the organic horizon or along the mineral-permafrost interface. Values are the average followed by the standard error in parentheses below, for: MDLT, material derived from linear terpenoids (0.6-1.6 ppm); CRAM, carboxylic-rich alicyclic material (1.6-3.2 ppm); CARB, carbohydrates (3.2-4.5 ppm); AROM, aromatics (6.5-8.5 ppm); regions I-V are related to EEMS indices described in *Figure 3.3*; SUVA, DOC normalized specific UV absorbance at 254 nm. The level of significance from the 2-way ANOVA model including landscape position (L), horizon (H), and their interaction (L*H) are reported as * $p < 0.05$, ** $p < 0.01$, *** $p < 0.001$, or non-significant (ns).

Site	Layer	MDLT (%)	CRAM (%)	CARB (%)	AROM (%)	Region I	Region II	Region III	Region IV	Region V	SUVA
Hillslope	Organic	13.15	16.24	8.07	20.41	16.27	36.76	23.00	16.11	7.86	2.61
		(0.25)	(0.13)	(0.13)	(0.40)	(2.31)	(0.87)	(1.26)	(0.25)	(0.53)	(0.11)
	Mineral	12.32	16.23	8.41	19.32	15.91	40.70	20.11	16.77	6.52	2.96
		(0.28)	(0.16)	(0.28)	(0.37)	(1.03)	(0.64)	(0.94)	(0.15)	(0.36)	(0.06)
Riparian	Organic	13.84	15.27	7.58	21.50	14.88	36.36	24.57	15.99	8.20	2.65
		(0.37)	(0.62)	(0.08)	(0.50)	(1.73)	(1.01)	(0.72)	(0.21)	(0.24)	(0.06)
	Mineral	12.68	16.30	7.95	20.04	13.44	40.96	21.43	17.23	6.94	2.83
		(0.43)	(0.19)	(0.26)	(0.56)	(0.87)	(0.63)	(0.44)	(0.24)	(0.14)	(0.08)
Source of variance											
L		ns	ns	ns	*	ns	ns	ns	ns	ns	ns
H		**	ns	ns	**		***	**	***	***	**
L*H		ns	*	*	ns	ns	ns	ns	ns	ns	**

REFERENCES

Adams RW, Holroyd CM, Aguilar JA, Nilsson M, Morris GA (2013) Perfecting WATERGATE: clean proton NMR spectra from aqueous solution Chemical Communications, 49(4), 358-360. *Chemical Communications*, **49**, 358–360.

Ameli AA, Amvrosiadi N, Grabs T, Laudon H, Creed IF, McDonnell JJ, Bishop K (2016) *Hillslope permeability architecture controls on subsurface transit time distribution and flow paths*, Vol. 543. 17-30 pp.

Anderson AE, Weiler M, Alila Y, Hudson RO (2008) Dye staining and excavation of a lateral preferential flow network. *Hydrology and Earth System Sciences Discussions*, **5**, 1043–1065.

Bates D, Maechler Martin, Walker S (2016) Package "lme4": Linear Mixed-Effects Models. *CRAN Repository*, 1–113.

Battin TJ, Luyssaert S, Kaplan LA, Aufdenkampe AK, Richter A, Tranvik LJ (2009a) The boundless carbon cycle. *Nature Geoscience*, **2**, 598–600.

Battin TJ, Kaplan L a., Findlay S et al. (2009b) Biophysical controls on organic carbon fluxes in fluvial networks. *Nature Geoscience*, **2**, 595–595.

Bergstrom A, Jensco K, McGlynn B (2016) Spatiotemporal processes that contribute to hydrologic exchange between hillslopes, valley bottoms, and streams. *Water Resources Research*, **52**, 4628–4645.

Bowden WB, Gooseff MN, Balser A, Green A, Peterson BJ, Bradford J (2008) Sediment and nutrient delivery from thermokarst features in the foothills of the North Slope, Alaska: Potential impacts on headwater stream ecosystems. *Journal of Geophysical Research: Biogeosciences*, **113**, 1–12.

Boye K, Noël V, Tfaily MM, Bone SE, Williams KH, Bargar JR, Fendorf S (2017) Thermodynamically controlled preservation of organic carbon in floodplains.

Carey SK, Woo MK (2000) The role of soil pipes as a slope runoff mechanism, Subarctic Yukon, Canada. *Journal of Hydrology*, **233**, 206–222.

Chen W, Westerhoff P, Leenheer JA, Booksh K (2003) Fluorescence Excitation - Emission Matrix Regional Integration to Quantify Spectra for Dissolved Organic Matter. *Environmental Science and Technology*, **37**, 5701–5710.

Cooper LW, Kane DL, Hinzmant LD (2017) Application of Oxygen-18 Tracer Techniques to Arctic Hydrological Processes Author (s): Lee W . Cooper , Corina Solis , Douglas L . Kane and Larry D . Hinzman Published by : INSTAAR , University of Colorado Stable URL : http://www.jstor.org/stable/15518. **25**, 247–255.

Cotrufo MF, Wallenstein MD, Boot CM, Denef K, Paul E (2013) The Microbial Efficiency-Matrix Stabilization (MEMS) framework integrates plant litter decomposition with soil organic matter stabilization: Do labile plant inputs form stable soil organic matter? *Global Change Biology*, **19**, 988–995.

Covino T (2016) Hydrologic connectivity as a framework for understanding biogeochemical flux through watersheds and along fluvial networks. *Geomorphology*, **277**, 133–144.

Danczak RE, Sawyer AH, Williams KH, Stegen JC, Hobson C, Wilkins MJ (2016) Seasonal hyporheic dynamics control coupled microbiology and geochemistry in Colorado River sediments. *Journal of Geophysical Research: Biogeosciences*, **121**, 2976–2987.

Davis SN, Thompson GM, Bentley HW, Stiles G (1980) Ground-Water Tracers — A Short Review. *Groundwater*, **18**, 14–23.
Djoumbou Feunang Y, Eisner R, Knox C et al. (2016) ClassyFire: automated chemical classification with a comprehensive, computable taxonomy. *Journal of Cheminformatics*, **8**, 1–20.
Duffy JE, Lefcheck JS, Stuart-Smith RD, Navarrete SA, Edgar GJ (2016) Biodiversity enhances reef fish biomass and resistance to climate change. *Proceedings of the National Academy of Sciences*, **113**, 6230–6235.
Ernakovich JG, Wallenstein MD (2015) Permafrost microbial community traits and functional diversity indicate low activity at in situ thaw temperatures. *Soil Biology and Biochemistry*, **87**, 78–89.
Ernakovich JG, Lynch LM, Brewer PE, Calderon FJ, Wallenstein MD (2017) Redox and temperature-sensitive changes in microbial communities and soil chemistry dictate greenhouse gas loss from thawed permafrost. *Biogeochemistry*.
Fontaine S, Barot S, Barré P, Bdioui N, Mary B, Rumpel C (2007) Stability of organic carbon in deep soil layers controlled by fresh carbon supply. *Nature*, **450**, 277–80.
Fox J, Monette G (1992) Generalized Collinearity Diagnostics. *Journal of the American Statistical Association*, **87**, 178–183.
Frey KE, McClelland JW (2009) Impacts of permafrost degradation on arctic river biogeochemistry. *Hydrological Processes*, **23**, 169–182.
Grootveld M (2014) *Introduction to the Applications of Chemometric Techniques in Omics Research: Common Pitfalls, Misconceptions and Rights and Wrongs*. 1-34 pp.
Hackstadt AJ, Hess AM (2009) Filtering for increased power for microarray data analysis. *BMC Bioinformatics*, **10**, 11.
Hertkorn N, Benner R, Frommberger M et al. (2006) Characterization of a major refractory component of marine dissolved organic matter. *Geochimica et Cosmochimica Acta*, **70**, 2990–3010.
Hinton MJ, Schiff SL, English MC (1994) Examining the contributions of glacial till water to storm runoff using two- and three-component hydrograph separations. *Water Resources Research*, **30**, 983–993.
Hinzman LD, Bettez ND, Bolton WR et al. (2005) Evidence and implications of recent climate change in northern Alaska and other arctic regions. *Climatic Change*, **72**, 251–298.
Hopp L, McDonnell JJ (2009) Connectivity at the hillslope scale: Identifying interactions between storm size, bedrock permeability, slope angle and soil depth. *Journal of Hydrology*, **376**, 378–391.
Iversen CM, Sloan VL, Sullivan PF et al. (2015) The unseen iceberg: Plant roots in arctic tundra. *New Phytologist*, **205**, 34–58.
Jansen B, Kalbitz K, McDowell WH (2014) Dissolved Organic Matter: Linking Soils and Aquatic Systems. *Vadose Zone Journal*, **13**, 0.
Jencso KG, McGlynn BL, Gooseff MN, Bencala KE, Wondzell SM (2010) Hillslope hydrologic connectivity controls riparian groundwater turnover: Implications of catchment structure for riparian buffering and stream water sources. *Water Resources Research*, **46**, 1–18.
Kaiser K, Kalbitz K (2012) Cycling downwards - dissolved organic matter in soils. *Soil Biology and Biochemistry*, **52**, 29–32.
Kalbitz K, Schwesig D, Schmerwitz J et al. (2003) Changes in properties of soil-derived dissolved organic matter induced by biodegradation. *Soil Biology and Biochemistry*, **35**,

1129–1142.
Kane DL, Hinzman LD, Benson CS, Everett KR (1989) Hydrology of Imnavait Creek, an arctic watershed. *Ecography*, **12**, 262–269.
Kellerman AM, Dittmar T, Kothawala DN, Tranvik LJ (2014) Chemodiversity of dissolved organic matter in lakes driven by climate and hydrology. *Nature Communications*, **5**, 1–8.
Kirchner JW (2003) INVITED COMMENTARY A double paradox in catchment hydrology and geochemistry. **874**, 871–874.
Klaus J, Zehe E, Elsner M, Külls C, McDonnell JJ (2013) Macropore flow of old water revisited: Experimental insights from a tile-drained hillslope. *Hydrology and Earth System Sciences*, **17**, 103–118.
Koch JC, Runkel RL, Striegl R, Mcknight DM (2013) Hydrologic controls on the transport and cycling of carbon and nitrogen in a boreal catchment underlain by continuous permafrost. *Journal of Geophysical Research: Biogeosciences*, **118**, 698–712.
Koven C, Friedlingstein P, Ciais P, Khvorostyanov D, Krinner G, Tarnocai C (2009) On the formation of high-latitude soil carbon stocks: Effects of cryoturbation and insulation by organic matter in a land surface model. *Geophysical Research Letters*, **36**, 1–5.
Lachenbruch AH (1962) Mechanics of thermal contraction cracks and ice-wedge polygons in permafrost. *Geological Society of America Special Papers*, **70**, 1–66.
Lehmann J, Kleber M (2015) Perspective The contentious nature of soil organic matter. *Nature*, **528**, 60–68.
Lenth R (2016) Package lsmeans: least-squares means. *CRAN Repository*.
Liang C, Schimel JP, Jastrow JD (2017) The importance of anabolism in microbial control over soil carbon storage. *Nature Microbiology*, **2**, 17105.
Lipson DA, Zona D, Raab T, Bozzolo F, Mauritz M, Oechel W (2012) Water-table heiught and microtopography control biogeochemical cycling in an Arctic coastal tundra ecosystem. *Biogeosciences*, **9**, 577–591.
Marín-Spiotta E, Gruley KE, Crawford J et al. (2014) Paradigm shifts in soil organic matter research affect interpretations of aquatic carbon cycling: Transcending disciplinary and ecosystem boundaries. *Biogeochemistry*, **117**, 279–297.
Mayer LM (1994) Relationships between mineral surfaces and organic carbon concentrations in soils and sediments. *Chemical Geology*, **114**, 347–363.
McCay RT (2009) Recent advances in solvent suppression for solution NMR: A practical reference. In: *Annual reports on NMR spectroscopy*, 66th edn (ed Webb GA), pp. 33–76. Academic Press.
Mu CC, Abbott BW, Wu XD et al. (2017) Thaw Depth Determines Dissolved Organic Carbon Concentration and Biodegradability on the Northern Qinghai-Tibetan Plateau. *Geophysical Research Letters*, **44**, 9389–9399.
Natali SM, Schuur EAG, Mauritz M et al. (2015) Journal of Geophysical Research: Biogeosciences. *Journal of Geophysical Research: Biogeosciences*, **120**, 1–13.
Osterkamp TE, Romanovsky VE (1999) Evidence for warming and thawing of discontinuous permafrost in Alaska. *Permafrost and Periglacial Processes*, **10**, 17–37.
Pautler BG, Simpson J, Mcnally DJ, Lamoureux SF (2010) Arctic Permafrost Active Layer Detachments Stimulate Microbial Activity and Degradation of Soil Organic Matter. *Environmental Science and Technology*, **44**, 4076–4082.
Peterson BJ, Holmes RM, McClelland JW et al. (2002) Increasing river discharge to the Arctic Ocean. *Science*, **298**, 2171–2173.

Plug L, West J (2009) Thaw lake expansion in a two-dimensional coupled model of heat transfer, thaw subsidence, and mass movement. *Journal of Geophysical Research*, **114**.
Quinton WL, Gray DM, Marsh P (2000) Subsurface drainage from hummock-covered hillslopes in the Arctic tundra. Journal of Hydrology, 237(1), 113-125. *Journal of Hydrology*, **237**, 113–125.
Roth V-N, Dittmar T, Gaupp R, Gleixner G (2014) Ecosystem-specific composition of dissolved organic matter. *Vadose Zone Journal*, **13**.
Rowland JC, Jones CE, Altmann G et al. (2010) Arctic landscapes in transition: Responses to thawing permafrost. *Eos*, **91**, 229–230.
Runkel RL (2015) On the use of rhodamine WT for the characterization of stream hydrodynamics and transient storage. *Water Resources Research*, **51**, 1–18.
Santeford HS (1978) Snow soil interactions in interior Alaska. *Modeling of snow cover runoff*, 311–318.
Schmidt MWI, Torn MS, Abiven S et al. (2011) Persistence of soil organic matter as an ecosystem property. *Nature*, **478**, 49–56.
Schuur EAG, Vogel JG, Crummer KG, Lee H, Sickman JO, Osterkamp TE (2009) The effect of permafrost thaw on old carbon release and net carbon exchange from tundra. *Nature*, **459**, 556–559.
Seibert J, Grabs T, Köhler S, Laudon H, Winterdahl M, Bishop K (2009) Linking soil-and stream-water chemistry based on a Riparian Flow-Concentration Integration Model. *Hydrol. Earth Syst. Sci*, **13**, 2287–2297.
Simpson AJ, Simpson MJ, Soong R (2012) Nuclear magnetic resonance spectroscopy and its key role in environmental research. *Environmental Science and Technology*, **46**, 11488–11496.
Spencer RGM, Mann PJ, Dittmar T et al. (2015) Detecting the signature of permafrost thaw in Arctic rivers. *Geophysical Research Letters*, **42**, 2830–2835.
Stieglitz M, Shaman J, McNamara JP, Engel V, Shanley J, Kling GW (2003) An approach to understanding hydrologic connectivity on the hillslope and the implications for nutrient transport. *Global Biogeochemical Cycles*, **17**, 1–15.
Sturm M, Racine C, Tape K (2001) Climate change. Increasing shrub abundance in the Arctic. *Nature*, **411**, 546–547.
Sutfin NA, Wohl E (2017) Substantial soil organic carbon retention along floodplains of mountain streams. *Journal of Geophysical Research: Earth Surface*, **122**, 1325–1338.
Tetzlaff D, Buttle J, Carey SK, Mcguire K, Laudon H, Soulsby C (2015) Tracer-based assessment of flow paths, storage and runoff generation in northern catchments: A review. *Hydrological Processes*, **29**, 3475–3490.
Vonk JE, Mann PJ, Davydov S et al. (2013) High biolability of ancient permafrost carbon upon thaw. *Geophysical Research Letters*, **40**, 2689–2693.
Vos M, Wolf A, Jennings S, Kowalchuk G (2013) Micro-scale determinants of bacterial diversity in soil. *FEMS Microbiology reviews*, **37**, 936–954.
Walker DA, Walker MD (1996) Terrain and vegetation of the Imnavait Creek watershed. In: *Landscape Function and Disturbance in Arctic Tundra*, pp. 73–108. Springer Berlin Heidelberg.
Walvoord MA, Kurylyk BL (2016) Hydrologic Impacts of Thawing Permafrost—A Review. *Vadose Zone Journal*, **15**, 0.
Ward CP, Cory RM (2015) Chemical composition of dissolved organic matter draining permafrost soils. *Geochimica et Cosmochimica Acta*, **167**, 63–79.

Wehrens R, Mevik B-H (2007) pls: Partial Least Squares Regression (PLSR) and Principal Component Regression (PCR). *R package version 2.1-0*.
Weiler M, McDonnell JJ (2006) Testing nutrient flushing hypotheses at the hillslope scale: A virtual experiment approach. *Journal of Hydrology*, **319**, 339–356.
Weishaar J, Aiken G, Bergamaschi B, Fram M, Fujii R, Mopper K (2003) Evaluation of specific ultra-violet absorbance as an indicator of the chemical content of dissolved organic carbon. *Environmental Science and Technology*, **37**, 4702–4708.
White D, Hinzman L, Alessa L et al. (2007) The arctic freshwater system: Changes and impacts. *Journal of Geophysical Research: Biogeosciences*, **112**, 1–21.
Wild B, Schnecker J, Alves RJE et al. (2014) Input of easily available organic C and N stimulates microbial decomposition of soil organic matter in arctic permafrost soil. *Soil Biology and Biochemistry*, **75**, 143–151.
Woo M (2012) *Permafrost Hydrology*. Springer Berlin Heidelberg, Berlin, Heidelberg.
Woods GC (2012) Structural Characterization of Freshwater Dissolved Organic Matter from Arctic and Temperate Climates Using Novel Analytical Approaches by.
Woods GC, Simpson MJ, Kelleher BP, McCaul M, Kingery WL, Simpson AJ (2009). (2009) Online high-performance size exclusion chromatography− nuclear magnetic resonance for the characterization of dissolved organic matter. *Environmental Science and Technology*, **44**, 624–630.
Woods GC, Simpson MJ, Koerner PJ, Napoli A, Simpson AJ (2011a) HILIC-NMR: toward the identification of individual molecular components in dissolved organic matter. *Environmental science & technology*, **45**, 3880–3886.
Woods GC, Simpson MJ, Pautler BG, Lamoureux SF, Lafrenière MJ, Simpson AJ (2011b) Woods, Gwen C., et al. "Evidence for the enhanced lability of dissolved organic matter following permafrost slope disturbance in the Canadian High Arctic. *Geochimica et Cosmochimica Acta*, **75**, 7226–7241.
Xia J, Wishart DS (2016) Using MetaboAnalyst 3.0 for Comprehensive Metabolomics Data Analysis. *Current Protocols in Bioinformatics*, **55**, 10.1-14.10.91.
Zhang X, Hutchings JA, Bianchi TS, Liu Y, Arellano AR, Schuur EAG (2017) Importance of lateral flux and its percolation depth on organic carbon export in Arctic tundra soil: Implications from a soil leaching experiment. *Journal of Geophysical Research: Biogeosciences*, **122**, 796–810.
Zhu Q, Iversen CM, Riley WJ, Slette IJ, Vander Stel HM (2016) Root traits explain observed tundra vegetation nitrogen uptake patterns: Implications for trait-based land models. *Journal of Geophysical Research: Biogeosciences*, **121**, 3101–3112.
Zuur AF, Ieno EN, Elphick CS (2010) A protocol for data exploration to avoid common statistical problems. *Methods in Ecology and Evolution*, **1**, 3–14.

CHAPTER 4- THE PATH TAKEN: STREAM COMPLEXITY AND HYDROLOGIC CONNECTIVITY SHIFT METABOLITE COMPOSITION AND DISSOLVED ORGANIC MATTER CHEMISTRY[3]

INTRODUCTION

Dissolved organic matter (DOM) is the dominant form of organic carbon (C) in aquatic environments (Weishaar *et al.*, 2003; Seitzinger *et al.*, 2005). Given the central role of DOM in global C cycling, nutrient export, and food web dynamics (Dittmar & Stubbins, 2013; Jansen *et al.*, 2014) it is important to unravel the processes that control its flux and transformation in watersheds. However, elucidating these controls is challenging because of the tremendous chemical heterogeneity of DOM, which comprises a complex mixture of compounds varying in physicochemical reactivity (Weishaar *et al.*, 2003; Seitzinger *et al.*, 2005), and the complexity of underlying spatiotemporal mechanisms influencing its composition. Headwater streams are particularly important to study as they exert disproportionate control on fluvial biogeochemistry by setting initial conditions that cascade to the entire watershed (Cole *et al.*, 2007). As headwater streams can be hotspots of C-cycling, with the potential to structure downstream metabolism (Vannote *et al.*, 1980; Battin *et al.*, 2009) and water quality (Sapkal & Valunjkar, 2013), it is essential to understand how geomorphic factors influence DOM transport and processing.

In mountainous watersheds, the majority of DOM enters the fluvial network in small tributaries within the subalpine zone. By some estimates, half of this C is metabolized and converted to CO_2 (Aufdenkampe *et al.*, 2011), while the fraction remaining within the watershed

[3] This manuscript is in preparation: Lynch, L.M., Sutfin, N.A., Fegel, T.S., Boot, C.M., Covino, T.P., Wallenstein, M.D. 2018. The path taken: Stream complexity and hydrologic connectivity shift metabolite composition and dissolved organic matter chemistry.

is either retained on floodplains or exported further downstream (Sutfin *et al.*, 2016; Sutfin & Wohl, 2017). The balance between retention and export is critical in determining the chemical energy available to shape downstream metabolism. Thus, geomorphic complexity—the physical heterogeneity in stream planform (Livers & Wohl, 2016)—is a critical factor controlling the residence time and concentration of DOM remaining within fluvial networks. This is particularly evident in mountainous channel networks, where streams alternate between segments with a single channel (simple), and segments with multiple channels of flow across the valley bottom (complex or multithread) (Wohl, 2013). Single-thread channel segments naturally occur in relatively confined, steep-gradient valleys and are characterized by high transport capacities and limited sediment, water, and fluvial carbon storage (Sutfin *et al.*, 2016). The lack of geomorphic complexity in single-thread segments results in rapid export of DOM through the landscape, reducing rates of ecosystem metabolism (Polvi & Wohl, 2013). As a result, DOM chemistry may be minimally altered during transport. The removal of beaver and/or channel-spanning logjams can also convert complex channels to more simplified single-thread channel systems (Wegener *et al.*, 2017). Ensuing simplification has a host of environmental consequences, including decreased stream-floodplain connectivity, drying of the valley floodplain, and reduced floodplain C storage (Polvi & Wohl, 2013). Channel simplification is widespread across developed countries (Gooseff *et al.*, 2007) and resulting impacts on ecosystem function likely translate to DOM processing dynamics.

Stable multi-thread channels develop in broad, relatively unconfined valleys of Rocky Mountain National Park where channel-spanning logjams and beaver (*Castor canadensis)* activity dissipate transport energy and create sites of flow diversion (Polvi & Wohl, 2013; Wohl, 2013). These retention zones enhance the transient storage of DOM (Gooseff *et al.*, 2007), likely

increasing geophysical opportunities for microbial metabolism (Battin *et al.*, 2009). Additionally, flume studies have shown physical complexity increases microbial community diversity and the uptake of chemically complex DOM (Besemer *et al.*, 2009; Singer *et al.*, 2010). Greater microbial diversity may translate into more extensive DOM processing by diversifying metabolic pathways and altering the balance between anabolic and catabolic growth. While geomorphic complexity appears to be an important driver of DOM composition, limited analytical resolution has precluded detailed investigation (Kellerman *et al.*, 2014). As a result, it remains unclear whether decomposition results in the convergence of DOM molecular composition toward a core set of metabolites, or persistence of the original, chemically diverse molecular profile (Liang *et al.*, 2017). Resolution of this debate is essential in determining how DOM is cycled within a landscape.

In snowmelt-dominated catchments, strong seasonal fluctuations in discharge likely interact with geomorphic complexity to control molecular patterns of DOM composition. During spring snowmelt, shallow flowpaths through riparian soils activate, mobilizing DOM with a wide gradient of physicochemical reactivity across the terrestrial-aquatic interface (Ward *et al.*, 2017). However, this DOM may be rapidly shunted through the fluvial network before microbial or photo-oxidative transformation can significantly alter its chemical profile (Raymond *et al.*, 2016). In contrast, during low-flow periods, lateral hydrologic connectivity, particularly across the stream-floodplain interface (Covino, 2016), decreases, and downstream conveyance of water and entrained DOM is disproportionately reduced in multi-channel relative to single-channel systems (Sutfin *et al.*, 2016). Longer residence times in complex stream segments facilitates metabolic diversification and uptake of low molecular weight and complex resources (Singer *et al.*, 2010). However, nutrient limitation may shift microbial communities from anabolic

metabolism toward catabolic respiration, resulting in lower substrate use efficiency and divergent metabolite profiles (Liang *et al.*, 2017). Although alpine and subalpine headwaters are an important source of chemical energy to downstream ecosystems[7], we currently lack a quantitative understanding of the relationship between seasonal hydrology, geomorphic complexity, and DOM reactivity.

The adoption of mass spectrometry has tremendously improved our understanding of DOM composition and cycling. Electron impact gas chromatography mass spectrometry (EI GC-MS) provides access to individual metabolites from complex mixtures of environmental DOM (Seitzinger *et al.*, 2005; Kind & Fiehn, 2010; Lei *et al.*, 2011). In addition to setting a useful baseline for the degradation potential of a system (Kellerman *et al.*, 2014), these approaches allow us to link metabolic pathways to the fate and cycling of DOM. While particularly adept at identifying volatile, low molecular weight compounds, such as primary metabolites, GC-MS can also profile secondary metabolites, such as polyphenols and lignin derivatives (Halket *et al.*, 2005). Using chemical profiles to infer microbial processes is central to understanding the reactivity and fate of DOM.

In this study, we use a suite of complementary approaches, including EI GC-MS and excitation-emission fluorescence spectroscopy (EEMS), to quantify spatial and temporal differences in DOM molecular composition. We also determine the potential role of geomorphic complexity, hydrologic connectivity, and stream discharge in structuring DOM molecular composition. We posit that (1) stream segments with high geomorphic complexity provide the geophysical opportunities necessary for microbial communities to metabolize DOM for energy and growth, increasing downstream export of newly synthesized metabolites, and (2) maximal chemical diversity occurs during snowmelt and declines over time as hydrograph recession

minimizes terrestrial-aquatic connectivity. With this rationale, we test two predictions: (1) Metabolite diversity is significantly higher in complex, multi-channel reaches compared to confined, single-channel reaches, and (2) Mean range of DOM composition is significantly higher during the rising limb and peak flow, and gradually converges toward a core set of metabolites with hydrograph recession.

METHODS

SITE DESCRIPTION

North Saint Vrain Creek (NSV) and Beaver Brook are headwater streams located in Rocky Mountain National Park, Colorado, USA. Both streams have nearly identical climate regimes and underlying geology, consisting of a granitic core (Braddock & JC, 1990), but differ substantially in channel complexity. The approximately four-kilometer study reach along NSV exhibits pronounced downstream variations in valley geometry and channel complexity (Table 4.1). Creek planform alternates between single- and multi-thread channel segments as a result of beaver activity (Wohl *et al.*, 2012). The total drainage area of the NSV study reach is ~90 km^2 with an elevation of ~2,560 m. Vegetation is typical of the Colorado Front Range and aspen (*Populus tremuloides*) and willow stands (*Salix spp.*) dominate the riparian zone, while Engelmann spruce (*Picea engelmannii*), lodge pole pine (*Pinus contorta*), and subalpine fir (*Abies lasiocarpa*) colonize upland sites (Veblen & Donnegan, 2005). We established a second, approximately three-kilometer long research site in Beaver Brook, herein referred to as Upper Beaver Meadow (UBM). This site was once a complex channel segment occupied by beavers, but has been abandoned since the early 20^{th} century, resulting in channel simplification (Wohl, 2013). As a result, a narrow (1-2 m wide), single-thread channel has incised (2-3 m) into legacy beaver meadow sediment (Kramer *et al.*, 2012). Within the portion of Rocky Mountain National

Park where these sites are located, mean annual temperature is 5°C with a summer average of 14°C, and mean annual precipitation is 861 mm, with 451 mm contributed as snowfall (Copeland Lake SNOTEL site # 412, 2621 m elevation, 40° 7' 22.0794"N by 105° 20' 26.5194"W).

Study reaches along UBM and NSV consist of three longitudinally adjacent stream segments (Figure 4.1) varying in geomorphic complexity (Table 4.1). At UBM, each site is separated by ~1,500 m, and there are no multi-thread channels within the study reach. At NSV we sampled a multi-thread, active beaver meadow complex bounded by relatively confined upstream and downstream single-thread segments. An upstream and downstream transect bounded each of the three NSV subreaches, and the NSV beaver meadow included an additional transect at the middle of the subreach. The NSV beaver meadow complex has the highest planform complexity, with multiple water impoundments behind beaver dams, as well as side channels and slough features that progressively disconnect from the main-channel with hydrograph recession (Wegener *et al.*, 2017). Samples were also collected from a beaver pond located along the upstream transect within the NSV beaver meadow, which has no surface water connectivity and sits ~3 m higher in elevation than the main-channel. The selection of these sites allows us to assess the temporally dynamic role of lateral connectivity (continuous, intermittent, absent) on fluvial biogeochemistry. At each sampling site, we recorded GPS coordinates and physical characteristics including stream (or pond) width and depth (Table 4.1). Stream discharge was recorded hourly at UBM from June 11 through September 30, 2015 and at NSV from April 1 through August 30, 2015, reported in Wegener et al. (2017).

SAMPLE COLLECTION AND PROCESSING

We collected paired surface water and hyporheic sediment samples eight times between May and September 2015 (n=48). Surface water samples were collected into sterile 50 mL amber borosilicate bottles and hyporheic sediments were collected into sterile 50 mL centrifuge vials. Additional large-volume surface water samples were collected into 10 L sterile containers and prepared for GC-MS analysis (see below). All samples were filtered within six hours of collection through 0.7 μm glass fiber filters pre-combusted at 400°C (Whatman GF/F). Samples analyzed for total dissolved organic carbon (DOC) and total dissolved nitrogen (TDN) were acidified to pH 3, to stabilize the samples, and refrigerated until analysis on a Shimadzu TOC-L (Shimadzu Corporation Columbia, MD). Subsamples analyzed for inorganic nitrogen (NO_3^- and NH_4^+) were frozen until analysis on an Alpkem flow solution IV automated wet chemistry system (O.I. Analytical College Station, TX).

EXCITATION-EMISSION MATRICS

We used excitation-emission matrices to study the seasonal variability of fluorescent DOM characteristics (Fellman *et al.*, 2010). To reduce inner-filter effects and normalize C concentrations, we diluted filtered samples to 5 mg C L^{-1} before analyzing them on an Aqualog spectrofluorometer with a xenon excitation source (Horiba-Jobin Yvone Scientific Edison, NJ). We set excitation and emission slits to a 3 nm band-pass, and incrementally increased wavelengths in 3 nm steps from 200 to 800 nm. A sealed cuvette was used as a blank and analyzed between every twenty samples to correct for instrument drift. Following spectral analysis, we corrected each sample for inner-filter effects, masked Rayleigh scatter using first and second grating orders, and normalized each sample spectra by the blank (Cory & McKnight, 2005). We quantified excitation-emission matrix (EEMS) spectra using the fluorescence regional

integration (FRI) approach, and identified five spectral regions as outlined by Chen et al. using Matlab version R2016b. EEMS regions I and II are related to simple aromatic proteins (tyrosine and tryptophan-like), region III to fulvic-acid type materials, region IV to soluble microbial byproduct-type materials, and region V to humic acid-type organics (Chen *et al.*, 2003). The FRI approach is better suited to capture the underlying heterogeneity of aromatic DOM as it quantifies entire regions of wavelength-dependent fluorescent intensities rather than utilizing only several data points per spectrum (Chen *et al.*, 2003).

ELECTRON IMPACT GAS CHROMATOGRAPHY-MASS SPECTROMETRY

We used EI-GC-MS to generate mass spectral fragments, permitting partial structural identification of metabolites present in each sample (Kind & Fiehn, 2010). We concentrated the C in each pre-filtered 10 L surface water sample using four Bond Elut PPL cartridges pre-conditioned with HPLC-grade methanol (Agilent Technologies). Following C concentration, each cartridge was extracted with 10 mL of HPLC-grade methanol into sterile borosilicate vials and evaporated under pure N_2 gas. Samples were prepared for GC-MS analysis at the Proteomics and Metabolomics Facility, Colorado State University. Samples were re-suspended in 5 mL of methanol and vortexed for 30 seconds. Next, 1 mL aliquots were collected and centrifuged for 10 minutes at 15,000 g and 4°C, and then 50 µL of N-methyl-N-trimethylsilyltrifluoroacetamide and 1% trimethylchlorosilane were added to volatilize nonpolar metabolites. Sample supernatants were incubated for 30 min at 60°C and then centrifuged for five minutes at 3000 *x*g. Next, 80 µL aliquots were transferred to a glass GC-MS autosampler vial and injected into a Trace GC Ultra coupled to a Thermo ISQ mass spectrometer (Thermo Scientific) in a 1:10 split ratio. A 30 m TG-5MS column (Thermo Scientific, 0.25 mm i.d., 0.25 µm film thickness), with a 1.2 mL/min helium gas flow rate, separated metabolites. Masses between 50-650 mass to charge (*m/z*) were

scanned at 5 scans/sec after electron impact ionization. Quality control samples were injected after every six samples. A matrix of molecular features, defined by retention time and *m/z*, were generated using XCMS software in R. Compounds were annotated based on spectral matching to NISTv12, Golm, Metlin, Massbank, and in-house metabolite databases (Broeckling *et al.*, 2014). We procured the InChI code for each annotated metabolite from PubChem and used ClassyFire to identify its chemical taxonomy (Djoumbou Feunang *et al.*, 2016).

STATISTICAL ANALYSIS

We used one-way ANOVA models to identify main effects of landscape position and collection period (Julian date) on each dependent variable of interest using the *lmtest* package (Hothorn *et al.*, 2015) in R version 3.3.1 ("R Core Team: A language and environment for statistical computing," 2014). We explored mean differences within each dependent variable using two-sample t-tests with unequal variances and Satterthwaite's approximation for degrees of freedom using the *lsmeans* package in R (Lenth, 2016). Data were log transformed when necessary to meet assumptions of normality, evaluated with Shapiro-Wilk tests. Model residuals were tested for constant and homogenous variance using Q-Q and residual versus fitted plots. Outliers were identified using Cook's distance and removed if $D_i \geq 1$.

We used multiple linear regression analysis to identify relationships between our dependent variable of interest (DOC, EEMS region I, or EEMS region III) and potential predictor variables. Due to high correlations among many possible explanatory variables, only those most consistent with past work or theory are included in our regression analyses (with $r \geq 0.6$). A correlation matrix of all possible predictors is included in Supplemental Figure 4.1. Potential variables for the initial regression analysis included channel width, stream discharge, precipitation, temperature, valley confinement, and valley topographic aspect. Stepwise multiple

linear regressions were conducted following Sutfin and Wohl (Sutfin & Wohl, 2017), using the *step* function in the R *stats* package ("R Core Team: A language and environment for statistical computing," 2014). We normalized DOC using the boxcox power transformation in the R *MASS* package, with $\lambda = -0.343434$. Boxcox transformations yielded normally distributed errors, assessed with Shapiro-Wilk tests of the residuals (0.85), and inspection of qqplots and histograms of model residuals.

We used MetaboAnalyst 3.0 for detailed metabolite processing and analysis (Xia & Wishart, 2016). We removed non-informative metabolites using interquartile range filtering, and normalized the data using a log transformation and Pareto variance scaling, which are common data pretreatment methods (van den Berg *et al.*, 2006). We identified significantly different metabolites using one-way ANOVA and Tukey's HSD post-hoc analyses, and determined whether samples clustered by categorical factors (landscape position or sampling period), using Partial Least Squares–Discriminant Analysis (PLS–DA), a method commonly applied to metabolomic and chemometric datasets (Grootveld, 2014). We performed PLS-DA regressions in MetaboAnalyst 3.0, which uses the *plsr* function in the R *pls* package (Wehrens & Mevik, 2007). We assessed the performance of each generated model using classification and 10-fold cross validation, and used prediction accuracy during training and B/W permutation tests to explore relationships between our metabolite distribution ('predictor' variables) and hypothetical classification system (landscape position or sampling period). For each PLS-DA model, we generated 2,000 permutations to test whether these classification systems were significantly better than those arising through random chance (Grootveld, 2014).

We used constrained analysis of principal components (capscale), an ordination method in the R *vegan* package that permits non-Euclidean dissimilarity indices (Oksanen *et al.*, 2007),

to test for an association of metabolite composition (as derived from GC-MS) with spatial, climate, and fluvial characteristics. We included nine potential environmental drivers in our ordination: discharge, channel width, the proportion of the watershed influenced by beaver activity, average monthly precipitation and temperature, snowpack extent, dissolved organic carbon, and the percent fluorescent intensity of EEMS regions I (soluble microbial-type proteins) and III (fulvic-type acids). We computed Bray-Curtis dissimilarities from normalized metabolite peak intensities and fit our environmental drivers to each ordination, with p-values calculated over 999 permutations. We extracted sample and metabolite information from the first two canonical axes to test for an association between metabolite characteristics (*m/z,* retention time, abundance), and retained ($p<0.01$) environmental drivers. We used an independent NMDS ordination to validate retention of the selected environmental drivers (stress: 0.05).

RESULTS

INFLUENCE OF GEOMORPHIC COMPLEXITY AND SEASONALITY ON FLUVIAL CHEMISTRY

Despite collecting samples at UBM (simple morphology) spanning three km, we found no evidence of downstream chemical transformation on any measured index of DOM composition, except for C115, an unidentified metabolite (*m/z* heaviest mass: 513.39, $p<0.01$). Therefore, we used the stream average across UBM sampling sites for subsequent statistical analysis. Bulk C concentrations collected from all sampling locations were significantly different across space and time ($p<0.01$, $F_{8,39}=3.55$; Table 4.2). Of all the potential explanatory geomorphic and environmental variables tested, only valley confinement was a significant predictor of DOC concentration ($p<0.001$, Supplemental Table 4.1). Within NSV, DOC concentrations increased by 158% during transport through the beaver meadow complex and

remained elevated during export through the downstream confined channel (Table 4.2). Intermediate flows exported higher DOC concentrations than peak or low flow conditions.

Total dissolved N (TDN) concentrations were twice as high in the beaver pond than all other sites ($p<0.01$) and decreased throughout the season ($p<=0.02$). Regressing TDN against discharge revealed N export was highest during peak discharge ($R^2=0.46$). Total C:N varied spatially and temporally ($F_{8,39}=4.22$; Table 4.2); relative N availability was higher in the beaver pond and UBM than the beaver meadow complex and downstream confined channel ($p<0.05$). We also observed an effect of landscape position on hyporheic C and N concentrations, such that sites with lower transport energy (beaver pond and beaver meadow) had higher C and N concentrations than freely flowing reaches ($F_{8,39}=2.44$; $p<0.05$).

Optical fluorescence characteristics exhibited strong temporal dynamics, but their relative fluorescence intensity was not influenced by geomorphic complexity (Table 4.2). We observed the lowest relative percent intensities of simple aromatic proteins (regions I and II) and soluble microbial-type proteins (region IV) during peak discharge, with intensities doubling throughout the summer (Region I: $F_{8,39}=2.84$; Figure 4.2a). In contrast, fulvic- (region III) and humic- (region V) type acids decreased in relative intensity by 60% throughout the season, except for a highly enriched signal exported during peak discharge (Region III: $F_{8,39}=2.84$; Figure 4.2b). Regressing region I against region III revealed a strong, negative relationship ($R^2 = 0.89$), suggesting high levels of autochthonous productivity occur during periods of low allochthonous subsidy (Supplemental Figure 4.2). Discharge alone was a significant predictor of Regions I ($p<0.01$, $R^2 = 0.27$) and III ($p<0.05$, $R^2 = 0.22$), supporting the control of seasonality on DOM fluorescence (Supplemental Table 4.1).

METABOLITE DISTRIBUTION

We identified a total of 2,472 mass spectral features using untargeted EI GC-MS. We resolved these features using cluster analysis, identifying 259 unique compounds that each consisted of between 3 and 57 mass spectral fragments (Broeckling *et al.*, 2014). We were able to annotate and classify 10% of these compounds (Dunn *et al.*, 2013; Djoumbou Feunang *et al.*, 2016), which primarily consisted of sugars, organic acids, lipids, and lignin-derived aromatics (Supplemental Table 4.2). Due to limitations in current mass spectral libraries we were not able to annotate the majority of compounds driving sample separation across geomorphic complexity and sampling period (Table 4.3). However, we were able to use changes in metabolite composition to separate samples in ordination space.

Over half of all profiled metabolites (both annotated and not) exhibited significant separation across regions of varying geomorphic complexity (Supplemental Figure 4.3a). Combined, PLS-DA components 1 and 2 explained 42.8% of the variance, and retention of four axes maximized classification performance (R^2=0.69; CV accuracy=0.56). The top five VIP compounds, or metabolites that contributed most to sample separation across geomorphic complexity, had slightly higher quasi-molecular ion *m/z* values (310.8) than average (259.9) (Table 4.3a). The beaver pond and simplified channel at UBM, which represent end-members of hydrologic (dis)connectivity, had divergent metabolite profiles (Figure 4.3a), indicating a strong influence of geomorphic complexity on metabolite distribution relative to sites that experience changes in hydrologic connectivity. Within NSV, the upper and lower confined reaches showed minimal overlap, while the beaver meadow complex, situated in physical space between the two sites, shared metabolites with each. The upper confined sites, however, have more dissimilarity with the beaver meadow complex, whereas the lower confined site contained metabolites very

similar to and within the range of the meadow site. We observed a similar pattern when considering only annotated metabolites. The top five VIP compounds contributing to metabolite separation across geomorphic complexity had the highest scores in the beaver pond and simplified UBM, the lowest scores in the upper confined channel, and relatively low scores within the beaver meadow complex and lower confined channel (Supplemental Figure 4.4a). These compounds are related to byproducts of decomposition, including nonanoic and dodecanoic acids (medium-chain saturated fatty acids), glyceric acid (a three C sugar acid), and isovanillic acid (a derivate of lignin degradation) (Supplemental Table 4.2) (Djoumbou Feunang *et al.*, 2016).

Metabolites also separated across sampling period (Figure 4.3b), although only 40% exhibited significant temporal variability (Supplemental Figure 4.3b). Together, the first two PLS-DA components explained 45.3% of the variance, with maximal classification performance achieved with five axes (R^2=0.96; CV accuracy=0.44). The top five VIP compounds separating samples across time had relatively lower quasi-molecular ion *m/z* values (190.8) than average (259.9) (Table 4.3). The top five annotated VIP compounds were typically enriched early in the season and included lumichrome (a flavin pigment), glycerol (a three-carbon sugar acid), 2-hydroxypyridine (potentially involved in DNA synthesis), and several polyethylene glycols (ether compounds) (Supplemental Figure 4.4b) (Djoumbou Feunang *et al.*, 2016).

Samples collected during the rising limb and peak discharge (Figure 4.3c) were composed of significantly different metabolites than samples collected during base flow (Figure 4.3d), with typically lower quasi-molecular ion *m/z* values. Early in the season, samples did not separate by landscape position (p=0.808), suggesting a core set of metabolites is exported during high flow periods (Figure 4.3c). In contrast, we observed significant sample separation across

geomorphic complexity during base flow conditions ($p=0.013$), suggesting metabolite profiles diverge during low flow periods (Figure 4.3D).

ENVIRONMENTAL DRIVERS OF METABOLITE DIVERSITY

We identified six environmental drivers associated with metabolite composition (Figure 4.4). Within ordination space, dimension 1 explained 43.09% of variation across the dataset and dimension 2 explained an additional 30.06%. Dissolved organic C emerged as the primary factor influencing metabolite composition, and was oppositely correlated with discharge (Figure 4.4), where high discharge exported metabolites with relatively lower quasi-molecular ion *m/z* values than low flow periods. In addition, metabolites clustering with higher DOC concentrations had significantly higher quasi-molecular ion *m/z* values than those associated with proteins (EEMS Region I, $p<0.003$) and snowpack extent ($p<0.006$), indicating lower chemical reactivity. Samples clustering with proteins were typically collected later in the summer, when low flows reduced hydrologic connectivity across the landscape. These patterns suggest fragmented landscapes export chemically distinct, reactive metabolites from multi-thread channels relative to their single-thread counterparts. Mean monthly precipitation and temperature were oppositely related to snowpack extent, highlighting the role of seasonality in structuring metabolite composition.

DISCUSSION

Our results suggest subalpine fluvial chemistry and DOM molecular composition are strongly influenced by seasonality and geomorphology. Broad indices of DOM composition, including optical fluorescence (EEMS) and bulk DOC and TDN concentrations, were strongly related to in-stream flows. While these bulk chemical approaches revealed the influence of seasonality, we found the application of non-targeted metabolomics—a higher-resolution

approach—was essential for resolving the influence of landscape complexity on DOM chemistry. Linking complex environmental drivers to ecosystem metabolism is critical in understanding network-level energetics, an area of significant research interest (Battin *et al.*, 2009; Besemer *et al.*, 2009; Singer *et al.*, 2012; Kellerman *et al.*, 2014; Fegel *et al.*, 2016; Wegener *et al.*, 2017).

We observed the highest and most variable relative fluorescent intensities of fulvic- and humic-type acids—EEMS regions III and V—prior to peak discharge, suggesting the landscape is integrated during snowpack thaw. Both components are associated with aromatic, terrestrial-derived organics (Chen *et al.*, 2003; Creed *et al.*, 2015) and linked to DOM mobilization across the terrestrial-aquatic interface (Burns *et al.*, 2016). In subalpine watersheds, initial changes in stream water chemistry are driven by pulses of solutes from the snowpack (Campbell *et al.*, 1995) and activation of shallow soil flowpaths (Ward *et al.*, 2017). Spring thaw rapidly increases landscape connectivity, releasing metabolites that have accumulated in isolated soil pores throughout the winter (Schimel *et al.*, 2007; Drotz *et al.*, 2010). Materials transported from near-surface soil compartments are enriched in reactive plant-derived compounds, especially phenolics and other lignin derivatives (Kaiser & Kalbitz, 2012). We observed high concentrations of metabolites with relatively low quasi-molecular ion *m/z* values, which support activation of shallow flowpaths and export of plant-derived materials (Hättenschwiler & Vitousek, 2000), including syringol and isovannilic acid, which are associated with lignin-type derivatives (Djoumbou Feunang *et al.*, 2016). As soil flowpaths deepen with snowmelt, compounds enriched in microbial-derivatives and nitrogen-bearing compounds are mobilized (Rumpel & Kögel-Knabner, 2011). Stream-water chemistries exported in the spring thus reflect activation of diverse soil flowpaths (Burns *et al.*, 2016), however, rapid export during peak flows

may result in mixing and convergence of the chemical profile. Furthermore, although high concentrations of potentially labile DOM are exported with snowmelt, cold temperatures and rapid flow velocities likely limit in-stream metabolism.

During peak flows, we observed strongly homogenized fluvial and metabolite chemistries, and hyporheic scouring in single-channel segments. We propose these simple reaches typify the 'pulse-shunt' concept proposed by Raymond et al. (2016) (2016), where high concentrations of terrestrial-derived DOM mobilized during snowmelt can bypass local metabolism due to rapid increases in stream velocity. Systems with low flow heterogeneity have also been linked with lower microbial biodiversity and DOM uptake relative to sites with longer residence time that facilitate opportunities for microbial metabolism (Singer *et al.*, 2010). The lack of upstream DOM processing thus redistributes C and nutrient cycling to downstream, higher-order rivers, with implications for headwater C storage and water quality.

Like many mountainous headwaters, North St. Vrain exhibits pronounced downstream variations in stream planform (Wohl *et al.*, 2012) that moderate pulse-shunt dynamics even during high-flow periods. Specifically, single-channel reaches alternate with broad, multi-thread complexes that promote hydrological buffering by dissipating transport energy (Sutfin *et al.*, 2016). Wegener et al. (2017) showed that the multi-thread beaver meadow complex exhibits variable sink-source dynamics, as a function of flow. During high flow periods, water and entrained nutrients are distributed laterally in floodplain surface-water bodies and are gradually released during low flow periods. The release of these components subsidizes downstream metabolism, integrating ecosystem metabolism with landscape connectivity (Marcatelli *et al.*, 2011).

Throughout the summer, we observed significant reductions in stream velocity and increasing indicators of autochthonous productivity, suggesting greater opportunities for in-stream metabolism (Fasching *et al.*, 2016). Increasing relative intensities of soluble microbial-type proteins and decomposition byproducts (FRI regions I, II, and IV) were particularly pronounced in the beaver pond and the beaver meadow complex. These low-flow sites have increased DOM residence times, and are typically warmer (Wegener *et al.*, 2017), enhancing geophysical opportunities for metabolism relative to high-flow sites (Battin *et al.*, 2009). Within the beaver pond, we observed high concentrations of saturated medium-chain (9:0 and 10:0) and long-chain (16:0 and 18:0) fatty acids, both of which have been linked to fungal and bacterial detritivores (Torres-Ruiz *et al.*, 2007), and can serve as significant energy sources for aquatic heterotrophs (Perry *et al.*, 1979). During summer baseflow we observed significant landscape fragmentation as side and main channels within the beaver meadow complex became hydrologically disconnected (Sutfin *et al.*, 2016). Resulting fluctuations in redox gradients have been linked to the activation of metabolic pathways utilizing alternate terminal electron acceptors to degrade DOM (Danczak *et al.*, 2016; Boye *et al.*, 2017). Together with photo-oxidative transformation, these conditions could contribute to observed increases in chemical diversity with hydrograph recession.

The divergence in DOM composition with hydrograph recession could also be explained by a shift from anabolic assimilation toward catabolic metabolism. As hydrologic connectivity decreased, we observed lower nutrient availability, warmer temperatures in disconnected slough features, and higher ecosystem respiration within the beaver meadow complex (Wegener *et al.*, 2017). These patterns suggest nutrient-limited microbial communities cycle DOM less efficiently during warmer, low-flow periods, promoting C release to the atmosphere rather than

incorporation in microbial biomass (Cotrufo *et al.*, 2013). Unlike anabolism, which promotes chemical convergence through assimilation, catabolic respiration preserves the inherent complexity of DOM (Liang *et al.*, 2017). Thus, we revise our initial hypothesis and propose instead that 1) carbon chemistry in subalpine streams tend toward chemostasis during snowmelt, when landscape connectivity and hydrologic drivers shunt DOM through the fluvial network, and 2) carbon complexity increases as a function of hydrologic fragmentation, shifting the balance from anabolic to catabolic metabolism (Figure 4.5).

Although still in its nascence, the ability to infer microbial functionality from metabolomics is a promising avenue of research (Seitzinger *et al.*, 2005; Djoumbou Feunang *et al.*, 2016). Unlike fluorescence, NMR, and FT-ICR-MS approaches, which broadly group DOM complexity into functional groups or compound classes, EI GC-MS provides fragmentation spectra useful for identifying individual metabolites. Currently, GC-MS databases are sparse for ecological purposes (Halket *et al.*, 2005), and products of secondary metabolism (aromatics, alkaloids, terpenoids, glycosides, phenolics, lignans) (Luckner, 2013) are not represented as well as those of primary metabolism (amino acids, sugars, organic acids, peptides) (Kind & Fiehn, 2010). We found that the majority of compounds separating samples by landscape position had relatively high quasi-molecular ion values *m/z* (> 200), potentially indicative of these secondary metabolites and compounds with relatively high molecular weights.

The role of secondary metabolites in structuring network-level energetics is an area of considerable research interest (Horner *et al.*, 1988; Williams *et al.*, 1989; Hättenschwiler & Vitousek, 2000; Challis & Hopwood, 2003; Price-Whelan *et al.*, 2006). The environmental ubiquity of these structurally complex compounds suggests they confer a competitive advantage upon the organisms producing them. Otherwise, the pressures of Darwinian natural selection

would preclude their synthesis (Williams *et al.*, 1989). Mounting evidence suggests these higher molecular weight metabolites are variously involved in gene expression and cellular growth (Price-Whelan *et al.*, 2006), with the potential to create more beneficial environmental conditions by, for instance, complexing iron and nutrients (Horner *et al.*, 1988). Others have suggested the production of diverse metabolites facilitates microbial adaptation to complex environmental stressors (Challis & Hopwood, 2003), which are pronounced in subalpine watersheds, particularly under a changing climate. Thus, although we could not annotate many of these compounds, by pairing metabolomics with fluorescence spectroscopy, we were able to link microbial metabolism and landscape-scale processes to make inference about how underlying metabolic pathways structure local patterns of DOM chemistry at the terrestrial-aquatic interface and throughout the fluvial network.

The ability of subalpine watersheds to store and process DOM is imperiled by widespread and systematic channel simplification, resulting from land use changes, flow regulation, and beaver removal (Bain *et al.*, 2012; Covino *et al.*, 2012; Wegener *et al.*, 2017). In addition to loss of geomorphic complexity, changes in hydrologic regime associated with reduced snowpack and stochasticity in the timing and magnitude of runoff have the potential to greatly alter the spatio-temporal dynamics of hydrologic connectivity at the terrestrial aquatic interface. These watersheds are also experiencing dramatic shifts in biogeochemical function, including increased N deposition from intensified industrial and agricultural production (Baron *et al.*, 2000), episodic acidification (Kendall *et al.*, 1999; Sullivan *et al.*, 2005), and reductions in DOM and water subsidies from shrinking glaciers (Fegel *et al.*, 2016). The combination of these factors reduces ecosystem function, with implications for human health (Trussell & MD, 1978), the value of water and storage-associated flow regimes (Maas *et al.*, 2017), fate and transport of

point and non-point source pollution (Puttock *et al.*, 2017), and stormwater management (Bernhardt & Palmer, 2007). Here, we suggest subalpine systems are particularly sensitive to channel simplification, because the loss of geomorphic complexity reduces metabolic opportunities for DOM processing. We also suggest seasonal reductions in hydrologic connectivity, exacerbated by widespread reductions in snowpack (Barnett *et al.*, 2008), will heighten catabolic metabolism by reducing nutrient availability in disconnected features. The propagation of these novel chemistries fuels downstream metabolism, tying local biogeochemical processing to network level energetics.

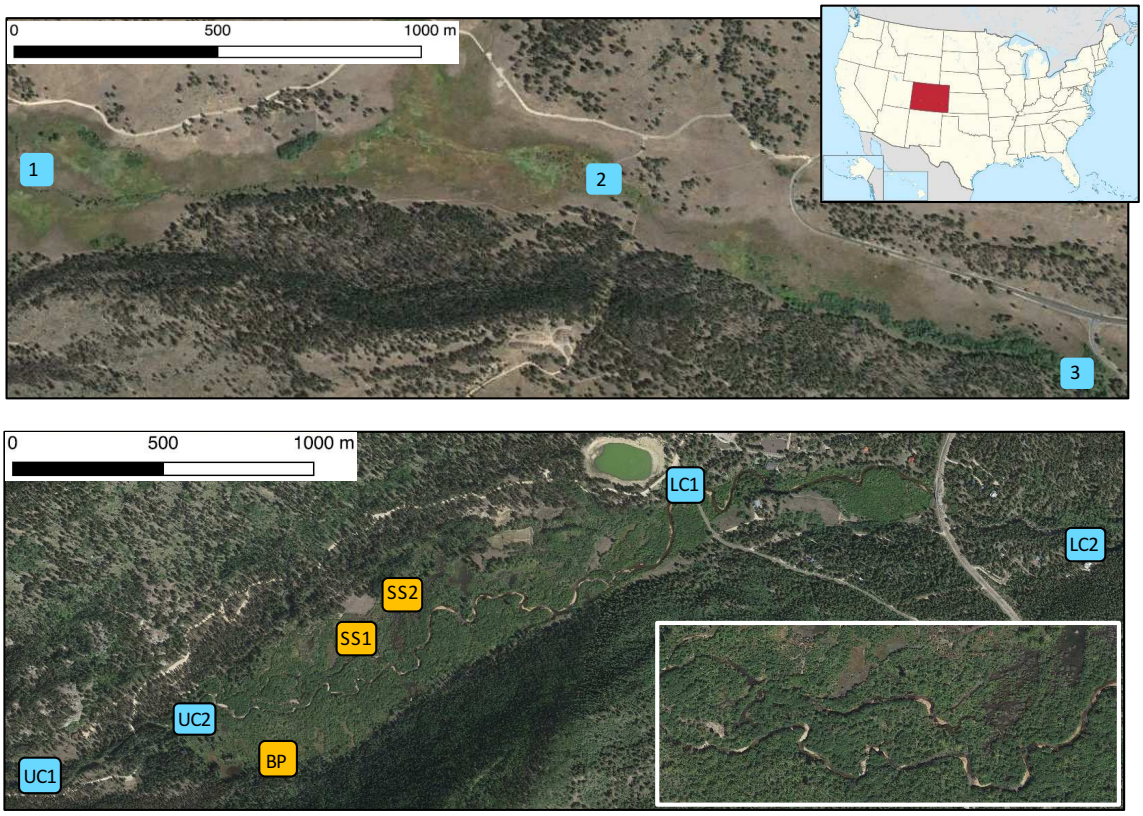

Figure 4.1. From the simplified Upper Beaver Meadows (UBM) system, we present data from three single-channel sites (1, 2, 3, upper panel). Single-channel segments bracket the beaver meadow complex at North Saint Vrain (NSV) Creek in Rocky Mountain National Park, Colorado (lower panel). From NSV, we present data from two main channel sites in the upper confined segment (UC1, UC2), two side-channel features in the active beaver meadow complex (SC1, SC2), two main channel sites in the lower confined segment (LC1, LC2), and a disconnected beaver pond (BP).

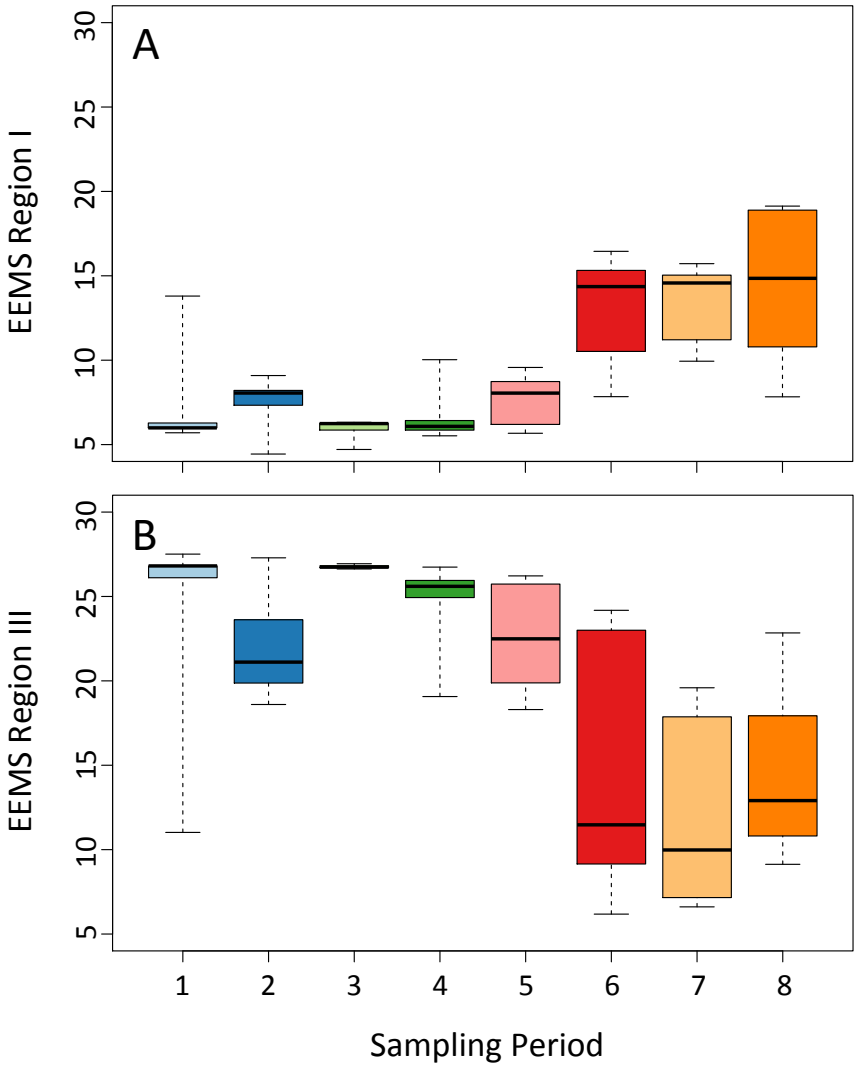

Figure 4.2. Boxplot representing seasonal distributions of EEMS region I: simple aromatic proteins (A), and EEMS region III: fulvic-type acids across sampling period (B) (n=49). Regions II and IV (simple aromatic proteins and soluble microbial byproducts) follow similar seasonal patterns as region I, while region III and V (humic-type acids) are related. Each box spans the interquartile range; whiskers extend to the minimum and maximum of the distribution.

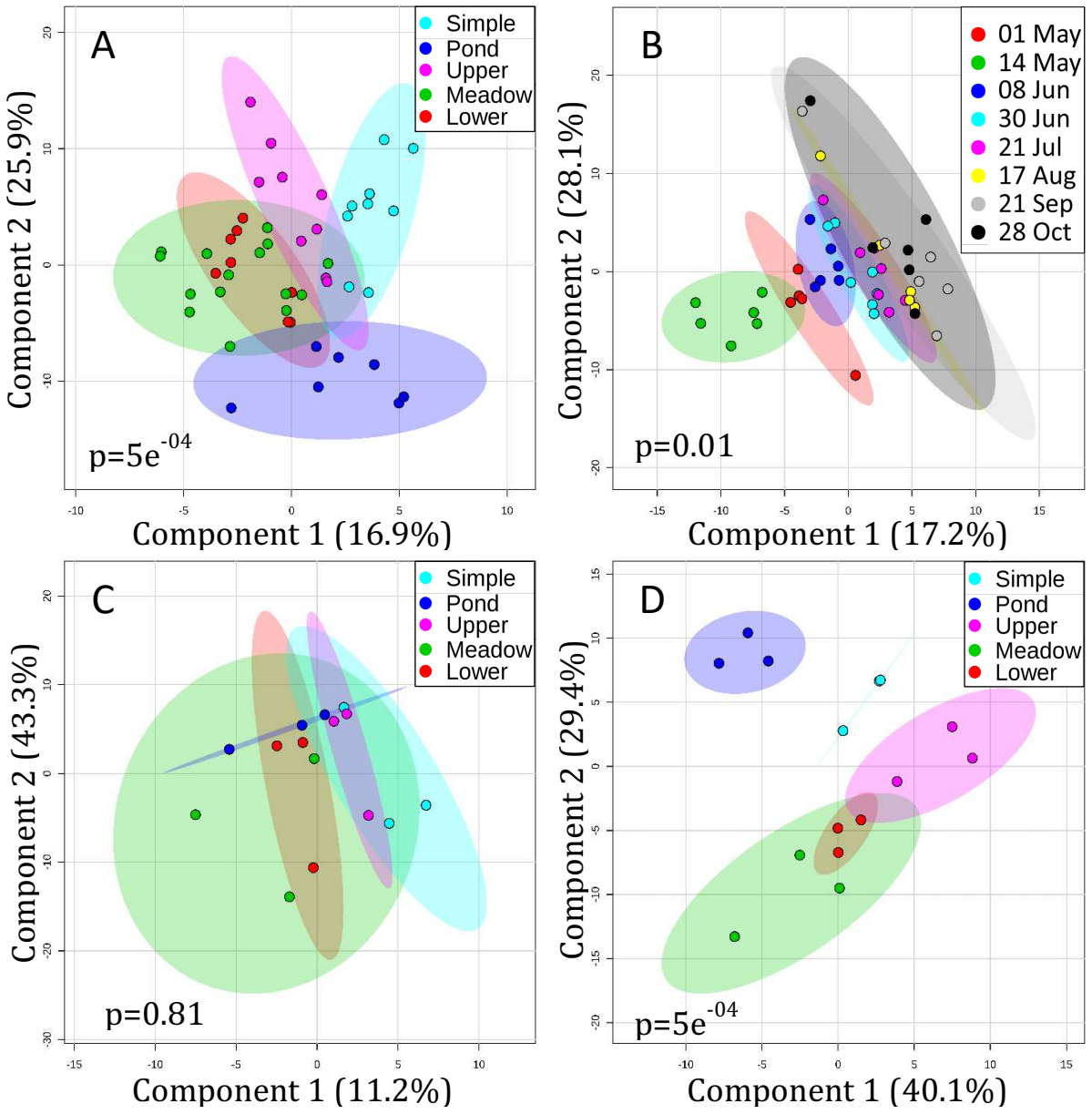

Figure 4.3. PLS-DA plot of metabolites clustered by landscape position (A), sampling period (B), rising limb, including only May 01, May 15, June 08 (C), or base flow, including only Aug 17, Sep 21, Oct 28 (D). Each circle represents a sample and shaded ellipses represent 95% confidence intervals for each *a-priori* cluster. Ellipse overlap signifies no significant difference between clusters. For each PLS-DA model, 2,000 permutations were generated to test whether our classification systems (landscape position and sampling period) were significantly better than those arising through random chance.

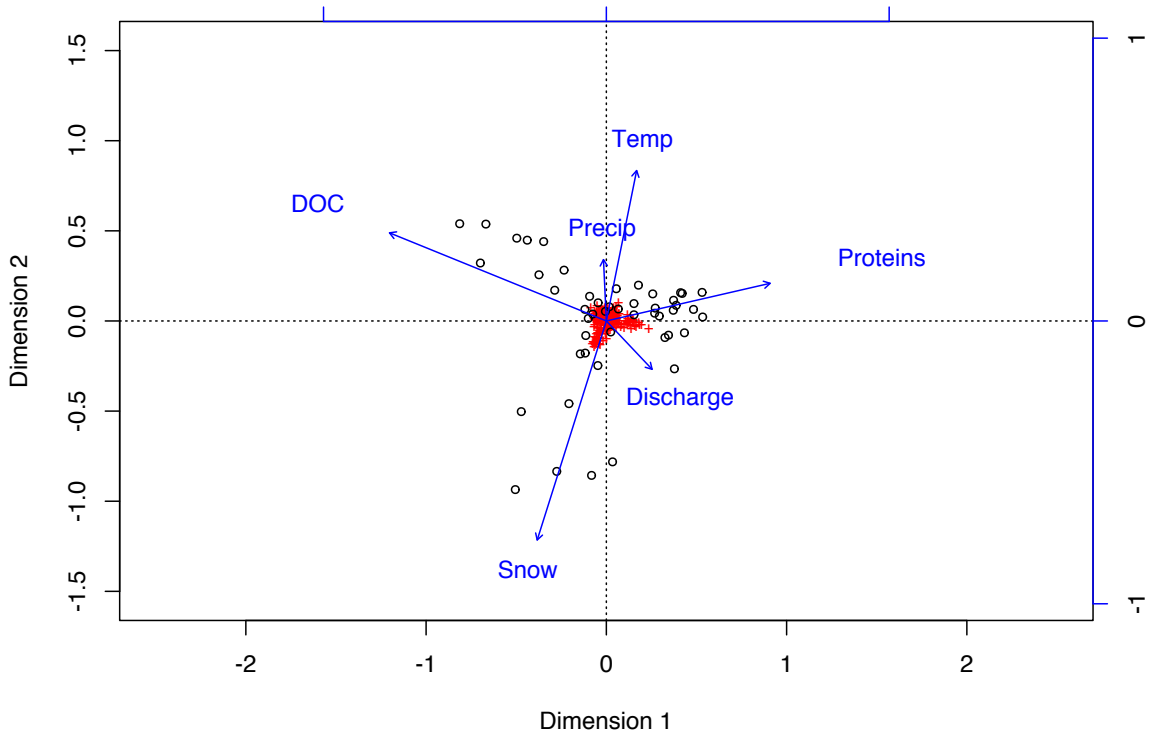

Figure 4.4. Multivariate analysis of metabolites and environmental drivers using constrained analysis of principal coordinates. Ordinations are based on Bray-Curtis dissimilarity, computed from normalized peak intensities, and used to test for an association of metabolite composition (as derived from GC-MS) with spatial, climate, and fluvial characteristics. Red crosses represent individual metabolites, black circles represent samples, blue vectors represent uncorrelated environmental variables with a significance level of <0.05. DOC, dissolved organic carbon; Precip, month-averaged precipitation; Temp, month-averaged temperature; Proteins, EEMS region I; Discharge, daily average; Snow, daily snow depth at Wild Basin.

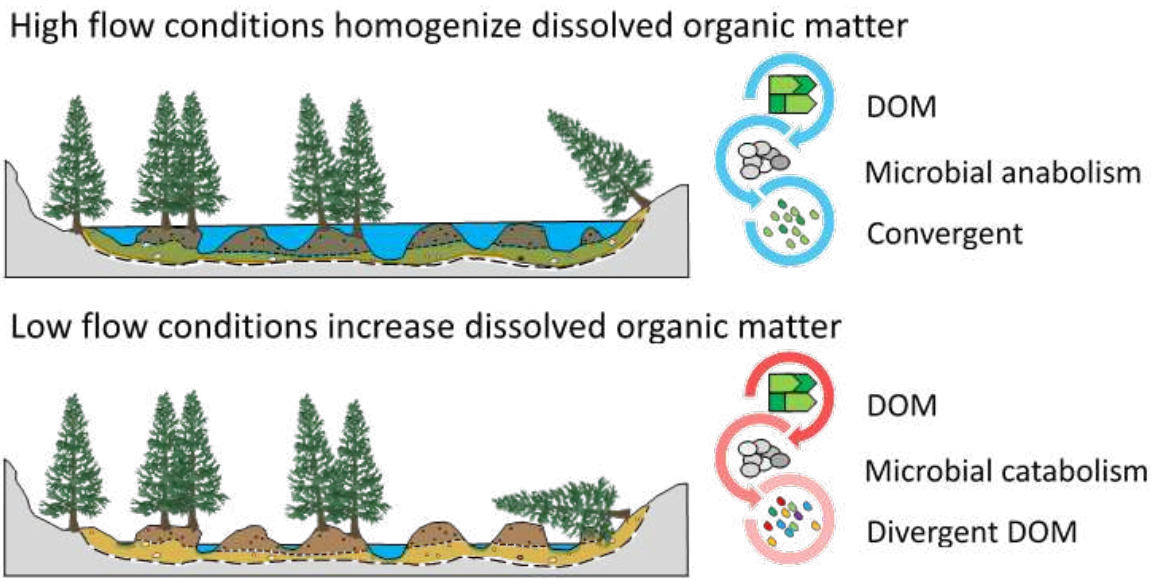

Figure 4.5. During peak discharge (upper left), high flows limit geophysical opportunities for microbial metabolism. Landscape fragmentation during summer base flow (lower left) increases water residence time and microbial processing of dissolved organic matter (DOM). With sufficient nutrient availability, microbial anabolism dominates (upper right), causing DOM chemistry to converge toward a core set of metabolites. As nutrient availability decreases in isolated side channel and slough features, catabolic pathways activate (lower right) and metabolite diversity increases.

Table 4.1. Physical characteristics of sampling sites located in Upper Beaver Meadow (UBM) and North Saint Vrain (NSV) creeks, Rocky Mountain National Park, Colorado. Channels with a confinement value >6 are considered '*unconfined'* while those will a confinement value <6 are considered '*confined'*.

	Simple	Upper	Meadow Complex	Lower	Pond
Watershed	UBM	NSV	NSV	NSV	NSV
Channel planform	Single-thread	Single-thread	Multithread	Single-thread	Groundwater
Lateral connectivity	Continuous	Continuous	Intermittent	Continuous	None
Number of sites	3	2	2	2	1
Watershed area (m)	21.6	88.9	88.9	88.9	88.9
Channel width (m)	0.71	12.2	14.5	20	12.8
Valley width (m)	163.9	59.6	246.8	27.5	246.9
Confinement (m)	230.85	4.89	17.02	1.38	19.29
Elevation (m)	2572.51	2561.08	2544.33	2519.76	2545.85

Table 4.2. Biogeochemical characteristics of surface water and hyporheic sediments by landscape position and collection period (discharge) at North St. Vrain (Pond, Upper, Meadow, Lower) and Upper Beaver Meadows (Simple). The average followed by the standard error (± 1 S.E.) in parentheses for dissolved C, N (TOC, TDN), inorganic N (NO_3, NH_4) and a metabolite chemodiversity index (Shanon-Weiner). The level of significance from the 2-way ANOVA model including site (S) and discharge (D) are reported as * $p < 0.05$, ** $p < 0.01$, *** $p < 0.001$, or non-significant (ns). For ns comparisons, a master mean, integrated across landscape position or collection period, is provided. Specific comparisons were explored using Tukey HSD t-tests with Satterthwaite-Welsch approximations for degrees of freedom (reported in Results section).

Landscape Position	TOC (mg L^{-1})	TDN (mg L^{-1})	NO_3 (mg L^{-1})	NH_4 (mg L^{-1})	Hyporheic TOC (mg L^{-1})	Hyporheic TDN (mg L^{-1})	Shannon-Weiner
Simple	4.00 (0.53)	0.25 (0.03)	0.08 (0.02)		4.81 (0.54)	0.35 (0.05)	
Pond	9.90 (1.95)	0.61 (0.15)	0.03 (0.01)		8.10 (1.49)	0.68 (0.23)	
Upper	2.70 (0.55)	0.33 (0.05)	0.11 (0.01)	0.07 (0.01)	3.41 (0.65)	0.58 (0.17)	3.45 (0.09)
Meadow	4.27 (0.49)	0.39 (0.05)	0.08 (0.02)		8.64 (2.29)	1.20 (0.29)	
Lower	3.42 (0.71)	0.31 (0.04)	0.09 (0.02)		4.41 (1.02)	0.73 (0.21)	
Collection Period							
1	6.49 (0.66)	0.49 (0.07)	0.11 (0.01)	0.17 (0.06)		2.13 (0.20)	
2	5.17 (0.67)	0.35 (0.02)	0.08 (0.02)	0.08 (0.01)		1.28 (0.47)	
3	4.72 (0.29)	0.47 (0.04)	0.11 (0.03)	0.08 (0.01)		0.54 (0.06)	
4	3.58 (0.49)	0.38 (0.04)	0.06 (0.02)	0.08 (0.01)	6.20 (1.76)	0.49 (0.08)	3.45 (0.12)
5	4.32 (1.75)	0.32 (0.06)	0.04 (0.01)	0.06 (0.01)		0.54 (0.11)	
6	8.22 (3.28)	0.49 (0.15)	0.03 (0.01)	0.05 (0.00)		0.37 (0.08)	
7	4.57 (2.68)	0.23 (0.11)	0.04 (0.01)	0.05 (0.00)		0.42 (0.09)	
8	4.64 (2.49)	0.43 (0.28)	0.06 (0.01)	0.05 (0.00)		0.31 (0.10)	
Source of variance							
S	**	***	***	ns	*	**	ns
D	**	**	*	***	ns	***	ns

Table 4.3. Metabolites ranked by variable importance to PLS-DA projection scores (VIP) for landscape position (a) and sampling period (b). VIP scores are calculated as the weighted sum of squares of the PLS-DA loadings, accounting for the amount of Y-variation explained in each dimension. The absolute ion intensity and quasi-molecular ion *m/z* values are reported for the largest ion fragment within each clustered spectrum (where each spectrum represents a single TMS-derived metabolite). Lower quasi-molecular ion *m/z* values indicate higher compound volatility and are typically associated with faster elution. The F statistic and p-values are calculated from Tukey HSD posthoc t-tests.

a) Landscape position

VIP rank	Component	*m/z*	Ion Intensity	Retention Time (sec)	F-value	p-value
1	115	513.39	5068750.55	848.05	26.32	4.50E-11
2	249	415.24	655021.76	844.39	20.18	2.04E-09
3	193	262.17	495548.72	427.67	20.10	2.16E-09
4	147	204.09	4384031.87	465.90	20.06	2.21E-09
5	62	160.11	5721841.99	539.88	18.41	7.02E-09

b) Sampling period

VIP rank	Component	*m/z*	Ion Intensity	Retention Time (sec)	F-value	p-value
1	10	162.11	3350524.58	836.24	13.75	6.63E-09
2	138	58.14	2629564.07	836.85	6.03	7.81E-05
3	112	118.15	16869278.30	914.96	20.75	1.82E-11
4	11	412.16	562885.68	754.30	7.76	6.50E-06
5	33	204.10	9955728.64	841.02	16.28	6.43E-10

REFERENCES

Aufdenkampe, A.K., Mayorga, E., Raymond, P.A., Melack, J.M., Doney, S.C., Alin, S.R., Aalto, R.E., Yoo, K., 2011. Riverine coupling of biogeochemical cycles between land, oceans, and atmosphere. Frontiers in Ecology and the Environment 9, 53–60. doi:10.1890/100014

Bain, D.J., Green, M.B., Campbell, J.L., Chamblee, J.F., Chaoka, S., Fraterrigo, J.M., Kaushal, S.S., Martin, S.L., Jordan, T.E., Parolari, A.J., Sobczak, W. V., Weller, D.E., WolLheim, W.M., Boose, E.R., Duncan, J.M., Gettel, G.M., Hall, B.R., Kumar, P., Thompson, J.R., Vose, J.M., Elliott, E.M., Leigh, D.S., 2012. Legacy Effects in Material Flux: Structural Catchment Changes Predate Long-Term Studies. BioScience 62, 575–584. doi:10.1525/bio.2012.62.6.8

Barnett, T.P., Pierce, D.W., Hidalgo, H.G., Bonfils, C., Santer, B.D., Das, T., Bala, G., Wood, A.W., Nozawa, T., Mirin, A.A., Cayan, D.R., Dettinger, M.D., 2008. Human-Induced Changes United States 319, 1080–1084.

Baron, J.S., Rueth, H.M., Wolfe, A.M., Nydick, K.R., Allstott, E.J., Minear, J.T., Moraska, B., 2000. Ecosystem Responses to Nitrogen Deposition in the Colorado Front Range. Ecosystems 3, 352–368. doi:10.1007/s100210000032

Battin, T.J., Kaplan, L. a., Findlay, S., Hopkinson, C.S., Marti, E., Packman, A.I., Newbold, J.D., Sabater, F., 2009. Biophysical controls on organic carbon fluxes in fluvial networks. Nature Geoscience 2, 595–595. doi:10.1038/ngeo602

Besemer, K., Singer, G., Hödl, I., Battin, T.J., 2009. Bacterial community composition of stream biofilms in spatially variable-flow environments. Applied and Environmental Microbiology 75, 7189–7195. doi:10.1128/AEM.01284-09

Boye, K., Noël, V., Tfaily, M.M., Bone, S.E., Williams, K.H., Bargar, J.R., Fendorf, S., 2017. Thermodynamically controlled preservation of organic carbon in floodplains. doi:10.1038/NGEO2940

Braddock, W., JC, C., 1990. Geologic map of Rocky Mountain National Park and vicinity: U.S. Geological Survey Miscellaneous Investigations Series Map I-1973, scale 1:50,000.

Broeckling, C.D., Afsar, F.A., Neumann, S., Ben-Hur, A., Prenni, J.E., 2014. RAMClust: A novel feature clustering method enables spectral-matching-based annotation for metabolomics data. Analytical Chemistry 86, 6812–6817. doi:10.1021/ac501530d

Burns, M.A., Barnard, H.R., Gabor, R.S., McKnight, D.M., Brooks, P.D., 2016. Dissolved organic matter transport reflects hillslope to stream connectivity during snowmelt in a montane catchment. Water Resources Research 52, 4905–4923. doi:10.1002/2015WR017878

Challis, G.L., Hopwood, D. a, 2003. Synergy and contingency as driving forces for the evolution of multiple secondary metabolite production by Streptomyces species. Proceedings of the National Academy of Sciences of the United States of America 100, 14555–14561. doi:10.1073/pnas.1934677100

Chen, W., Westerhoff, P., Leenheer, J.A., Booksh, K., 2003. Fluorescence Excitation - Emission Matrix Regional Integration to Quantify Spectra for Dissolved Organic Matter. Environmental Science and Technology 37, 5701–5710.

Cole, J.J., Prairie, Y.T., Caraco, N.F., McDowell, W.H., Tranvik, L.J., Striegl, R.G., Duarte, C.M., Kortelainen, P., Downing, J.A., Middelburg, J.J., Melack, J., 2007. Plumbing the

global carbon cycle: Integrating inland waters into the terrestrial carbon budget. Ecosystems 10, 171–184. doi:10.1007/s10021-006-9013-8
Cory, R.M., Harrold, K.H., Neilson, B.T., Kling, G.W., 2015. Controls on dissolved organic matter (DOM) degradation in a headwater stream: The influence of photochemical and hydrological conditions in determining light-limitation or substrate-limitation of photo-degradation. Biogeosciences 12, 6669–6685. doi:10.5194/bg-12-6669-2015
Cory, R.M., McKnight, D.M., 2005. Fluorescence spectroscopy reveals ubiquitous presence of oxidized and reduced quinones in dissolved organic matter. Environmental Science and Technology 39, 8142–8149. doi:10.1021/es0506962
Cotrufo, M.F., Wallenstein, M.D., Boot, C.M., Denef, K., Paul, E., 2013. The Microbial Efficiency-Matrix Stabilization (MEMS) framework integrates plant litter decomposition with soil organic matter stabilization: Do labile plant inputs form stable soil organic matter? Global Change Biology 19, 988–995. doi:10.1111/gcb.12113
Covino, T., 2017. Hydrologic connectivity as a framework for understanding biogeochemical flux through watersheds and along fluvial networks. Geomorphology 277, 133–144. doi:10.1016/j.geomorph.2016.09.030
Covino, T., McGlynn, B., McNamara, R., 2012. Land use/land cover and scale influences on in-stream nitrogen uptake kinetics. Journal of Geophysical Research: Biogeosciences 117, 1–13. doi:10.1029/2011JG001874
Creed, I.I.F., Mcknight, D.D.M., Pellerin, B.A., Green, M.B., Bergamaschi, B.A., Aiken, G.R., Burns, D.A., Findlay, S.E.G., Shanley, J.B., Striegl, R.G., Aulenbach, B.T., Clow, D.W., Laudon, H., Mcglynn, B.L., Mcguire, K.J., Smith, R.A., Stackpoole, S.M., 2015. The river as a chemostat : fresh perspectives on dissolved organic matter flowing down the river continuum. Canadian Journal of Fisheries and Aquatic Sciences 14, 1–14. doi:10.1139/cjfas-2014-0400
Danczak, R.E., Sawyer, A.H., Williams, K.H., Stegen, J.C., Hobson, C., Wilkins, M.J., 2016. Seasonal hyporheic dynamics control coupled microbiology and geochemistry in Colorado River sediments. Journal of Geophysical Research: Biogeosciences 121, 2976–2987. doi:10.1002/2016JG003527
Djoumbou Feunang, Y., Eisner, R., Knox, C., Chepelev, L., Hastings, J., Owen, G., Fahy, E., Steinbeck, C., Subramanian, S., Bolton, E., Greiner, R., Wishart, D.S., 2016. ClassyFire: automated chemical classification with a comprehensive, computable taxonomy. Journal of Cheminformatics 8, 1–20. doi:10.1186/s13321-016-0174-y
Drotz, S.H., Sparrman, T., Nilsson, M.B., Schleucher, J., Öquist, M.G., 2010. Both catabolic and anabolic heterotrophic microbial activity proceed in frozen soils. Proceedings of the National Academy of Sciences of the United States of America 107, 21046–21051. doi:10.1073/pnas.1008885107
Dunn, W.B., Erban, A., Weber, R.J.M., Creek, D.J., Brown, M., Breitling, R., Hankemeier, T., Goodacre, R., Neumann, S., Kopka, J., Viant, M.R., 2013. Mass appeal: Metabolite identification in mass spectrometry-focused untargeted metabolomics. Metabolomics 9, 44–66. doi:10.1007/s11306-012-0434-4
Fasching, C., Ulseth, A.J., Schelker, J., Steniczka, G., Battin, T.J., 2016. Hydrology controls dissolved organic matter export and composition in an Alpine stream and its hyporheic zone. Limnology and Oceanography 61, 558–571. doi:10.1002/lno.10232
Fegel, T.S., Baron, J.S., Fountain, A.G., Johnson, G.F., Hall, E.K., 2016. The differing biogeochemical signatures of glaciers and rock glaciers. Journal of Geophysical Research:

Biogeosciences 121, 919–932. doi:10.1002/2015JG003236.Received
Fellman, J.B., Hood, E., Spencer, R.G.M., 2010. Fluorescence spectroscopy opens new windows into dissolved organic matter dynamics in freshwater ecosystems: A review. Limnology and Oceanography 55, 2452–2462. doi:10.4319/lo.2010.55.6.2452
Gooseff, M.N., Hall, R.O., Tank, J.L., 2007. Relating transient storage to channel complexity in streams of varying land use in Jackson Hole, Wyoming. Water Resources Research 43, 1–10. doi:10.1029/2005WR004626
Grootveld, M., 2014. Introduction to the Applications of Chemometric Techniques in Omics Research: Common Pitfalls, Misconceptions and Rights and Wrongs, Metabolic Profiling: Disease and Xenobiotics. doi:10.1039/9781849735162-00001
Halket, J.M., Waterman, D., Przyborowska, A.M., Patel, R.K.P., Fraser, P.D., Bramley, P.M., 2005. Chemical derivatization and mass spectral libraries in metabolic profiling by GC/MS and LC/MS/MS. Journal of Experimental Botany 56, 219–243. doi:10.1093/jxb/eri069
Hättenschwiler, S., Vitousek, P.M., 2000. The role of polyphenols in terrestrial ecoystems nutrient cycling. Tree 15, 238–243.
Horner, J.D., Gosz, J.R., Cates, R.G., 1988. The Role of Carbon-Based Plant Secondary Metabolites in Decomposition in Terrestrial Ecosystems. The American Naturalist 132, 869–883.
Hothorn, T., Zeileis, A., Farebrother, R.W., Cummins, C., Millo, G., Mitchell, D., 2015. lmtest: Testing linear regression models [WWW Document]. R Package Version 0.9-3.4.
Jansen, B., Kalbitz, K., McDowell, W.H., 2014. Dissolved Organic Matter: Linking Soils and Aquatic Systems. Vadose Zone Journal 13, 0. doi:10.2136/vzj2014.05.0051
Kaiser, K., Kalbitz, K., 2012. Cycling downwards - dissolved organic matter in soils. Soil Biology and Biochemistry 52, 29–32. doi:10.1016/j.soilbio.2012.04.002
Kellerman, A.M., Dittmar, T., Kothawala, D.N., Tranvik, L.J., 2014. Chemodiversity of dissolved organic matter in lakes driven by climate and hydrology. Nature Communications 5, 1–8. doi:10.1038/ncomms4804
Kendall, K.A., Shanley, J.B., Mcdonnell, J., 1999. A Hydrometric and Geochemical Approach to Test the Transmissivity Feedback Hypothesis during Snowmelt feedback hypothesis during snowmelt. Journal of Hydrology 219, 188–205. doi:10.1016/S0022-1694(99)00059-1
Kind, T., Fiehn, O., 2010. Advances in structure elucidation of small molecules using mass spectrometry. Bioanalytical Reviews 2, 23–60. doi:10.1007/s12566-010-0015-9
Kramer, N., Wohl, E.E., Harry, D.L., 2012. Using ground penetrating radar to “unearth” buried beaver dams. Geology 40, 43–46.
Lenth, R., 2016. Package lsmeans: least-squares means. CRAN Repository.
Liang, C., Schimel, J.P., Jastrow, J.D., 2017. The importance of anabolism in microbial control over soil carbon storage. Nature Microbiology 2, 17105. doi:10.1038/nmicrobiol.2017.105
Livers, B., Wohl, E., 2016. Sources and interpretation of channel complexity in forested subalpine streams of the Southern Rocky Mountains. Water Resources Research 52, 3910–3929. doi:10.1002/2015WR018306
Maas, A., Dozier, A., Manning, D.T., Goemans, C., 2017. Water storage in a changing environment: The impact of allocation institutions on value. Water Resources Research 53, 672–687. doi:10.1002/2016WR019239
Marcatelli, A.., Baxter, C.V., Mineau, M.M., Hall, R.O., 2011. Quantity and quality: unifying food web and exosystem perspectives on the role of resource subsidies in freswhaters. Ecology 92, 1215–1225. doi:10.1890/10-2240.1

Oksanen, J., Kindt, R., Legendre, P., O'Hara, B., Stevens, H.H., 2007. The vegan package.
Opsahl, S.P., Zepp, R.G., 2001. Photochemically-induced alteration of stable carbon isotope ratios (delta C-13) in terrigenous dissolved organic carbon. Geophysical Research Letters 28, 2417–2420. doi:10.1029/2000GL012686
Polvi, L.E., Wohl, E., 2013. Biotic Drivers of Stream Planform. BioScience 63, 439–452. doi:10.1525/bio.2013.63.6.6
Price-Whelan, A., Dietrich, L.E.P., Newman, D.K., 2006. Rethinking "secondary" metabolism: physiological roles for phenazine antibiotics. Nature Chemical Biology 2, 71–78. doi:10.1038/nchembio764
Puttock, A., Graham, H.A., Cunliffe, A.M., Elliott, M., Brazier, R.E., 2017. Eurasian beaver activity increases water storage, attenuates flow and mitigates diffuse pollution from intensively-managed grasslands. Science of the Total Environment 576, 430–443. doi:10.1016/j.scitotenv.2016.10.122
R Core Team: A language and environment for statistical computing, 2014.
Raymond, P.A., Saiers, J.E., Sobczak, W. V., 2016. Hydrological and biogeochemical controls on watershed dissolved organic matter transport: Pulse- shunt concept. Ecology 97, 5–16. doi:10.1890/14-1684.1
Rumpel, C., Kögel-Knabner, I., 2011. Deep soil organic matter-a key but poorly understood component of terrestrial C cycle. Plant and Soil 338, 143–158. doi:10.1007/s11104-010-0391-5
Sapkal, R.S., Valunjkar, S.S., 2013. Development and Sensitivity Analysis of Water Quality Index for Evaluation of Surface Water for Drinking Purpose. Internation Journal of Civil Engineering and Technology 4, 119–134.
Schimel, J., Balser, T., Wallenstein, M., 2007. Microbial stress-response physiology and its implications for ecosystem function. Ecology 88, 1386–1394.
Seitzinger, S.P., Hartnett, H., Lauck, R., Mazurek, M., Minegishi, T., Spyres, G., Styles, R., 2005. Molecular-level chemical characterization and bioavailability of dissolved organic matter in stream water using electrospray-ionization mass spectrometry. Limnology and Oceanography 50, 1–12. doi:10.4319/lo.2005.50.1.0001
Singer, G. a., Fasching, C., Wilhelm, L., Niggemann, J., Steier, P., Dittmar, T., Battin, T.J., 2012. Biogeochemically diverse organic matter in Alpine glaciers and its downstream fate. Nature Geoscience 5, 710–714. doi:10.1038/ngeo1581
Singer, G., Besemer, K., Schmitt-Kopplin, P., Hödl, I., Battin, T.J., 2010. Physical heterogeneity increases biofilm resource use and its molecular diversity in stream mesocosms. PLoS ONE 5. doi:10.1371/journal.pone.0009988
Sutfin, N.A., Wohl, E., 2017. Substantial soil organic carbon retention along floodplains of mountain streams. Journal of Geophysical Research: Earth Surface 122, 1325–1338. doi:10.1002/2016JF004004
Sutfin, N.A., Wohl, E.E., Dwire, K.A., 2016. Banking carbon: A review of organic carbon storage and physical factors influencing retention in floodplains and riparian ecosystems. Earth Surface Processes and Landforms 41, 38–60. doi:10.1002/esp.3857
Torres-Ruiz, M., Wehr, J.D., Perrone, A. a., 2007. Trophic relations in a stream food web: importance of fatty acids for macroinvertebrate consumers. Journal of the North American Benthological Society 26, 509–522. doi:10.1899/06-070.1
Trussell, R., MD, U., 1978. The formation of trihalomethanes. American Water Works Association Journal 70, 604–612.

van den Berg, R.A., Hoefsloot, H.C.J., Westerhuis, J.A., Smilde, A.K., van der Werf, M.J., 2006. Centering, scaling, and transformations: improving the biological information content of metabolomics data. BMC Genomics 7, 142. doi:10.1186/1471-2164-7-142

Vannote, R.L., Minshall, W.G., Cummins, K.W., Sedell, J.R., Cushing, C.E., 1980. The river continuum concept. Canadian Journal of Fisheries and Aquatic Sciences 37, 130–137.

Ward, N.D., Bianchi, T.S., Medeiros, P.M., Seidel, M., Richey, J.E., Keil, R.G., Sawakuchi, H.O., 2017. Where Carbon Goes When Water Flows: Carbon Cycling across the Aquatic Continuum. Frontiers in Marine Science 4. doi:10.3389/fmars.2017.00007

Wegener, P., Covino, T., Wohl, E., 2017. Beaver- mediated lateral hydrologic connectivity, fluvial carbon and nutrient flux, and aquatic ecosystem metabolism. Water Resources Research 53, 4606–4623.

Wehrens, R., Mevik, B.-H., 2007. pls: Partial Least Squares Regression (PLSR) and Principal Component Regression (PCR). R Package Version 2.1-0.

Weishaar, J., Aiken, G., Bergamaschi, B., Fram, M., Fujii, R., Mopper, K., 2003. Evaluation of specific ultra-violet absorbance as an indicator of the chemical content of dissolved organic carbon. Environmental Science and Technology 37, 4702–4708. doi:10.1021/es030360x

Williams, D.H., Stone, M.J., Hauck, P.R., Rahman, S.K., 1989. Why Are Secondary Metabolites (Natural Products) Biosynthesized? Journal of Natural Products 52, 1189–1208. doi:10.1021/np50066a001

Wohl, E., 2013. Landscape-scale carbon storage associated with beaver dams. Geophysical Research Letters 40, 3631–3636. doi:10.1002/grl.50710

Wohl, E., Dwire, K., Sutfin, N., Polvi, L., Bazan, R., 2012. Mechanisms of carbon storage in mountainous headwater rivers. Nature Communications 3, 1263. doi:10.1038/ncomms2274

Xia, J., Wishart, D.S., 2016. Using MetaboAnalyst 3.0 for Comprehensive Metabolomics Data Analysis. Current Protocols in Bioinformatics 55, 10.1-14.10.91.

CHAPTER 5- CONCLUSIONS

SUMMARY

Arctic and alpine watersheds are experiencing dramatic shifts in function resulting from climate changes. The ability of these sensitive ecosystems to transform and sequester carbon (C) is jeopardized, although results from this dissertation suggest both systems are remarkably resilient to destabilizing change. Shrub expansion across northern hemispheres is increasing the relative efficiency of microbial metabolism, sequestering new C inputs belowground while protecting older C sources from priming. The downslope transport of dissolved organic matter (DOM), which integrates hillslope and riparian regions and increases connectivity across the terrestrial-aquatic interface, transforms the chemical composition of mobilized organic matter. As microbial communities sequentially process DOM flowing downslope, they release compounds that resist further turnover to adjacent stream ecosystems. The accumulation of similar products in the ocean suggests deposition and burial of these microbial derivatives could reduce CO_2 efflux of terrestrial-derived organic matter to the atmosphere. We also found that the preservation of ecosystem complexity facilitates interactions between microbial decomposers and substrates that facilitate ecosystem function. Together, our results suggest that complex, functioning ecosystems are intrinsically valuable, providing critical ecosystem services including C sequestration and climate change resilience.

RECOMMENDATIONS FOR FUTURE WORK

A critical, yet poorly constrained variable in our ecological understanding of soils and sediments is the sorption potential of metabolites on the mineral matrix. If newly exposed minerals—at the permafrost thaw front or recently scoured hyporheic zone—are highly sorptive, terrestrial-derived products could be stabilized, increasing organic matter formation and

minimizing CO_2 feedbacks to climate change. Additionally, downslope or downstream mobility of DOM could be limited by physicochemical stabilization, reducing fluxes between pore spaces and substrate delivery across the terrestrial-aquatic interface. Thus, it is critical to quantify the leaching potential of new DOM inputs and the duration that microbial byproducts remain sorbed on the mineral matrix.

Despite remarkable ecosystem resilience, there are thresholds beyond which exist rapid and irreversible environmental change. Thus, it is imperative we adopt a watershed perspective when modeling ecosystem responses to, and modification of, global climate. In particular, we must determine how complex hydrobiogeochemical systems function, and explicitly parameterize the efficiency of microbial metabolism across multiple temporal and spatial scales.

SUPPLEMENTAL INFORMATION- CHAPTER 2

Supplemental Table 2.1. Mean (± 1 S.E.) annual soil temperatures (at different depths belowground) and cumulative precipitation for the years of this study (2014, 2015) and the ten-year average (2005-2015).

Year	Surface soil temperature (°C)	Soil temperature at 5 cm (°C)	Soil temperature at 10 cm (°C)	Soil temperature at 20 cm (°C)	Cumulative precipitation (mm)
2014	5.2 (0.1)	5.7 (0.2)	3.4 (0.1)	3.4 (0.1)	238.8
2015	5.4 (0.1)	6.8 (0.2)	4.2 (0.1)	4.1 (0.1)	209.3
10-year average	5.6 (0.2)	5.8 (0.2)	3.5 (0.1)	3.1 (0.1)	206.3

Supplemental Table 2.2. Biogeochemical characteristics of organic and mineral soil horizons underlying *B. nana* and *E. vaginatum* (conditional on month). The average followed by the standard error (± 1 S.E.) in parentheses for soil C and N, dissolved C and N (DOC, TDN), and microbial biomass C and N (MBC, MBN) (n=4). The level of significance from the 3-way ANOVA model including soil depth (D), vegetation (V), treatment (T), all 2-way and 3-way interactions are reported as * $p < 0.05$, ** $p < 0.01$, *** $p < 0.001$, or non-significant (ns).

July

Depth	Vegetation/ Treatment	Soil C ($g\ m^{-2}$)	Soil N ($g\ m^{-2}$)	TOC ($g\ m^{-2}$)	TDN ($g\ m^{-2}$)	TIN ($g\ m^{-2}$)	MBC ($g\ m^{-2}$)	MBN ($g\ m^{-2}$)
	B. nana							
Lower								
	Control	2634.49 (875.21)	114.63 (33.40)	7.38 (3.48)	0.91 (0.47)	11.46 (7.67)	12.49 (8.40)	3.33 (1.38)
	Amended	4255.49 (530.57)	148.20 (8.89)	5.72 (3.93)	1.09 (0.48)	17.90 (11.29)	27.96 (19.90)	3.78 (2.65)
	E. vaginatum							
	Control	3385.44 (1467.15)	42.40 (16.96)	3.84 (1.42)	0.21 (0.08)	5.63 (2.43)	21.16 (10.24)	2.07 (1.09)
	Amended	2911.85 (762.47)	117.36 (41.66)	2.06 (0.59)	0.13 (0.01)	2.47 (0.86)	14.79 (5.10)	1.59 (0.44)
Upper	*B. nana*							
	Control	2401.40 (34.00)	57.28 (7.96)	6.39 (2.03)	0.23 (0.07)	1.99 (1.11)	26.81 (11.58)	3.04 (1.38)
	Amended	2415.64 (44.44)	51.29 (16.92)	2.38 (1.17)	0.16 (0.05)	26.59 (14.71)	9.15 (3.46)	1.01 (0.51)
	E. vaginatum							
	Control	2120.01 (72.31)	38.28 (12.00)	2.12 (1.32)	0.07 (0.04)	1.14 (0.83)	6.71 (3.44)	0.63 (0.38)
	Amended	2436.32 (32.61)	26.14 (5.28)	3.02 (0.60)	0.19 (0.08)	4.19 (2.06)	14.65 (3.82)	2.96 (1.24)
D		ns	***	ns	ns	*	ns	ns
V		ns	*	ns	ns	**	ns	ns
T		ns	ns	ns	ns	ns	ns	ns
D*V		ns	ns	ns	ns	ns	ns	ns
D*T		ns	ns	ns	ns	ns	ns	ns
V*T		ns	ns	ns	ns	ns	ns	ns
D*V*T		ns	ns	ns	ns	ns	ns	ns

September

Depth	Vegetation/ Treatment	Soil C (g m^{-2})	Soil N (g m^{-2})	TOC (g m^{-2})	TDN (g m^{-2})	TIN (g m^{-2})	MBC (g m^{-2})	MBN (g m^{-2})
Lower	*B. nana*							
	Control	837.86 (342.95)	12.93 (2.00)	0.87 (0.29)	0.12 (0.04)	1.74 (0.64)	2.69 (0.89)	0.10 (0.07)
	Amended	2319.04 (1076.70)	80.14 (34.12)	1.92 (1.44)	0.24 (0.13)	4.16 (2.06)	2.48 (1.21)	0.42 (0.15)
	E. vaginatum							
	Control	1857.14 (707.02)	58.05 (23.25)	2.67 (1.15)	0.21 (0.56)	11.09 (7.16)	13.01 (7.17)	1.17 (0.61)
	Amended	4249.82 (266.17)	115.91 (11.22)	2.80 (1.09)	0.56 (0.31)	19.22 (9.90)	9.69 (3.61)	0.93 (0.40)
Upper	*B. nana*							
	Control	1452.39 (629.49)	27.50 (19.15)	1.98 (0.96)	0.09 (0.03)	3.14 (1.79)	12.62 (10.15)	0.83 (0.56)
	Amended	2242.58 (41.30)	53.87 (3.53)	1.76 (0.46)	0.09 (0.03)	1.46 (0.86)	8.97 (3.47)	0.96 (0.48)
	E. vaginatum							
	Control	1877.90 (303.74)	29.53 (7.30)	1.79 (0.74)	0.09 (0.03)	3.49 (1.19)	11.11 (3.80)	0.95 (0.43)
	Amended	2322.94 (52.22)	30.96 (12.44)	2.45 (0.35)	0.11 (0.01)	1.60 (0.12)	12.14 (1.11)	1.27 (0.16)
D		ns	*	ns	*	ns	ns	*
V		*	ns	ns	ns	*	ns	ns
T		**	**	ns	ns	ns	ns	*
D*V		ns	ns	ns	ns	ns	ns	ns
D*T		ns	ns	ns	ns	ns	ns	ns
V*T		ns	ns	ns	ns	ns	ns	ns
D*V*T		ns	ns	ns	ns	ns	ns	ns

May

Depth	Vegetation/ Treatment	Soil C ($g\ m^{-2}$)	Soil N ($g\ m^{-2}$)	TOC ($g\ m^{-2}$)	TDN ($g\ m^{-2}$)	TIN ($g\ m^{-2}$)	MBC ($g\ m^{-2}$)	MBN ($g\ m^{-2}$)
Lower	*B. nana*							
	Control	1438. 41 (713.34)	73.56 (37.31)	4.86 (1.72)	0.42 (0.26)	6.71 (4.16)	15.34 (5.99)	1.09 (0.66)
	Amended	1973.06 (739.63)	102.91 (35.05)	5.14 (2.23)	0.94 (0.44)	14.85 (6.59)	24.52 (13.22)	2.62 (1.51)
	E. vaginatum							
	Control	2068.51 (1391.96)	50.27 (31.61)	2.85 (1.60)	0.18 (0.10)	1.38 (0.54)	21.87 (17.49)	1.96 (1.75)
	Amended	3689.49 (773.18)	102.80 (24.69)	7.13 (2.00)	0.55 (0.21)	9.43 (4.53)	48.31 (14.87)	3.74 (1.20)
Upper	*B. nana*							
	Control	1951.19 (165.00)	53.95 (3.47)	6.95 (0.82)	0.42 (0.19)	7.35 (5.37)	41.21 (8.22)	3.29 (0.60)
	Amended	1899.22 (442.18)	52.35 (11.82)	4.30 (1.31)	0.29 (0.08)	4.37 (2.29)	46.92 (28.02)	2.72 (0.96)
	E. vaginatum							
	Control	1641.00 (502.48)	30.79 (6.95)	3.34 (1.10)	0.12 (0.03)	1.29 (0.13)	9.88 (3.30)	0.92 (0.30)
	Amended	2466.89 (46.92)	50.91 (3.40)	7.13 (1.58)	0.20 (0.03)	0.98 (0.13)	39.41 (9.67)	1.99 (0.26)
D		ns	*	ns	ns	*	ns	ns
V		ns	ns	ns	ns	*	ns	ns
T		ns	ns	ns	ns	ns	*	*
D*V		ns	ns	ns	ns	ns	ns	ns
D*T		ns	ns	ns	ns	*	ns	ns
V*T		ns	ns	*	ns	ns	*	ns
D*V*T		ns	ns	ns	ns	ns	ns	ns

Supplemental Table 2.3a**.** Biogeochemical characteristics of soils underlying *B. nana* and *E. vaginatum* for total CO_2 efflux, LMW-C conversion to CO_2, soil organic matter-derived CO_2 (SOM-CO_2), priming-derived CO_2 (primed pool and %), microbial substrate use efficiency (SUE), LMW-C retention efficiency (Ret. Eff.), dissolved C, total N, inorganic N (TOC, TDN, TIN), and microbial biomass C and N (MBC, MBN) (n=4). All values are reported on a g m^{-2} basis, unless otherwise noted. The level of significance from the 3-way ANOVA model including vegetation (V), treatment (T), month (M), all 2-way and 3-way interactions are reported as * $p < 0.05$, ** $p < 0.01$, *** $p < 0.001$, or non-significant (ns). The level of significance from the 3-way ANOVA model for soil C is reported numerically with bolded text for significant results.

Source of variance	CO_2 Flux	LWM C-CO_2	SOM-CO_2	Priming (%)	SUE	Ret. Eff.	TOC	TDN	TIN (ug m^{-2})	MBC	MBN
Soil C	0.94	0.31	0.99	0.78	0.51	0.38	0.23	0.18	**0.02**	**0.001**	0.06
T	***						*	ns	ns	ns	ns
V	**	***	ns	ns	ns	*	ns	***	ns	ns	ns
M	***	ns	**	ns	**	ns	***	ns	ns	***	**
T*V	**						***	ns	ns	ns	ns
T*M	***						ns	ns	ns	ns	ns
V*M	ns	ns	ns	ns	ns	ns	ns	ns	*	ns	ns
T*V*M	ns						*	ns	ns	ns	ns

Supplemental Table 2.3b. Biogeochemical characteristics of soils underlying *B. nana* and *E. vaginatum* where microbial biomass C (MBC) and total inorganic N (TIN) are normalized to soil C content (g^{-1} soil C). The level of significance from the 3-way ANOVA model including vegetation (V), treatment (T), month (M), all 2-way and 3-way interactions are reported as * $p < 0.05$, ** $p < 0.01$, *** $p < 0.001$, or non-significant (ns).

Source of variance	MBC (g C g^{-1} soil C)	TIN (µg N g^{-1} soil C)
T	ns	ns
V	ns	ns
M	***	ns
T*V	ns	ns
T*M	ns	ns
V*M	ns	*
T*V*M	ns	ns

Supplemental Table 2.4. Biogeochemical characteristics of soils underlying *B. nana* and *E. vaginatum* normalized to soil C. The average followed by the standard error (± 1 S.E.) in parentheses for soil C and N, dissolved C and N (TOC, TDN), and microbial biomass C and N (MBC, MBN) (n=4). All values are reported on a g per gram soil C basis. The level of significance from the 3-way ANOVA model including treatment (T), vegetation (V), and month (M), all 2-way and 3-way interactions are reported as * $p < 0.05$, ** $p < 0.01$, *** $p < 0.001$, or non-significant (ns).

Month	Vegetation/ Treatment	CO_2	DOC	Soil N	TDN	TIN	MBC	MBN
July	*B. nana*							
	Control	2.11 (0.25)	10.53 (2.03)	31.08 (0.99)	0.73 (0.25)	0.004 (0.002)	22.64 (7.41)	2.71 (0.99)
	Amended	3.54 (0.76)	3.19 (0.96)	28.1 (4.83)	0.46 (0.11)	0.012 (0.005)	15.48 (2.79)	1.77 (0.19)
	E. vaginatum							
	Control	2.64 (0.56)	5.08 (1.06)	15.56 (2.09)	0.23 (0.05)	0.002 (0.001)	18.54 (1.97)	1.65 (0.24)
	Amended	6.67 (0.18)	4.32 (0.88)	23.09 (8.21)	0.26 (0.07)	0.002 (0.001)	23.96 (5.53)	4.04 (1.51)
September	*B. nana*							
	Control	5.93 (2.28)	5.29 (1.67)	13.89 (7.91)	0.42 (0.06)	0.002 (0.001)	23.69 (12.10)	1.61 (0.69)
	Amended	4.47 (0.82)	3.64 (0.93)	27.92 (3.14)	0.32 (0.10)	0.002 (0.001)	15.33 (3.25)	1.63 (0.45)
	E. vaginatum							
	Control	3.11 (0.73)	5.15 (0.86)	19.45 (3.83)	0.40 (0.12)	0.005 (0.002)	23.58 (5.47)	1.95 (0.57)
	Amended	7.57 (2.16)	8.69 (1.87)	23.63 (2.48)	0.35 (0.02)	0.002 (0.001)	48.73 (10.42)	2.88 (0.41)
May	*B. nana*							
	Control	0.78 (0.16)	15.32 (3.72)	33.17 (1.90)	0.95 (0.29)	0.005 (0.002)	65.71 (16.93)	5.08 (0.89)
	Amended	8.57 (3.72)	7.19 (0.41)	34.22 (3.15)	0.67 (0.16)	0.006 (0.002)	55.44 (17.97)	3.60 (0.54)
	E. vaginatum							
	Control	0.57 (0.06)	4.93 (1.31)	13.20 (3.26)	0.23 (0.04)	0.001 (0.00)	18.61 (5.81)	1.57 (0.49)
	Amended	4.60 (0.49)	2.77 (0.45)	23.16 (2.36)	0.25 (0.08)	0.005 (0.002)	12.45 (1.81)	1.25 (0.18)

Source of variance							
T	***	*	**	ns	ns	ns	ns
V	ns	ns	**	***	ns	ns	ns
M	***	**	ns	ns	ns	***	**
T*V	*	*	ns	ns	ns	ns	ns
T*M	***	ns	ns	ns	ns	ns	ns
V*M	ns	ns	**	ns	**	ns	ns
T*V*M	ns	*	*	ns	ns	ns	ns

Supplemental Table 2.5. LMW-C fate in soils underlying *B. nana* and *E. vaginatum*. The average followed by the standard error (± 1 S.E.) in parentheses for LMW-C conversion to CO_2, soil organic matter-derived CO_2 (SOM-CO_2), priming-derived CO_2 (primed pool and %), microbial substrate use efficiency (SUE), and LMW-C retention efficiency (Ret. Eff.) (n=4). The level of significance from the 2-way ANOVA model including vegetation (V) and month (M), and all 2-way interactions are reported as * $p < 0.05$, ** $p < 0.01$, *** $p < 0.001$, or non-significant (ns).

Month	Vegetation/ Treatment	LWM C-CO_2 (g m^{-2})	SOM-CO_2 (g m^{-2})	Primed (g m^{-2})	Primed (%)	SUE	Ret. Eff.
July	*B. nana*						
	Amended	3.85 (3.22)	8.27 (1.28)	8.27 (1.28)	-17.12 (16.64)	0.47 (0.15)	3.06 (1.83)
	E. vaginatum						
	Amended	6.38 (1.22)	13.03 (2.65)	13.02 (2.65)	5.36 (15.35)	0.35 (0.09)	1.46 (0.48)
September	*B. nana*						
	Amended	5.23 (1.75)	5.23 (0.71)	5.23 (0.71)	-30.44 (14.50)	0.28 (0.05)	2.85 (0.58)
	E. vaginatum						
	Amended	12.37 (3.03)	3.04 (0.94)	3.04 (0.94)	-24.54 (7.03)	0.09 (0.04)	0.84 (0.36)
May	*B. nana*						
	Amended	5.19 (3.84)	7.71 (1.17)	7.71 (1.17)	-29.95 (10.40)	0.50 (0.15)	8.20 (3.14)
	E. vaginatum						
	Amended	15.46 (6.81)	8.09 (2.80)	8.09 (2.80)	-23.11 (16.07)	0.66 (0.04)	0.88 (0.34)
Source of variance							
V		***	ns	ns	ns	ns	**
M		*	**	ns	ns	**	ns
V*M		ns	ns	ns	ns	ns	ns

Supplemental Table 2.6. Potential extracellular enzyme activities of soils underlying *B. nana* and *E. vaginatum*. The average followed by the standard error (± 1 S.E.) in parentheses for seven hydrolytic enzymes (n=4). Potential activities are reported in nmol activity g dry soil^{-1} hr^{-1}. The level of significance from the 3-way ANOVA model including vegetation (V), treatment (T), month (M), all 2-way and 3-way interactions are reported as * $p < 0.05$, ** $p < 0.01$, *** $p < 0.001$, or non-significant (ns).

Month	Vegetation/ Treatment	CB	AG	BG	XYL	LAP	NAG	AP
July	*B. nana*							
	Control	4553.48 (742.21)	429.23 (142.10)	1040.04 (257.82)	570.59 (125.84)	2537.18 (920.81)	141.85 (23.36)	8217.36 (1223.42)
	Amended	3615.39 (729.55)	231.98 (73.78)	545.76 (117.62)	477.95 (76.49)	2375.87 (395.55)	207.36 (46.47)	10453.93 (2975.87)
	E. vaginatum							
	Control	1572.87 (240.63)	159.90 (57.36)	330.38 (101.56)	358.78 (93.74)	798.31 (399.16)	75.86 (13.93)	5153.81 (1737.06)
	Amended	2898.37 (402.32)	213.91 (37.59)	900.59 (253.43)	389.36 (43.37)	1059.70 (200.97)	87.33 (21.19)	4209.36 (318.81)
September	*B. nana*							
	Control	965.42 (438.27)	191.50 (174.21)	86.62 (67.14)	237.67 (120.37)	1007.64 (651.01)	109.51 (56.13)	5679.99 (3230.04)
	Amended	3107.00 (596.83)	311.35 (75.88)	689.92 (253.43)	462.17 (102.17)	1477.13 (375.88)	147.00 (3.35)	6369.95 (1179.31)
	E. vaginatum							
	Control	2392.63 (721.80)	232.58 (81.94)	305.14 (148.47)	419.46 (128.81)	947.87 (305.70)	130.27 (39.71)	4568.26 (1326.97)
	Amended	3989.83 (316.60)	265.08 (99.44)	1087.86 (263.10)	673.41 (164.01)	1710.74 (351.47)	158.745 (24.62)	7288.91 (1628.80)
May	*B. nana*							
	Control	689.70 (182.05)	70.31 (23.03)	186.15 (81.17)	103.54 (19.62)	456.15 (94.69)	38.60 (1.37)	1301.82 (83.57)
	Amended	913.95 (203.89)	205.48 (121.58)	350.60 (75.90)	247.45 (112.64)	565.99 (113.28)	58.10 (3.51)	1469.47 (426.73)
	E. vaginatum							
	Control	869.40 (197.59)	191.83 (121.52)	351.53 (101.87)	270.70 (109.53)	500.93 (155.44)	35.20 (3.95)	872.61 (211.27)
	Amended	651.19 (61.00)	185.27 (141.23)	246.78 (11.98)	219.89 (126.47)	456.37 (48.07)	41.02 (4.66)	977.80 (147.40)

Source of variance							
T	ns	ns	**	ns	ns	ns	ns
V	*	ns	ns	ns	ns	ns	ns
M	ns	ns	ns	**	***	***	ns
T*V	ns	ns	ns	ns	ns	ns	ns
T*M	ns	ns	ns	ns	ns	ns	ns
V*M	ns	ns	ns	ns	*	ns	ns
T*V*M	ns	**	ns	ns	ns	ns	ns

SUPPLEMENTAL INFORMATION- CHAPTER 3

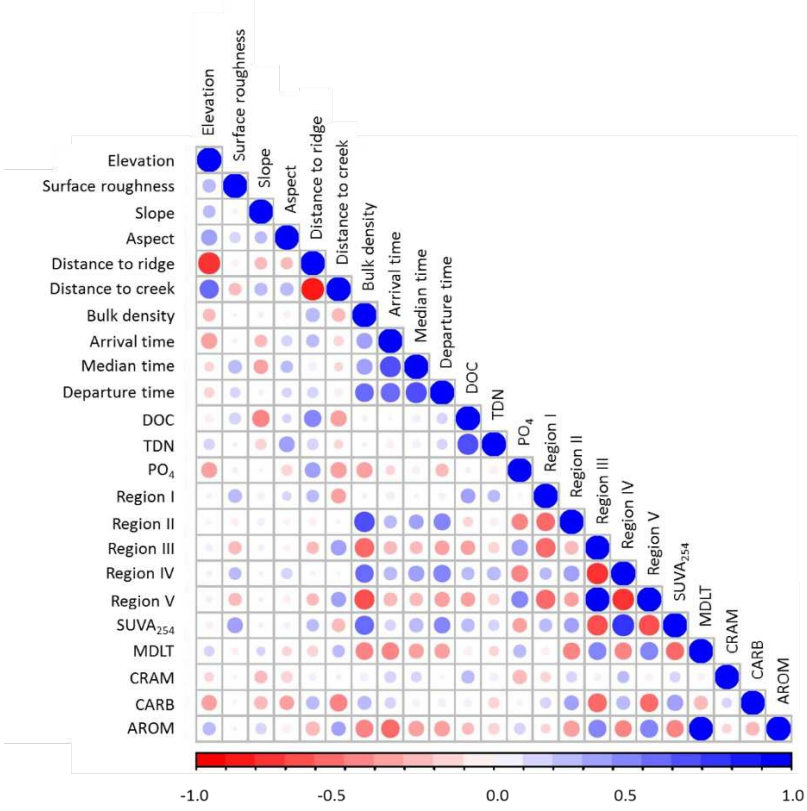

Supplemental Figure 3.1. Correlation plot displays a matrix of variables. The color scale indicates Spearman correlations between spatial variables, bromide interception, bulk chemistry, fluorescence spectroscopy, and NMR spectroscopy (red, negative; blue, positive). Spatial characteristics include elevation (m); surface roughness, a measure of terrain; slope angle (degrees); aspect, relative to true north (degrees), distance from hillslope ridge or from Imnavait Creek (m); bulk density (g cm^{-3}). Arrival, median, and departure times refer to the interception of 5%, 50%, or 95% of the bromide tracer. DOC, dissolved organic carbon (umol L-1); TDN, total dissolved nitrogen; PO_4, phosphate; Regions I and II are related to simple aromatic proteins, region III to fulvic-type acids, region IV to soluble microbial-type proteins, region V to humic-type acids; $SUVA_{254}$, DOC normalized specific UV absorbance at 254 nm. MDLT, material derived from linear terpenoids (0.6-1.6 ppm); CRAM, carboxylic-rich alicylic material (1.6-3.2 ppm); CARB, carbohydrates (3.2-4.5 ppm); AROM, aromatics (6.5-8.5 ppm), in percent relative to the integration of all NMR spectra.

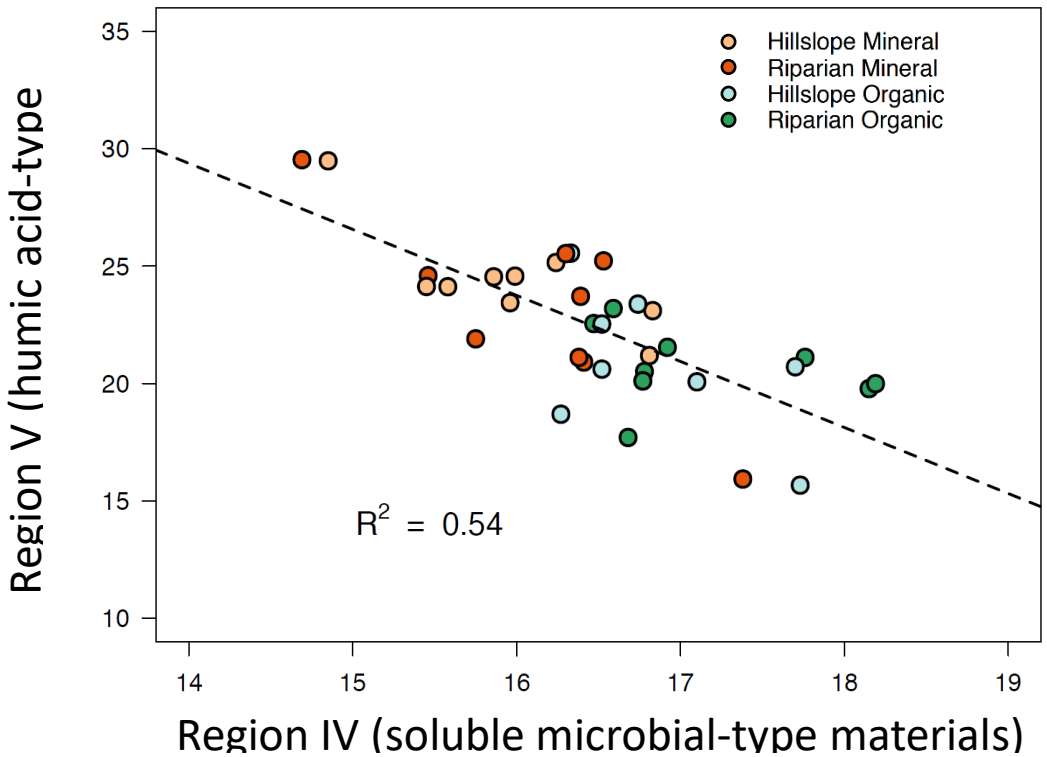

Supplemental Figure 3.2. Linear regression of EEMS region IV (soluble microbial-type products) against EEMS region V (humic-type acids). Samples collected from the mineral horizon are displayed in red colors, those collected from the organic horizon are displayed in green colors. Samples do not separate across landscape position.

Supplemental Table 3.3. Transit distribution times for recovered bromide. At each site, samples were collected from the organic horizon or along the mineral-permafrost interface at hillslope or riparian sites over a ten-day sampling period. Values are the mean number of hours it took to intercept 5% (arrival), 50% (median), or 100% (departure) of the added bromide, with standard errors reported in parentheses (n=9). The level of significance from the repeated measures ANOVA model including site (S), depth (D), distance from application (X), time (T), and all interactions are reported as * $p < 0.05$, ** $p < 0.01$, *** $p < 0.001$, or non-significant (ns).

Site	Depth	Arrival Time (hr)	Median Arrival (hr)	Departure Time (hr)	Arrival velocity (m hr^{-1})	Median velocity (m hr^{-1})	Departure velocity (m hr^{-1})
Hillslope	Mineral	58.94 (10.08)	140.64 (14.76)	225.50 (4.77)	69.55 (15.86)	162.84 (27.38)	271.44 (46.14)
	Organic	43.69 (10.74)	115.55 (15.82)	201.18 (17.63)	60.91 (12.14)	193.21 (47.15)	370.24 (97.88)
Riparian	Mineral	41.54 (8.77)	144.86 (19.17)	227.85 (4.97)	52.79 (19.70)	163.50 (34.74)	275.23 (47.55)
	Organic	23.37 (5.48)	86.03 (14.32)	185.19 (17.94)	44.72 (15.31)	167.84 (54.37)	325.75 (79.81)

Repeat measures	Time	Velocity
S	ns	ns
D	**	ns
X	ns	**
T	***	***
S*D	ns	ns
S*X	ns	ns
S*T	ns	ns
D*X	*	ns
D*T	*	ns
X*T	ns	***
S*D*X	***	*
S*D*T	***	***
D*X*T	***	***
S*D*X*T	***	***

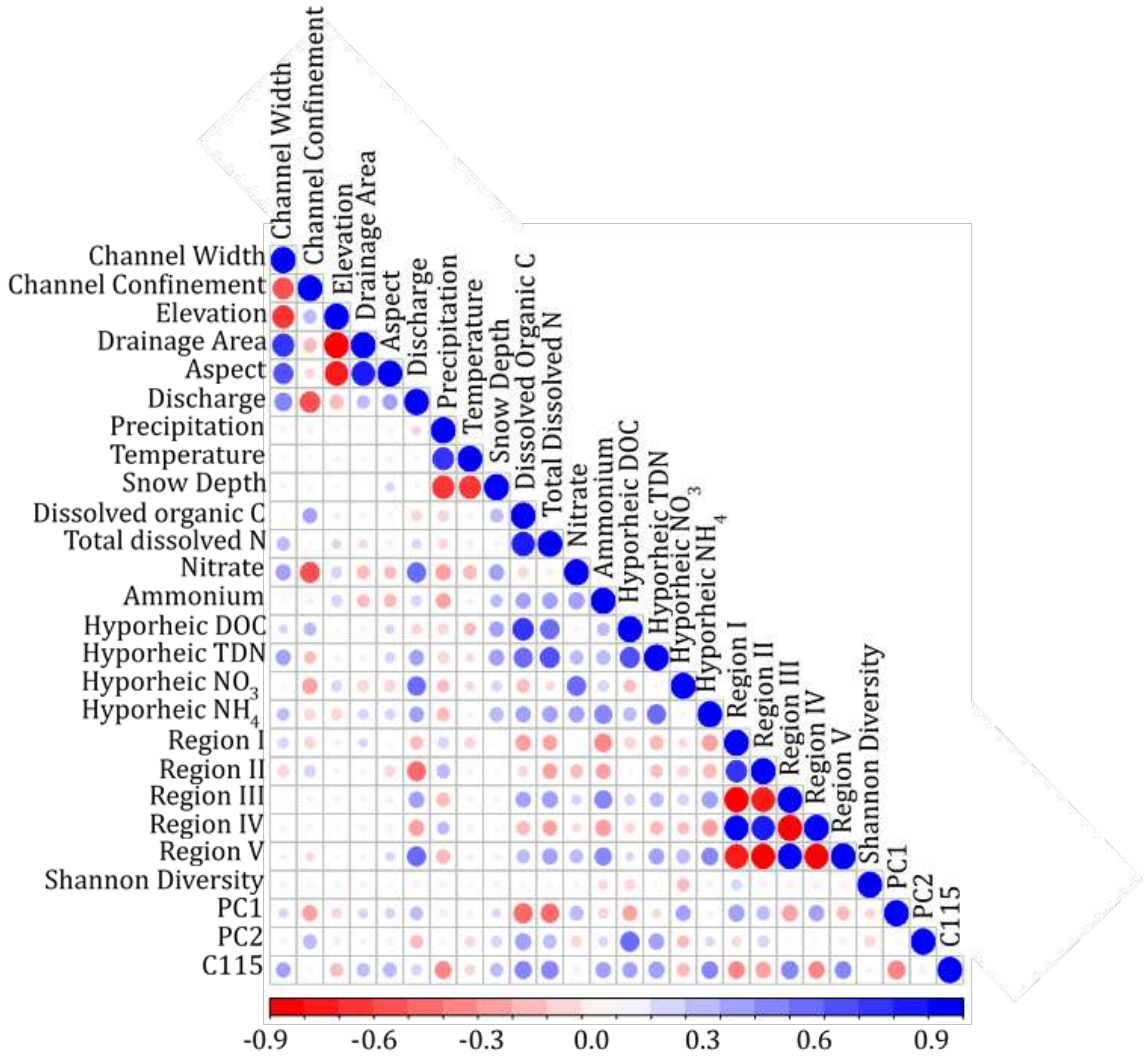

Supplemental Figure 4.1. Correlation plot displays a matrix of potential predictor variables. The color scale indicates Spearman correlations between geomorphology, bulk chemistry, fluorescence spectroscopy, and the intensity of individual metabolites (red, negative; blue, positive). DOC, dissolved organic carbon; TDN, total dissolved nitrogen; NO_3, nitrate; NH_4, ammonium, Region I-V corresponds to EEMS indices; Shannon Diversity, calculated for normalized metabolites; PC1 and PC2, PCA principal components 1 and 2 extracted for metabolites; C115, non-annotated metabolites.

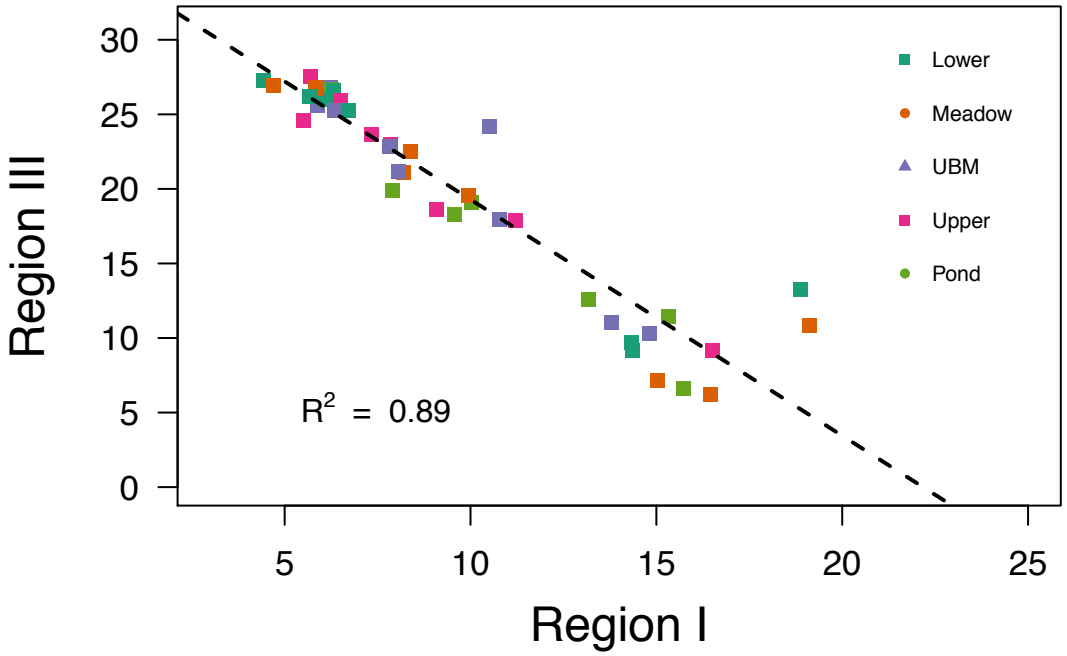

Supplemental Figure 4.2. Linear regression of EEMS region III (fulvic-type acids) against EEMS region I (soluble microbial-type proteins).

a

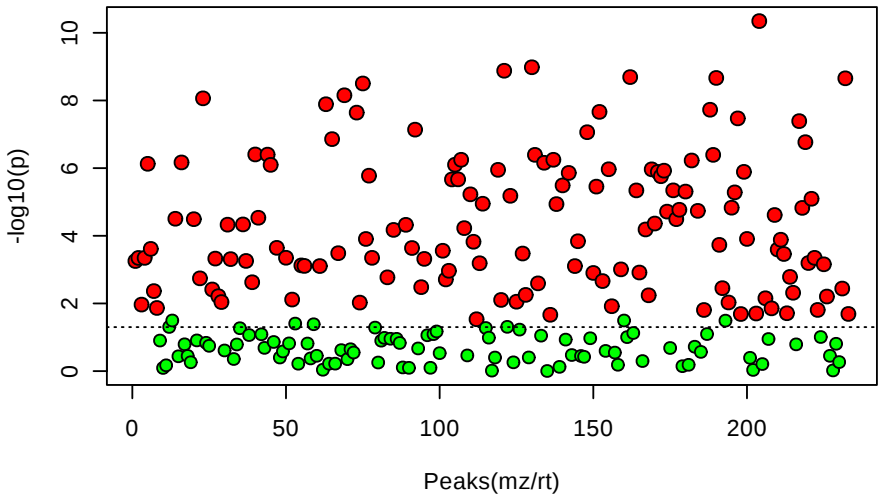

b

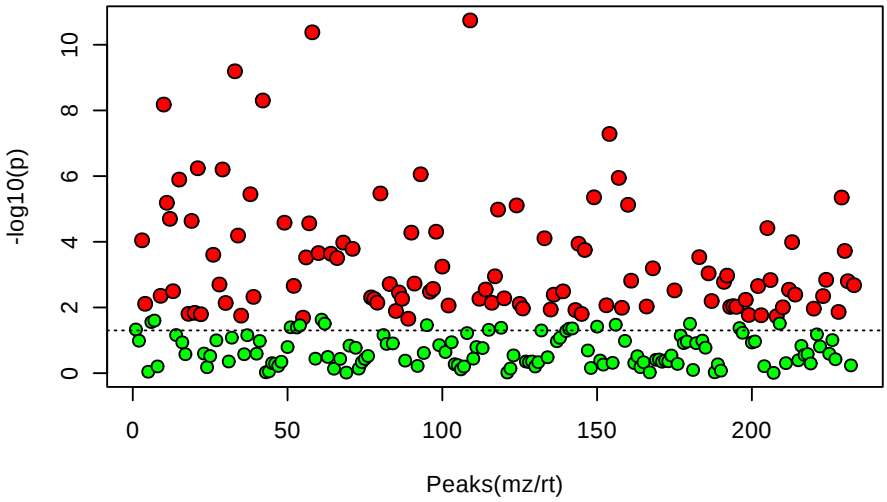

Supplemental Figure 4.3. Metabolites identified by ANOVA analysis that differ significantly across landscape position (upper panel) and sampling period (lower panel) are shown in red. Metabolites that are not significantly different across comparisons are shown in green. Overall, 141 significant features were identified for landscape position and 106 significant features were identified for sampling period.

a

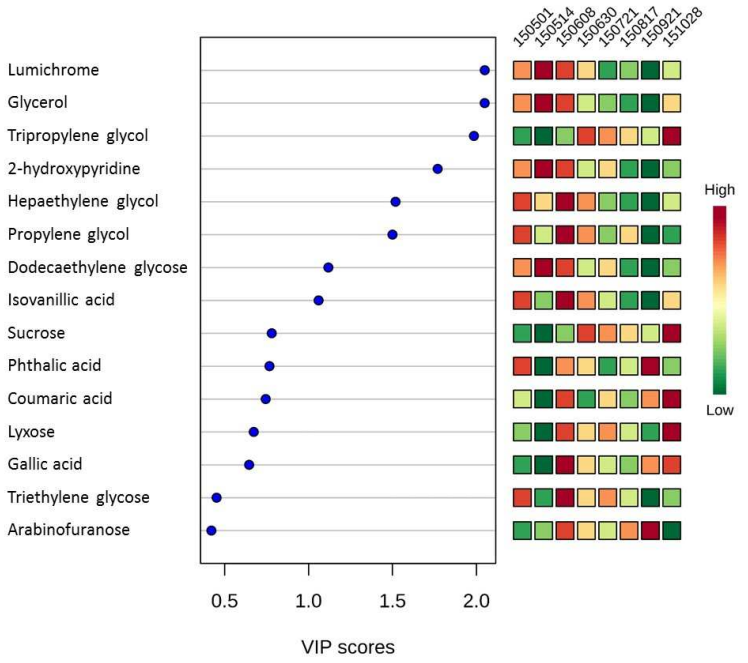

b

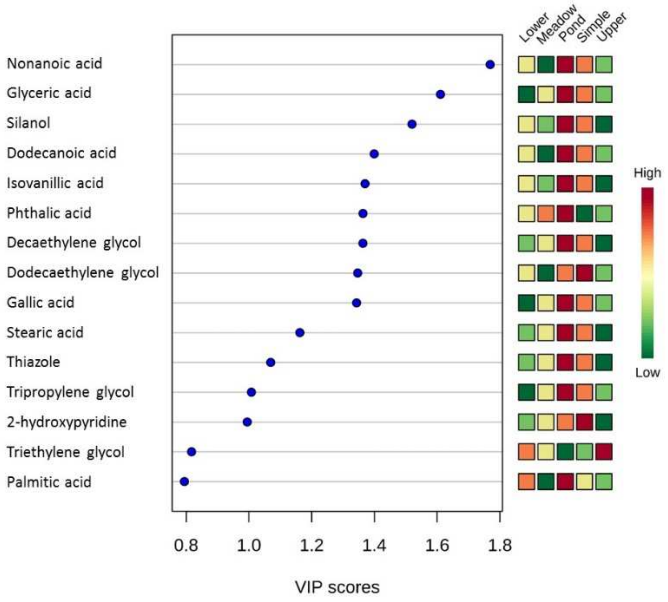

Supplemental Figure 4.4. VIP (variable importance in projection) scores for the top 15 annotated metabolites that separate groups by landscape position (upper) and sampling period (lower). See Supplemental Table 4.1 for metabolite classification.

Supplemental Table 4.1. Results of stepwise multiple liner regression models evaluating relationships between dissolved organic carbon (A), EEMS Region I (B), or EEMS Region III (C), with uncorrelated spatial and environmental components.

A) Dissolved organic carbon

	Estimate	Standard Error	t-value	p-value
(Intercept)	-3.57E+02	3.30E+02	-1.084	0.287
Width	-9.81E-03	9.85E-03	-0.996	0.326
Confine	-1.42E-02	3.36E-03	-4.211	<0.001***
Aspect	8.05E-05	7.41E-05	1.086	0.285
Discharge	-2.05E-02	1.44E-02	-1.428	0.163
Precip	-5.72E-03	6.56E-03	-0.872	0.390
Temp	7.25E-03	1.20E-02	0.603	0.551

Adjusted R^2: 0.29; F statistic: 3.54 on 6 and 32 DF; p-value: 0.01

B) EEMS Region I (simple aromatic proteins)

	Estimate	Standard Error	t-value	p-value
(Intercept)	-7.04E+03	8.69E+03	-0.810	0.424
Width	-1.02E-01	2.59E-01	-0.394	0.696
Confine	-1.09E-01	8.85E-02	-1.235	0.226
Aspect	1.59E-03	1.95E-03	0.812	0.423
Discharge	-1.28E+00	3.78E-01	-3.372	0.002**
Precip	-1.46E-01	1.73E-01	-0.844	0.405
Temp	-1.17E-02	3.17E-01	-0.037	0.971

Adjusted R^2: 0.27; F statistic: 3.36 on 6 and 32 DF; p-value: 0.01

C) EEMS Region III (fulvic-type acids)

	Estimate	Standard Error	t-value	p-value
(Intercept)	9.38E+03	1.49E+04	0.629	0.534
Width	1.07E-01	4.45E-01	0.239	0.812
Confine	1.36E-01	1.52E-01	0.897	0.377
Aspect	-2.11E-03	3.35E-03	-0.628	0.534
Discharge	2.30E+00	6.49E-01	3.542	0.001**
Precip	-3.37E-02	2.97E-01	-0.114	0.910
Temp	3.14E-01	5.44E-01	0.577	0.568

Adjusted R^2: 0.22; F statistic: 2.77 on 6 and 32 DF; p-value: 0.03

Supplemental Table 4.2. Annotated metabolites collected from subalpine watersheds. The absolute ion intensity and quasi-molecular ion *m/z* values are reported for the largest ion fragment within each clustered spectrum (where each spectrum represents a single TMS-derived metabolite). Lower quasi-molecular ion *m/z* values indicate higher compound volatility, and are typically associated with faster elution. Compounds were annotated by querying NIST Standard Reference and KEGG databases, and classified using ClassyFire, a taxonomic database. InChI identifiers were acquired using the PubChem database.

Compound	Absolute Ion Intensity	*m/z*	Retention Time (sec)	Molecular weight (g/mol)	Annotation
Lyxose	106559108.56	73.09	905.41	150.13	Carbohydrate (pentose sugar)
Gallic acid	3830376.39	105.09	990.18	170.12	Gallic acid and derivatives
Dodecaethylene glycol	104264734.57	117.11	1048.61	546.65	Ether (Polyethylene glycols)
2-hydroxypyridine	91460309.74	117.12	883.29	95.10	Pyridinones
Glycerol	288549182.08	131.12	842.33	92.09	Sugar alcohol
Triethylene glycol	548194767.73	144.14	157.86	150.17	Ether (Polyethylene glycols)
Galactose	72522312.97	144.14	259.73	180.16	Hexose (carbohydrate)
Phthalic acid	52173327.64	147.09	616.52	166.14	Benzoic acid
Tripropylene glycol mono-n-butyl ether	20202276.27	151.08	360.78	248.36	Ether (Polyethylene glycols)
Syringic acid	193476048.25	152.07	191.13	198.17	Gallic acid and derivatives
Lumichrome	236666175.84	187.16	755.85	242.23	Flavin pigment
Palmitic acid	5255961.83	189.09	344.35	256.42	Long-chain fatty acid
Arabinofuranose	35731903.90	217.12	457.45	150.13	Pentose (carbohydrate)
Isovanillic acid	3202688.05	219.14	848.21	168.15	P-methoxybenzoic acids and derivatives
Heptaethylene glycol	1331759.18	295.16	738.69	326.39	Ether (Polyethylene glycols)
Propylene glycol	15867163.02	297.10	551.73	76.09	Secondary alcohol
Benzoic acid	5883468.49	317.16	563.13	122.12	Benzoic acid
Coumaric acid	3021280.76	361.17	1033.60	164.05	Hydroxycinnamic acids and derivatives
Sucrose	27919103.56	371.29	848.38	342.30	O-glycosyl compound (disaccharide)
Dodecanoic acid	1361788.52	455.29	1008.71	200.32	Medium-chain fatty acid (lipids)
Stearic acid	1002115.97	473.23	994.22	284.48	Long-chain fatty acid (lipids)
Glyceric acid	1150664.31	502.20	1018.32	106.08	Sugar acids and derivatives
Nonanoic acid	943194.96	506.07	983.12	158.23	Medium-chain fatty acid (lipids)
Silanol	737215.71	519.13	974.00	45.09	Inorganic
Thiazole	1066433.76	521.79	943.04	85.13	Thiazole
Decaethylene glycol	669496.78	589.26	1024.46	458.55	Ether (Polyethylene glycols)

Supplemental Table 4.2 *continued.*

Compound	InChiKey
Lyxose	InChI=1S/C5H10O5/c6-2-1-10-5(9)4(8)3(2)7/h2-9H,1H2/t2-,3+,4+,5?/m1/s1
Gallic acid	InChI=1S/C7H6O5/c8-4-1-3(7(11)12)2-5(9)6(4)10/h1-2,8-10H,(H,11,12)
Dodecaethylene glycol	InChI=1S/C24H50O13/c25-1-3-27-5-7-29-9-11-31-13-15-33-17-19-35-21-23-37-24-22-36-20-18-34-16-14-32-12-10-30-8-6-28-4-2-26/h25-26H,1-24H2
2-hydroxypyridine	InChI=1S/C5H5NO/c7-5-3-1-2-4-6-5/h1-4H,(H,6,7)
Glycerol	InChI=1S/C3H8O3/c4-1-3(6)2-5/h3-6H,1-2H2
Triethylene glycol	InChI=1S/C6H14O4/c7-1-3-9-5-6-10-4-2-8/h7-8H,1-6H2
Galactose	InChI=1S/C6H12O6/c7-1-2-3(8)4(9)5(10)6(11)12-2/h2-11H,1H2/t2-,3+,4+,5-,6?/m1/s1
Phthalic acid	InChI=1S/C8H6O4/c9-7(10)5-3-1-2-4-6(5)8(11)12/h1-4H,(H,9,10)(H,11,12)
Tripropylene glycol mono-n-butyl ether	InChI=1S/C10H22O4/c1-2-3-5-12-7-9-14-10-8-13-6-4-11/h11H,2-10H2,1H3
Syringic acid	InChI=1S/C9H10O5/c1-13-6-3-5(9(11)12)4-7(14-2)8(6)10/h3-4,10H,1-2H3,(H,11,12)
Lumichrome	InChI=1S/C12H10N4O2/c1-5-3-7-8(4-6(5)2)14-10-9(13-7)11(17)16-12(18)15-10/h3-4H,1-2H3,(H2,14,15,16,17,18)
Palmitic acid	InChI=1S/C16H32O2/c1-2-3-4-5-6-7-8-9-10-11-12-13-14-15-16(17)18/h2-15H2,1H3,(H,17,18)
Arabinofuranose	InChI=1S/C5H10O5/c6-1-2-3(7)4(8)5(9)10-2/h2-9H,1H2/t2-,3-,4+,5+/m1/s1
Isovanillic acid	InChI=1S/C8H8O4/c1-12-7-3-2-5(8(10)11)4-6(7)9/h2-4,9H,1H3,(H,10,11)
Heptaethylene glycol	InChI=1S/C14H30O8/c15-1-3-17-5-7-19-9-11-21-13-14-22-12-10-20-8-6-18-4-2-16/h15-16H,1-14H2
Propylene glycol	InChI=1S/C3H8O2/c1-3(5)2-4/h3-5H,2H2,1H3
Benzoic acid	InChI=1S/C7H6O2/c8-7(9)6-4-2-1-3-5-6/h1-5H,(H,8,9)
Coumaric acid	InChI=1S/C9H8O3/c10-8-4-1-7(2-5-8)3-6-9(11)12/h1-6,10H,(H,11,12)/b6-3+
Sucrose	InChI=1S/C12H22O11/c13-1-4-6(16)8(18)9(19)11(21-4)23-12(3-15)10(20)7(17)5(2-14)22-12/h4-11,13-20H,1-3H2/t4-,5-,6-,7-,8+,9-,10+,11-,12+/m1/s1
Dodecanoic acid	InChI=1S/C10H20O2/c1-2-3-4-5-6-7-8-9-10(11)12/h2-9H2,1H3,(H,11,12)
Stearic acid	InChI=1S/C18H36O2/c1-2-3-4-5-6-7-8-9-10-11-12-13-14-15-16-17-18(19)20/h2-17H2,1H3,(H,19,20)
Glyceric acid	InChI=1S/C3H6O4/c4-1-2(5)3(6)7/h2,4-5H,1H2,(H,6,7)/t2-/m1/s1
Nonanoic acid	InChI=1S/C9H18O2/c1-2-3-4-5-6-7-8-9(10)11/h2-8H2,1H3,(H,10,11)
Silanol	InChI=1S/HOSi/c1-2/h1H
Thiazole	InChI=1S/C3H3NS/c1-2-5-3-4-1/h1-3H
Decaethylene glycol	InChI=1S/C20H42O11/c21-1-3-23-5-7-25-9-11-27-13-15-29-17-19-31-20-18-30-16-14-28-12-10-26-8-6-24-4-2-22/h21-22H,1-20H2